ANKARA YILDIRIM BEYAZIT UNIVERSITY

GRADUATE SCHOOL OF NATURAL AND APPLIED SCIENCES

ACTIVE CELL BALANCING WITH BIDIRECTIONAL CUK CONVERTER

M.Sc. Thesis by

Eyüp KÖSEOĞLU

Department of Defense Technologies

May, 2023

ANKARA

ACTIVE CELL BALANCING WITH BIDIRECTIONAL CUK CONVERTER

A Thesis Submitted to

The Graduate School of Natural and Applied Sciences of

Ankara Yıldırım Beyazıt University

In Partial Fulfillment of the Requirements for the Degree of Master of Science in Defense Technologies, Department of Defense Technologies

by

Eyüp KÖSEOĞLU

May, 2023

ANKARA

M.Sc. THESIS EXAMINATION RESULT FORM

We have read the thesis entitled **"ACTIVE CELL BALANCING WITH BIDIRECTIONAL CUK CONVERTER"** completed by **EYÜP KÖSEOĞLU** under the supervision of **PROF. DR. AHMET KARAARSLAN** and we certify that in our opinion it is fully adequate, in scope and in quality, as a thesis for the degree of Master of Science.

PROF. DR. AHMET KARAARSLAN

Supervisor

ASSOC. PROF. DR. EMRE ÖZKOP

Jury Member

PROF. DR. HÜSEYİN CANBOLAT

Jury Member

PROF. DR. SADETTİN ORHAN

Director

Graduate School of Natural and Applied Sciences

ETHICAL DECLARATION

I hereby declare that, in this thesis which has been prepared in accordance with the Thesis Writing Manual of Graduate School of Natural and Applied Sciences,

- All data, information and documents are obtained in the framework of academic and ethical rules,
- All information, documents and assessments are presented in accordance with scientific ethics and morals,
- All the materials that have been utilized are fully cited and referenced,
- No change has been made on the utilized materials,
- All the works presented are original,

and in any contrary case of above statements, I accept to renounce all my legal rights.

Date: 2023, May **Signature:**

Name & Surname: Eyüp KÖSEOĞLU

ACKNOWLEDGMENTS

Firstly, I would like to express my sincere gratitude to my supervisor, Prof. Dr. Ahmet KARAARSLAN, for his tremendous support and motivation during my study. His immense knowledge and precious recommendations constituted the milestones of this study. His guidance assisted me throughout my research and while writing this thesis.

I would like to dedicate this thesis to my wife Gülsemin and my daughters Ülkü, Aybüke and Umay. I would like to sincerely thank my mother who has always supported me throughout my education.

2023, 1 May **Eyüp KÖSEOĞLU**

ACTIVE CELL BALANCING WITH BIDIRECTIONAL CUK CONVERTER

ABSTRACT

In multi-cell battery packs, the battery management system is the safety system of the battery and is responsible for keeping values such as voltage, current, and temperature within safe limits. One of its most important functions is eliminating the imbalances caused by the voltage difference between the battery cells connected in series. Active and passive topologies are used to compensate for voltage differences between cells. In passive cell balancing, excess energy is dissipated as heat energy over a resistor, while in active cell balancing systems, excess energy is transferred between cells, thus increasing efficiency. In this study, a modular and converter-based active balancing topology is presented. In the design, isolated cuk converter modules perform bidirectional energy transfer corresponding to each battery cell connected in series. Such a modular design has good flexibility and extensibility for balancing series-connected battery cells. By designing an isolated bi-directional cuk converter circuit and equalization controller, five battery cells connected in series were tested separately in charging, discharging, and idle states. The proportional integral control and fuzzy logic control methods have been applied to the proposed topology and verified with the Matlab/Simulink program.

Keywords: Modified cuk converter, active cell balancing, battery management system, battery equalization.

ÇİFT YÖNLÜ CUK DÖNÜŞTÜRÜCÜ İLE AKTİF HÜCRE DENGELEME

ÖZ

Çok hücreli pil paketlerinde batarya yönetim sistemi pilin güvenlik sistemidir ve voltaj, akım, sıcaklık gibi değerlerin güvenli sınırlar içinde tutulmasından sorumludur. En önemli işlevlerinden biri seri bağlı akü hücreleri arasındaki gerilim farkından kaynaklanan dengesizlikleri ortadan kaldırmaktır. Aktif ve pasif topolojiler, hücreler arasındaki voltaj farklarını telafi etmek için kullanılır. Pasif hücre dengelemede fazla enerji bir direnç üzerinden ısı enerjisi olarak dağıtılırken, aktif hücre dengeleme sistemlerinde fazla enerji hücreler arasında aktarılarak verim artırılır. Bu çalışmada, modüler ve dönüştürücü tabanlı bir aktif dengeleme topolojisi sunulmaktadır. Tasarımda izole cuk çevirici modüller seri bağlı her akü hücresine karşılık gelen çift yönlü enerji aktarımı gerçekleştirmektedir. Böyle bir modüler tasarım, seri bağlı pil hücrelerinin dengelenmesi için iyi bir esnekliğe ve genişletilebilirliğe sahiptir. İzole çift yönlü cuk çevirici devresi ve denkleştirme denetleyicisi tasarlanarak seri bağlı beş pil hücresi şarj, deşarj ve boşta durumlarında ayrı ayrı test edilmiştir. Önerilen topolojiye oransal integral kontrol ve bulanık mantık kontrol yöntemleri uygulanmış ve Matlab/Simulink programı ile doğrulanmıştır.

Anahtar Kelimeler: Değiştirilmiş cuk dönüştürücü, aktif hücre dengeleme, batarya yönetim sistemi, pil dengeleme.

CONTENTS

M.Sc. THESIS EXAMINATION RESULT FORM ii
ETHICAL DECLARATION iii
ACKNOWLEDGMENTS iv
ABSTRACT v
ÖZ vi
NOMENCLATURE ix
LIST OF TABLES x
LIST OF FIGURES xi
CHAPTER 1 - INTRODUCTION 1
CHAPTER 2 - BATTERIES 5
2.1 Lead-acid batteries 6
2.2 Nickel-Cadmium Batteries 7
2.3 Nickel Metal Hydride Batteries 8
2.4 Lithium Based Batteries 9
2.5 Solid State Batteries 12
2.6 Supercapacitors 13
2.7 Comparison of Rechargeable Batteries 14
CHAPTER 3 - BATTERY MANAGEMENT SYSTEM 16
3.1 BMS Functions 16
3.2 BMS Topologies 18
3.3 Cell Balancing Topologies 20
3.3.1 Passive Cell Balancing 21
3.3.2 Active Cell Balancing 22
3.3.2.1 Capacitor-Based Active Balancing Methods 22
3.3.2.2 Inductor and Transformer Based Active Balancing Methods 24
3.3.2.3 Converter-Based Active Cell Balancing Methods 26
CHAPTER 4 - PROPOSED CONVERTER BASED TOPOLOGY AND CONTROL TECHNIQUES 37
4.1 Proposed Topology 37
4.2 Cuk Converter 38
4.2.1 State Space Equations of Cuk Converter 40
4.3 Modified Isolated Bidirectional Cuk Converter 45

4.4 Equalization Circuit and Balancing Algorithm 48
4.5 Commonly Used Control Methods in DC-DC Converters 52
4.5.1 Voltage Mode Control of DC-DC Converter 52
4.5.2 Current Mode Control of DC-DC Converter 53
4.5.3 Hysteretic Control 54
4.5.4 Sliding Mode Control 55
4.5.5 PID Control 56
4.5.6 Fuzzy Logic Control 58
4.5.6.1 Fuzzy Logic 58
4.5.6.2 Fuzzy Set 59
4.5.6.3 Membership Functions 61
4.5.6.4 Fuzzy Logic Structure 62
4.6 Designed PI Controller 67
4.7 Designed Fuzzy Logic Controller 73
CHAPTER 5 - SIMULATION RESULTS 82
CHAPTER 6 - CONCLUSION 86
REFERENCES 87
CURRICULUM VITAE 92

NOMENCLATURE

Acronyms

BMS	BatteryManagement System
CAN	Controller Area Network
FLC	Fuzzy Logic Control
LCO	Lithium Cobalt Oxide
LFP	Lithium Iron Phosphate
LIN	Local Interconnect Network
LMO	Lithium Manganese Oxide
LTO	Lithium Titanate Oxide
LVDS	Low Voltage Differential Signaling
NCA	Lithium Nickel Cobalt Aluminium Oxide
NMC	Lithium Nickel Manganese Cobalt Oxide
PI	Proportional Integral
PID	Proportional Integral Derivative
PVC	Polyvinyl Chloride
SMB	Server Message Block
SOC	State of Charge
SOH	State of Health
SPI	Serial Peripheral Interface
TTL	Transistor-Transistor Logic
USB	Universal Serial Bus

LIST OF TABLES

Table 2.1 Comparison of rechargeable batteries 14
Table 4.1 Cuk converter design parameters 39
Table 4.2 Values of components in the cuk converter circuit 40
Table 4.3 The rules 75
Table 5.1 Balancing time comparison 83
Table 5.2 Comparison of current and voltage changes 85

LIST OF FIGURES

Figure 1.1 SOC imbalance situation 2
Figure 2.1 Different shapes of lithium-ion batteries 10
Figure 2.2 The types of lithium-ion batteries 11
Figure 2.3 Schematic diagram of an solid-state battery 13
Figure 2.4 Supercapacitor 13
Figure 3.1 Centralized topology block diagram 19
Figure 3.2 Modular topology block diagram 19
Figure 3.3 Master-slave topology block diagram 20
Figure 3.4 Distributed topology block diagram 20
Figure 3.5 Passive balancing methods 21
Figure 3.6 Capacitor-based cell-balancing methods 23
Figure 3.7 Single inductor based cell balancing 24
Figure 3.8 Multiple inductors based cell balancing 25
Figure 3.9 Multi-winding transformer based cell balancing method 26
Figure 3.10 Multiple transformer based cell balancing 26
Figure 3.11 Buck-boost converter based cell balancing 27
Figure 3.12 Cuk converter-based cell balancing 28
Figure 3.13 Resonant converter-based cell balancing 29
Figure 3.14 Unidirectional flyback-based based cell balancing 30
Figure 3.15 Bi-directional flyback converter based cell balancing 31
Figure 3.16 Full-bridge converter based cell balancing 32
Figure 3.17 Dual active bridge converter based cell balancing 33
Figure 3.18 Dual half-bridge converter based cell balancing 34
Figure 3.19 Push-pull converter based cell balancing 35
Figure 3.20 Forward converter based cell balancing 36
Figure 4.1 Active topologies 37
Figure 4.2 Cuk converter operating modes 38
Figure 4.3 Average large signal 43
Figure 4.4 The modified isolated bidirectional cuk converter 46
Figure 4.5 Mode-1 interval-1 46
Figure 4.6 Mode-1 interval-2 46
Figure 4.7 Mode-2 interval-1 47

Figure 4.8 Mode-2 interval-2 47
Figure 4.9 The modified cuk converter with component values 47
Figure 4.10 Proposed bus topology 49
Figure 4.11 The modified cuk converters Matlab/Simulink block diagram 50
Figure 4.12 The flow chart of proposed active cell balancing control algorithm 51
Figure 4.13 Voltage mode control of asynchronous buck converter] 52
Figure 4.14 Current mode control of asynchronous buck converter 53
Figure 4.15 Hysteretic control of asynchronous buck converter 54
Figure 4.16 Voltage ripple of hysteretic control 55
Figure 4.17 Working principle of sliding mode control 55
Figure 4.18 Block diagram of PI controller with cuk converter 58
Figure 4.19 Classic set 60
Figure 4.20 Fuzzy set 60
Figure 4.21 The most commonly used membership function types 61
Figure 4.22 Block diagram of a fuzzy control system 62
Figure 4.23 Mamdani fuzzy inference system 64
Figure 4.24 Centroid defuzzification method 65
Figure 4.25 Weighted Average defuzzification method 66
Figure 4.26 Max membership defuzzification method 66
Figure 4.27 Mean max membership defuzzification method 67
Figure 4.28 Mode-1 double loop PI control Matlab/Simulink block diagram 67
Figure 4.29 The converter with double loop PI control Matlab/Simulink block diagram for mode-1 68
Figure 4.30 Mode-2 Matlab/Simulink block diagram 68
Figure 4.31 The converter with PI control Matlab/Simulink block diagram for mode-2 69
Figure 4.32 Modified bidirectional cuk converter Matlab/Simulink block diagram for PI control 70
Figure 4.33 Equalization control function Matlab/Simulink block diagram for PI control 71
Figure 4. 34 Mode-1 discharging control Matlab/Simulink block diagram for PI controller 72
Figure 4.35 Mode-2 charging control Matlab/Simulink block diagram for PI controller 73
Figure 4.36 Fuzzy logic designer 74
Figure 4.37 The Membership functions 75

Figure 4.38 Rule surface 76
Figure 4.39 The converter with FLC Matlab/Simulink block diagram for mode 1 .. 77
Figure 4.40 The converter with FLC Matlab/Simulink block diagram for mode 2 .. 77
Figure 4.41 Modified bidirectional cuk converter Matlab/Simulink block diagram for FLC 78
Figure 4.42 Equalization control function Matlab/Simulink block diagram for FLC 79
Figure 4.43 Mode-1 discharging Matlab/Simulink block diagram for FLC 80
Figure 4.44 Mode-2 charging Matlab/Simulink block diagram for FLC 81
Figure 5.1 SOC variation at idle state; a) PI control, b) FLC 82
Figure 5.2 SOC variation at charging state; a) PI control, b) FLC 83
Figure 5.3 SOC variation at discharging state; a) PI control, b) FLC 83
Figure 5.4 Cell current variation in the balancing process 84
Figure 5.5 Bus voltage variation; a) PI control, b) FLC 85

CHAPTER 1

INTRODUCTION

With the increasing world population and the innovations in many industrial and technological fields, the energy demand is constantly increasing. Although fossil fuels meet many areas' energy needs, the trend towards alternative and renewable energy sources has increased as fossil fuel reserves have depleted and environmental problems have arisen. In order to benefit from renewable and alternative energy sources uninterruptedly and increase energy efficiency, energy must be stored appropriately. In addition, many systems, such as mobile phones, computers, electric vehicles, satellites, space systems, communication systems, and defense systems need light, cheap, reliable energy sources with high energy potential. This situation has further increased the importance of energy storage. Batteries, which have an an extensive wide usage area, store electrical energy as chemical energy. It is a common practice to use battery packs built with lithium-based battery cells in systems that require high energy capacity and are designed to operate entirely on battery power or battery support. Lithium-based battery cells are widely used due to some advantages over other batteries. These advantages are high energy density, high reliability, long cycle life, low cost, low self-discharge, and a faster charge and discharge rate.

Lithium-based cells are also divided into many different subspecies. However, in general, their common feature is the necessity of constantly monitoring their voltages, temperatures, and currents during use. Lithium cells must thus be kept within a safe working area. Cells not kept within the safe operating zone may lose their capacity early, deteriorate, or even burn and explode, causing severe safety problems. Battery management system units are used in the battery to keep the batteries and the cells that make up the battery in a safe working area, calculate the battery capacity, make the battery charge and discharge correctly, and use the battery efficiently. The BMS is the most critical unit of a battery, and the features and performance of the BMS directly determine the performance of the battery [1].

The desired energy capacity is obtained by connecting the battery cells in series and parallel to each other. When connected in series, the voltage increases; when connected in parallel, the current increases. However, in series and parallel connected battery cells, leakage, state of charge (SOC), resistance, and capacitance differences may occur in the cells due to the manufacturing process or charging history. These differences can cause some cells to overheat, swell, or even explode due to overcharging, or cause the battery to become unusable due to over-discharge. For this reason, BMS is needed to use lithium-based batteries healthily and efficiently [2].

Because of the variability in SOC between cells, as shown in Figure 1.1, the maximum charge is limited by the cell with the greatest SOC level, whereas the minimum charge is limited by the cell with the least SOC level. Because of this, the battery pack's usable capacity has significantly decreased [3].

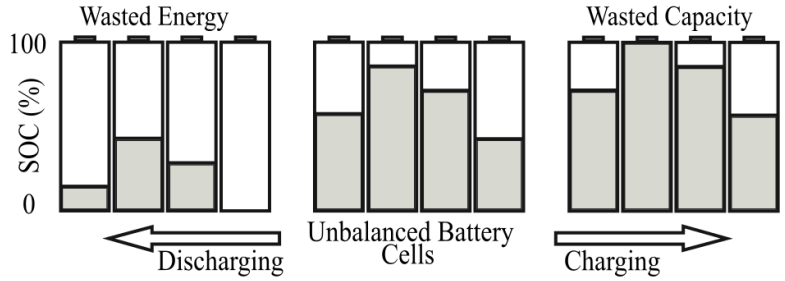

Figure 1.1 SOC imbalance situation

Balancing the cells' energy is one of BMS's other vital responsibilities. Due to the differences that occur during production and use, not every cell is identical, and the differences between cells may increase during use. When the charging and discharging processes are terminated depends on the lowest and highest battery cell capacities. For this reason, balancing is done by decreasing the energy of the cell that reaches the target value at the end of the charge and by increasing the energy of the cell that is finished at the end of the discharge. Thanks to the balancing process, the battery uses its full capacity [2]. In the literature, various cell-balancing topologies are under the main headings of passive and active balancing. Both passive and active balancing techniques have benefits and drawbacks. Passive balancing is simple and inexpensive in design but has low efficiency as energy is wasted. Excess energy is dissipated as

heat through a resistor, so low balancing currents are used. Active balancing is complex and costly to design but highly efficient as excess energy is transferred to weaker cells. In active balancing, balancing can be done at very high currents compared to passive balancing.

A thorough study of BMS design and selection for battery packs manufactured using lithium batteries is given in [2] and [4]. The structure of lithium batteries, charge-discharge characteristics, different BMS topologies, various cell balancing methods, and practical studies are presented.

A thorough presentation of active battery balancing systems based on DC-DC converters and the balancing control algorithms utilized in these systems can be found in [5].

In [6-10], active and passive cell balancing methods are presented, and their advantages and disadvantages are mentioned.

An adaptive sliding-mode control is proposed in [11] along with the analysis and modeling of the improved isolated cuk converter based equalizer.

In [12], a modified cuk equalizer for the energy bus-based distributed equalization network is suggested, and the equalization effectiveness is increased by using a synchronous control technique.

The energy-bus equalizer for dynamic battery equalization is created in [13] based on the isolated cuk converters. Furthermore, a model-predictive control technique was put out to address variations in an operating state and the dynamic equalization of an electric vehicle's battery during charging, discharging, and driving moments.

A bidirectional flyback converter-based equalization circuit was constructed in [14], and a PI controller was used to manage the converter's output power.

Active balancing topologies are very important in terms of energy efficiency. In active balancing, there are capacitive, inductive, and converter-based topologies.

Converter-based topologies stand out due to their energy efficiency and balancing speed [10].

The aim of the thesis is to model an active balancing topology that provides fast and efficient balancing to eliminate voltage imbalances in series-connected battery cells and to compare the results obtained with different control methods. By designing the balancing circuit and equalization controller, five battery cells connected in series with different SOC values were separately tested in charge, discharge, and idle. The proposed topology and balancing algorithm are simulated in Matlab/Simulink program using PI and FLC methods.

In the second part, the BMS is introduced, and BMS functions and topologies are presented. Basic information about topologies used in passive and active balancing methods is given.

In the third chapter, the state equations are derived by detailed analysis of the cuk converter. A small signal model was obtained for the transfer functions required for the control design. A modified isolated bidirectional cuk converter circuit has been designed, and a balancing algorithm has been presented. Finally, proposed control methods, FLC and PI controller designs, are presented.

The fourth chapter compares simulation results with FLC and PI control methods.

The fifth chapter is the conclusion part, where a brief summary of what has been done in the thesis is presented and future studies are mentioned.

CHAPTER 2

BATTERIES

Batteries are units that store electrical energy as chemical energy, and they are used in many devices and fields such as mobile phones, radios, laptops, electric vehicles, satellite systems, communication systems, and defense systems. Batteries function because that electrochemical redox processes transform the chemical energy they store into electrical energy. Through an electrical circuit, electrons move from one substance to another during redox reactions. In order to achieve the necessary output voltage and capacity, one or more cells are connected in series, parallel, or both in series and parallel [15]. Parallel connections increase the capacity and current that can be drawn, while series connections increase the voltage. The battery's capacity is measured in milliampere-hours (mAh) or amp-hours (Ah) [16].

Each cell consists of a metal anode (negative electrode), a metal oxide cathode (positive electrode), and an electrolyte that provides the chemical reaction between these two electrodes. In electrolysis, the ionic exchange process causes an electric current to flow at the cathode while the anode corrodes. The electrical energy generated from this reaction is used to power various tools. The characteristics of the batteries are determined by the type of cells used in the batteries, the number of cells, the serial-parallel connection structure of the cells, and other hardware elements other than the cells used in the batteries [15].

Batteries can be classified as either rechargeable or non-rechargeable. Rechargeable batteries are referred to as "secondary batteries," whereas non-rechargeable batteries are referred to as "primary batteries" [15-17].

Primary batteries are non-rechargeable, in other words, batteries that cannot be charged and reused when the chemical energy inside is depleted. These batteries are also called dry cells and are named according to the material they contain. There are varieties, such as zinc batteries and alkaline batteries. Primary batteries are disposable, although they offer a quick solution in case of need [18].

They are generally the preferred battery types in systems with low current consumption and low frequency of use. Although they have high energy densities, they have low power densities. Although their energy density is low, they are used in many areas of our daily lives due to their low prices and long waiting times. Zinc-carbon batteries are suitable for low-power and low-cost applications. However, the electrolyte of these batteries flowing out of the battery over time can do more harm than good to the system. Zinc chloride batteries have a longer life than zinc carbon batteries. Shelf life is relatively high. Alkaline batteries are employed in low-cost devices that need a lot of power. However, silver oxide batteries have a high energy density despite their small size. They are used in hearing aids. Lithium batteries are widely used in clocks and computer clocks due to their long standby times and high energy density [15].

Rechargeable, that is, secondary batteries, are battery types that can be used after being fully charged. They have a long service life because they can be charged. High power density, high discharge rate, flat discharge curves, and good low-temperature performance are characteristics of secondary batteries [15,18]. Secondary-type batteries are preferred in systems with high power consumption and total energy demand. In current battery studies, batteries are classified according to the type of electrode and/or electrolyte used: nickel-metal hydride, lead-acid, nickel-cadmium, lithium-ion, and lithium-sulfur batteries [15].

2.1 Lead-acid batteries

Electronics frequently include the element lead. Lead, for instance, may be used as the primary ingredient in solders and lead oxides in the glass of cathode ray tubes, while lead acid can be used as a stabilizing agent in batteries and specific PVC cables. The usage of lead-acid batteries is widespread and dates back many years. The French physicist Gaston Plante created the first rechargeable battery used commercially in 1859. Lead-acid batteries are today's most widely used battery type in the automobile, transportation, and telecommunications industries. Lead-acid batteries also contain lead at the anode and lead dioxide at the cathode. It has a positive plate made of brown lead dioxide and a negative plate made of lead metal, both submerged in diluted

sulfuric acid, which serves as the electrolyte. The lead-acid battery stores electrical energy that can be changed from chemical energy to electrical energy [15].

Lead-acid batteries have features such as strong recovery capability, low cost, excellent safety performance, a long life cycle in use, a low self-discharge rate, low maintenance, large quantities available in various sizes and designs, and the ability to operate effectively over a wide temperature range. The disadvantages of these batteries include limited energy density, relatively low cycle life, long charging time, environmental pollution, high mass, thermal instability, and permanent capacity loss [19]. Self-discharge rates are high in storage. Overcharging causes irreversible polarisation of the electrodes and sulfate production during long-term storage while discharged. Lead-acid batteries' nominal voltage and energy density are lower than other battery technologies. The 2V voltage value of lead-acid batteries is insufficient compared to lithium-ion batteries [15,16].

2.2 Nickel-Cadmium Batteries

Strong, ductile, silvery-white nickel has an excellent resistance to corrosion and heat deterioration. Ni-Cd batteries contain cadmium metal at the anode and $Ni(OH)_2$ at the cathode. Electrons released from the positive electrode go to the negative electrode with cadmium and hydroxide, and cadmium hydroxide is formed. Its electrolyte is potassium hydroxide. Since the reaction is reversible, the battery can be charged. Applications that call for Ni-Cd batteries include those that need them for their high energy capacity, extended operational lifetimes, high dependability, quick charging, and high discharge rates. In addition, they have advantages such as a wide operating temperature range, almost entirely recyclable, maintenance-free, high resistance to mechanical and electrical abuse, trouble-free charging at high currents, and generate little heat during operation [15].

Due to their higher energy densities, longer cycle lifetimes, and lower maintenance needs than lead-acid batteries, Ni-Cd batteries have emerged as a desirable substitute in typical applications [19]. However, the widespread use of Ni-Cd batteries, due to the heavy metals in their structure, increases environmental pollution and harms the environment [20]. Therefore, its use is limited. Residues in the structure of the battery

form small blocks of cadmium, causing a problem called the memory effect that significantly affects battery performance. The memory effect is its biggest weakness. It has a high self-discharge feature. It is an expensive energy storage system due to the high cost of the cadmium element. The energy density is poor when compared to other battery types. Because of its detrimental impact on the environment, it has resulted in the development of nickel-metal hydride batteries, which do not utilize cadmium [15,16].

2.3 Nickel Metal Hydride Batteries

Ni-MH batteries are one of the best technologies commercialized in the 1990s. It is the most common kind of nickel-containing battery used in various gadgets, including cameras, computers, medical equipment, and countless other portable electronic devices. Additionally, it is utilized in hybrid and electric vehicles. Ni-MH batteries contain metal hydride, which has hydrogen-adsorbing properties at the anode, and $Ni(OH)_2$ at the cathode, as in Ni-Cd batteries. The electrolyte used is a potassium solution. Polyamide or polypropylene felt or gauze is usually used as a separator between the two electrodes. The battery is housed in a steel case. In cylindrical cells, anode, cathode, and separator strips are laminated and spirally wound. The electrolyte is filled into the center of the cell, and then the cell is closed. The electrochemical performance of Ni-MH batteries is strongly dependent on the metal hydride negative electrode material, which can reversibly store hydrogen. When a battery is discharged, $Ni(OH)_2$ is formed at the positive electrode, and the metal hydride at the negative electrode undergoes oxidation to produce a metal alloy. During charging, the reverse reaction occurs and energy is stored [15].

Due to their fundamental qualities, such as excellent safety, low cost, long cycle life, environmental friendliness, high discharge capacity at low temperatures, overcharge and discharge tolerance, good activation ability, non-toxicity, and high power output, Ni-MH batteries have gained acceptance as an ideal energy source. The significant limitations of these batteries are their high self-discharge rate, low power, and high energy density at high operating temperatures compared to other secondary cells. Another disadvantage is the lack of capacity retention. On the other hand, it is a more

ecologically friendly battery since it does not include lead or cadmium compared to lead-acid and Ni-Cd batteries. It is also more cost-effective than lithium-ion batteries [15,16,21].

If Ni-MH batteries are charged with excessive current, there is a severe decrease of their cycle life. During charging, it needs to be charged with a complex algorithm. Compared to Ni-Cd batteries, the charging time is longer, and their self-discharge is higher. Before lithium-ion battery technology, it had been preferred in the electric vehicle industry because it is a low-cost and mature technology [22].

2.4 Lithium Based Batteries

Energy storage units in which lithium ions are used as charge carriers are generally called Li-ion batteries. Lithium ions are left on the negative electrode during charging by the positive electrode according to the Li-ion battery's operating principle. Conversely, lithium ions are delivered to the positive electrode by the negative electrode during discharge [23]. Because of their high cycle count, these batteries were first made available for purchase by Sony in 1991 and are now often used in portable electronic devices (including smartphones, laptops, and tablets), electric cars, and medical equipment. A lithium-ion battery's cathode and anode electrodes are separated by a porous separator and submerged in an organic liquid electrolyte. The lithium atom donates electrons during charging and forms the Li+ cation, which dissolves from the cathode into the non-aqueous electrolyte, crossing from the cathode to the anode side through the electrolyte. Li+ ions do not react directly; they settle in the anode/cathode structure and separate [15].

High energy and power density, cheap cost, minimal self-discharge, low environmental pollution, reversible and lengthy working durations, high reliability, lengthy cycle lifetimes, and quick charge and discharge rates are just a few of the advantages of lithium-ion batteries. These batteries have the highest voltage per cell and energy density per mass compared to other batteries of today's era. The advantages of lithium-ion batteries over other battery types are their lack of memory effect, extremely low self-discharge rates, and long cycle lives [16].

Lithium-ion batteries have a vast working temperature range since they may be utilized between -20°C and +60°C in the charge state and between -40°C and +65°C during discharge. Furthermore, the voltage range of lithium-ion battery cells is 2.5V to 4.2V, roughly three times that of other battery types. In Figure 2.1, different designed lithium batteries are shown.

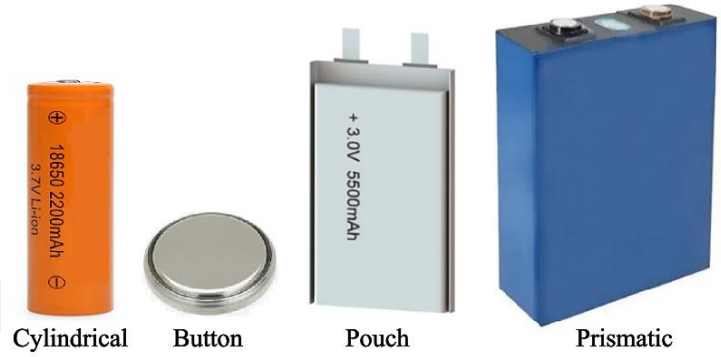

Figure 2.1 Different shapes of lithium-ion batteries

Due to lithium's high degree of reactivity, there is a chance of an explosion or burning during use. The disadvantages that stand out the most are the capacity limitation and explosion danger brought on by the volume expansion of the electrodes while charging and discharging. Dangerous circumstances can occur when lithium-ion batteries are exposed to strong heat or direct sunshine. The charging procedure should be done at a steady current until the charging voltage reaches 80% of the battery voltage at its maximum value. Following that, a constant voltage should be used to continue charging. Finally, the charging process should be stopped when the charging current reaches a particular level [16]. Lithium-ion battery cells need safety circuits to prevent overcharging and overdischarging when connected in series and parallel to form a battery pack [24]. In Figure 2.2, the photo of types of lithium-ion batteries are shown.

Various battery types have emerged by using different materials in lithium-ion batteries. These are LCO, LMO, LFP, NMC, LTO, and NCA batteries. Regarding specific energy, LCO, NMC, and NCA batteries stand out, whilst NCA batteries take the lead in terms of specific power. LTO batteries come to the fore regarding safety, performance, cost, and cycle life [16].

Figure 2.2 The types of lithium-ion batteries [25]

Lithium polymer batteries differ from lithium-ion batteries in that polymer material is used as the electrolyte. The polymer electrolyte material has a high electrical conductivity. Due to the presence of liquid electrolytes in its structure, the battery is covered with metal foils to prevent leaks. LiPO batteries are a type of battery that can be found in desired sizes. They are usually produced specially to meet the demands of large device manufacturers. Therefore, it is used in portable electronic devices. Because it has a flammable and explosive structure, care should be taken during its use. Even if LiPO batteries are thrown into the water while burning, they continue to burn due to the chemical density inside. Due to their chemical structure, they are light and more resistant to excessive discharge. The low self-discharge rate is also a feature that makes this battery type stand out [16]. Due to the low conductivity of LiPO batteries, they provide better performance at high temperatures. It has lower energy density and fewer cycles compared to lithium-ion batteries. Compared to Ni-Cd and Ni-MH batteries, LiPO batteries offer a better energy density and a longer lifespan [26].

High power density, safety, and cycle rate batteries include lithium-iron phosphate batteries. However, compared to lithium-ion batteries, it is seen as a disadvantage because it has a lower energy density, capacity [26].

Sulfur is one of the most abundant elements in nature. The maximum theoretical power density and capacity of any known cathode are possessed by sulfur. Lithium-sulfur batteries contain lithium at the anode and sulfur in powder form at the cathode. Energy

production occurs through multi-step reduction and oxidation reactions between lithium and sulfur. Lithium sulfur batteries have a higher energy potential than lithium-ion batteries, are lighter, and are more resistant to sudden temperature changes. While lithium-sulfur (Li-S) batteries are in the new-generation battery class, they have a high energy potential (3.5 times higher than lithium-ion batteries). It has a wide operating temperature range, is lightweight, and resists unexpected temperature fluctuations. It has a high storage capacity, is environmentally friendly, requires no maintenance, and has a very long shelf life. The abundance of sulfur in nature and its cheapness make the battery a low-cost system. However, it has drawbacks like a short cycle life, poor charging efficiency, inadequate safety, and a high self-discharge rate [15].

2.5 Solid State Batteries

Solid-state batteries are a type of battery technology that uses solid electrolytes instead of the liquid or gel electrolytes used in conventional batteries. Since they do not contain flammable liquid electrolytes, the risk of ignition and explosion is less. It has the potential to store more energy per unit volume, which means longer battery life and smaller, more compact batteries. Solid-state batteries have the potential to charge faster and are especially useful for electric vehicles and other applications where fast charging is important. Its challenges are improving solid electrolyte conductivity and reducing production costs [27].

The anode is made of lithium metal or lithium-ion storage material such as graphite. The cathode is made of a lithium-ion storage material such as lithium cobalt oxide, lithium iron phosphate, or lithium manganese oxide. The solid electrolyte, which enables ion movement between the anode and cathode, is the most crucial part of the solid-state battery. The solid electrolyte can be made from various materials, including ceramics, glasses, or polymers. However, the most commonly used solid electrolyte materials are lithium phosphorus oxynitride (LiPON), lithium thiophosphate (Li_3PS_4), and lithium garnet ($Li_7La_3Zr_2O_{12}$) [28]. Figure 2.3 shows the solid-state battery structure.

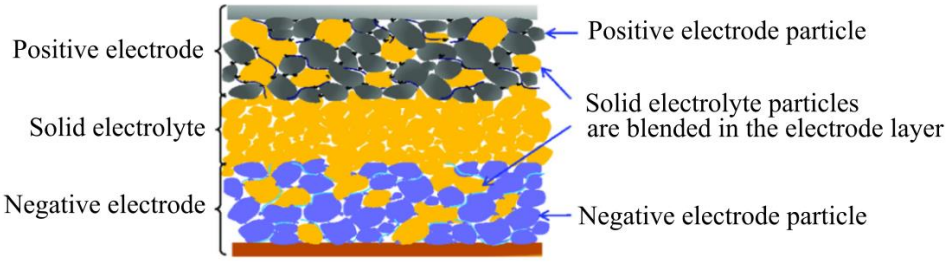

Figure 2.3 Schematic diagram of an solid-state battery [29]

2.6 Supercapacitors

In contrast to batteries, which store energy through a chemical process, supercapacitors, often referred to as ultracapacitors or electrochemical capacitors, store energy in an electric field. They can charge and discharge energy fast because they have a high power density. In addition, they have a long cycle life, with the ability to be charged and discharged hundreds of thousands of times without deterioration. A supercapacitor consists of two electrodes separated by an electrolyte. It stores energy by accumulating an electric charge on the surface of the electrodes [30].

Because they use electrode materials with a large surface area, like activated carbon, which provides a large surface area for charge accumulation, supercapacitors can store much more energy than conventional capacitors. The electrolyte used in supercapacitors is typically an organic solvent containing an electrolyte salt such as potassium hydroxide, sodium chloride, or lithium sulphate. Batteries have a higher energy density than supercapacitors. In comparison to batteries, they also self-discharge more quickly. Due to their high power densities, lengthy cycle lifetimes, and capacity to function across a broad temperature range, supercapacitors stand out [30].

Figure 2.4 Supercapacitor [31]

Figure 2.4 shows a supercapacitor.

2.7 Comparison of Rechargeable Batteries

Because of their affordability, dependability, and availability, lead-acid batteries are often utilized in a wide range of applications. Although they have low energy densities, they have high power densities. They are used in applications such as starting car engines and powering UPS systems. The energy density of nickel-cadmium batteries is high, and they have a long cycle life. Since they contain environmentally harmful cadmium, their use has increased in different batteries. Since nickel-metal hydride batteries do not contain toxic metals, they are more environmentally friendly than Ni-Cd batteries. They have less cycle life than lithium-ion batteries but a better energy density than lead-acid batteries.

Table 2.1 Comparison of rechargeable batteries [32,33]

Battery Type	Rated Cell Voltage (V)	Energy Density (Wh/kg)	Number of Cycles	Cost
Lead-acid	2,0	35	1000	Low
Ni-Cd (Nickel Cadmium)	1.2	50-80	2000	Low
Ni-MH (Nickel Metal Hydride)	1.2	70-95	<3000	Low
LCO (Lithium Cobalt Oxide)	3.7-3.9	150	500-1000	Medium
NCA (Lithium Nickel Cobalt Aluminium Oxides)	3.65	130	500	Medium
NMC (Lithium-Nickel-Manganese-Cobalt-Oxide)	3.8-4.0	170	1000-2000	Medium
LMO (Lithium Manganese Oxide)	4	120	300-700	Medium
LFP (Lithium Iron Phosphate)	3.3	130	1000-2000	High
LTO (Lithium Titanate Oxide)	2.3-2.5	85	3000-7000	High
Li-S (Lithium Sulfur)	2.5	350-650	300	Low
Solid State Battery	3.6	250-1000	>10000	High
Supercapacitor	2.3 to 2.75	4-8	500000-20000000	High

Today, lithium-ion batteries are the most widely used kind of battery for electric vehicles and portable electronic devices. They feature a significant cycle life, a high energy density, and quick charging periods. Solid-state batteries have potentially

higher energy densities, faster charge times, and longer cycle lives than conventional batteries. However, they are still under development and are more expensive to manufacture than conventional batteries. Supercapacitors can store and release energy quickly, with a higher power density and faster charge times than batteries. However, compared to batteries, they have a lower energy density. Table 2.1 compares rechargeable batteries with regard to voltage, energy density, cycle life, and cost.

CHAPTER 3

BATTERY MANAGEMENT SYSTEM

Battery groups of various capacities may be built by connecting the battery cells in series and parallel, depending on the requirements. It is crucial to monitor and regulate the battery cells' current, voltage, and temperature during charge-discharge, particularly in lithium-based battery packs. In order to use the battery cells in the battery pack in a healthy, safe, and effective manner, battery management systems are created. A rechargeable battery is monitored and managed by a BMS. Electric cars, renewable energy systems, portable electronics, aerospace and defense systems, and many more applications depend on battery management systems.

3.1 BMS Functions

There are some general functions that a BMS should have. BMS is a system that performs functions such as battery safety and protection, charge control, SOC estimation, SOH estimation, cell monitoring, thermal management, cell balancing, and communication.

Battery monitoring is one of the BMS's primary responsibilities. The BMS continually measures the battery cells' voltage, current, and temperature measurements. For the battery to operate safely and effectively, it's crucial that cell voltages and temperatures stay within the operating range. It is essential for safety that the operating temperature of Li-ion batteries, which is one of the most preferred battery types, is under control, and the operating temperature should be kept under constant control, if possible, by taking measurements from each cell or with the help of sensors homogeneously distributed in the battery pack. BMS evaluates all the data it receives from the battery pack with the help of various sensors and presents various information about the battery to the user. SOC and SOH are some of this information. The SOC of a cell measures how much energy is now held in the battery in relation to the maximum amount that can be held when it is fully charged. It is frequently expressed as a

percentage, where 100% corresponds to a fully charged battery and 0% to an empty or entirely exhausted battery.

A BMS function that calculates SOC estimates how much energy is kept in a rechargeable battery. The SOC gives a reading of the battery's energy level and is expressed as a percentage of the battery's total capacity. Battery voltage and current are measured, and SOC of the battery is calculated using this data.

SOH gauges a rechargeable battery's performance as compared to when it was new. It details the battery's capability to store and discharge energy over time and is stated as a percentage of the battery's initial capacity. The SOH is an important parameter for battery management, as it indicates its performance and remaining life. It is used to determine when to replace the battery and optimise its performance. The SOH is also used to ensure the battery is operated within its safe working range and to eliminate issues caused by battery deterioration. Monitoring the battery's numerous characteristics, including voltage, current, temperature, and aging, allows for the estimation of the SOH [2].

BMS is a system that constantly communicates with other control units in the electronic structure in which it is used, using various protocols. It should be able to share various information about the battery with other systems or with the user connected from the outside and be able to apply commands from outside or other units healthily. The BMS can communicate via various wired and wireless communication technologies. SMB, CAN, RS-232, TTL, USB, LIN, RS485, LVDS, Ethernet, Bluetooth, and WIFI are some examples [4]. A BMS’s communication interface will be determined by its intended purpose as well as the requirements of the systems and devices with which it must communicate. The communication interface is a key component of the BMS since it allows the BMS to receive and communicate data from other systems and devices, and regulate and monitor the battery system.

Over-temperature protection is a function in BMS that guards against damage caused by high temperatures. Over-temperature protection is performed by monitoring the battery's temperature and acting when it exceeds a predetermined limit. For example, the BMS could reduce the charging or discharge current, disconnect the charging

source or load, or shut down the system that is using the battery. Lithium-ion batteries typically operate in a temperature range of -20°C to 60°C [34].

The BMS opens the circuit to cut off energy flow between the battery pack and the system it is linked to when abnormal conditions arise in the battery. For example, when any cell in the battery pack achieves maximum voltage, charging should be stopped, even if the other cells in the array are not yet full. Otherwise, the cell will be overcharged. Similarly, even if the other cells in the array are not yet empty, the discharge must stop when any battery pack cell approaches the minimum voltage. Otherwise, the cell will be overcharged.

It ensures that the battery works with optimum efficiency by controlling the relevant parameters during charging and discharging. During charging, it regulates the charging current according to the battery charge rate. During discharge, it notifies the system of the current that can instantly be drawn from the battery. In addition, it detects voltage imbalances between battery cells and ensures that all cells are at equal voltage with various balancing methods.

A BMS feature called cell balancing ensures that all cells in a battery pack are charged and discharged uniformly. The voltage levels and charge-discharge rates of the battery cells in the battery pack might vary. The performance of the battery pack may deteriorate over time and may even become useless, leading to unfavourable outcomes like explosions, if this imbalance between the cells is not addressed. A well-made cell balancing mechanism increases the battery pack's overall performance and increases the battery pack's lifespan.

3.2 BMS Topologies

BMS topology refers to the architecture of the BMS system, which includes the hardware and software components used to manage the battery. BMSs can have different topologies depending on the number and structure of electronic cards they have. Different topologies can be used for BMS: centralized, distributed, modular, and master-slave.

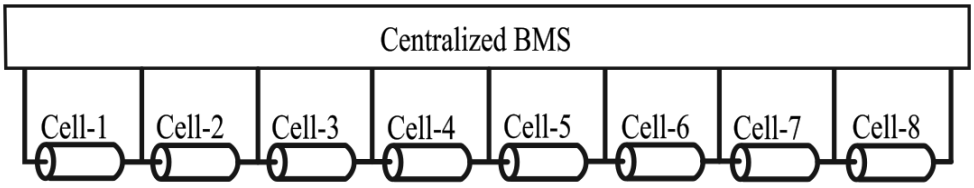

Figure 3.1 Centralized topology block diagram

In the central topology, a central main control unit is directly connected to each battery pack cell, as shown in Figure 3.1. There is a single electronic card in the central topology, which performs all the tasks of the BMS. Measurements such as cell voltages and temperatures, measurement of battery current, SOC and SOH calculations, heater, cooler control, and communication tasks with other units are performed by a single card. As a result, it's compact and easier to troubleshoot when problems occur [2].

In a modular BMS, as shown in Figure 3.2, battery groups are controlled by multiple modules. Two or more electronic cards form a hierarchical structure. Usually, the modular structure consists of "master" and "slave" cards. Using a digital communication interface like CAN bus, RS-482, or SPI, each slave card receives data from the cells in a particular battery area and transmits it to the master card. The master card makes the necessary calculations and evaluations and performs the main tasks of the BMS. In applications where multiple batteries need to work harmoniously, a more competent electronic unit can be placed on the master cards. It has almost the same advantages as the central topology. Cables are easier to manage, as each module is placed close to its respective battery pack. Larger battery packs can be obtained by increasing the number of modules. However, the cost is slightly higher than the central topology [2].

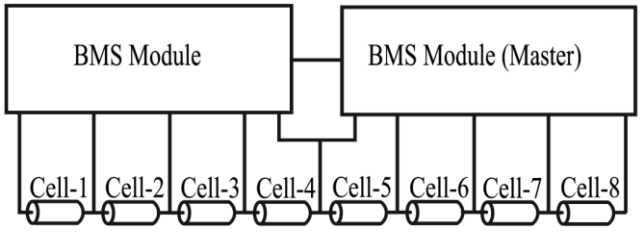

Figure 3.2 Modular topology block diagram

A master-slave BMS is shown in Figure 3.3. Each slave module is responsible for a specific battery group, and as such, it resembles a modular topology. However, master modules are different and deal only with computation and communication [2]. A distributed BMS is significantly different from other topologies, as shown in Figure 3.4. A distributed BMS has circuit boards that are placed directly in the cells. A BMS controller manages circuit boards linked to battery cells. The computations and communication are controlled by the BMS controller [2]. It consists of a single card, on which the main operations are carried out, and auxiliary cards.

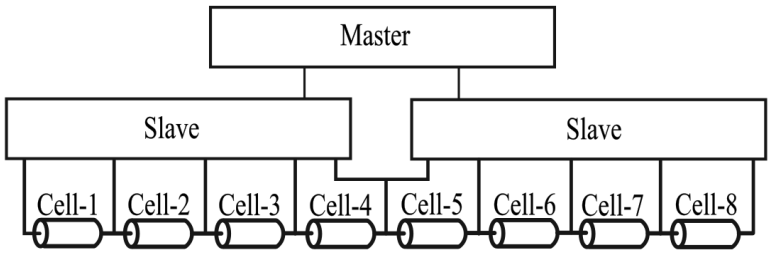

Figure 3.3 Master-slave topology block diagram

Having a card for each cell ensures that it is less affected by electromagnetic noise, as there are no measurement cables, and prevents malfunctions with a simpler connection. Since the number of electronic cards used in the dispersed topology will increase, the cost will increase even more than other methods.

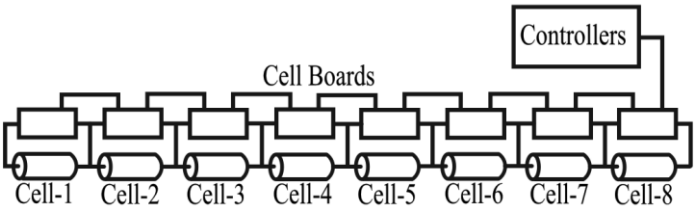

Figure 3.4 Distributed topology block diagram

3.3 Cell Balancing Topologies

Batteries made of parallel-connected cells pressurize one another to equalize voltage. Consequently, cells that are linked in parallel automatically balance one another. The capacity of the battery cells varies since they do not charge and discharge equally. In

an unbalanced battery pack, one or more series-connected cells will charge up to their maximum capacity earlier than the others. If the battery is not fully charged, the unfinished cells will exhaust themselves before the other cells in the series. These voltage imbalances over time may cause cell damage or decrease the battery pack's overall capacity and performance. Cell balancing is needed to eliminate intercellular capacity differences. Until the cells with a low level of charge in the battery are full, the cells with a high charge ratio are prevented from charging more. The cell-balancing mechanism is crucial to maximize energy efficiency and extend battery life. Passive and active cell balancing are the two primary categories under which cell balancing techniques may be analyzed.

3.3.1 Passive Cell Balancing

Passive cell balancing is a quick and affordable way to balance the charge among the cells in a battery pack. Shunting resistors are used and linked in parallel to each battery pack cell. A shunting resistor linked to a cell begins to release energy as heat when the cell's SOC rises beyond a given threshold, which lowers the cell's SOC. The balancing speed depends on the value and power of the resistor. Figure 3.5 (a) shows the fixed shunt resistor and Figure 3.5 (b) shows the switched shunt resistor method. Also, it is used in charging mode only [6].

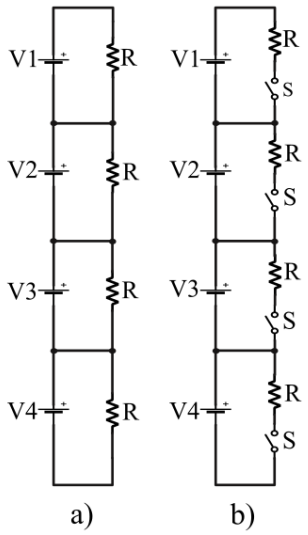

Figure 3.5 Passive balancing methods

The fixed shunt resistor method is typically used in lead-acid and nickel-cadmium batteries, where the cells can tolerate higher levels of heat generation without significant degradation. However, the increased sensitivity of lithium-ion cells to high temperatures prevents them from being widely employed in lithium-ion battery systems [10].

Using electronic switches in the switched shunt resistor balancing method makes it more efficient than the fixed shunt resistor balancing method. With a switched shunt resistor, the BMS can selectively couple the shunt resistor to cells that must be balanced at a given time. This means that the shunt resistor will only dissipate energy when it is needed, rather than constantly wasting energy as with a fixed shunt resistor [10]. The switched shunt resistor balancing method is suitable for lithium-ion batteries [6]. When the battery discharges, using this balancing method is useless because no energy can be saved [7].

3.3.2 Active Cell Balancing

In active cell balancing, the energy of cells with a high SOC level is taken and transferred to cells with a low SOC level. Compared to the passive balancing method, the active balancing method completes the balancing process faster and more effectively. This technique may be applied to a battery that is both charging and draining. Capacitive, inductive, or converter types of balancing can be used for active cell balancing [6,9,10].

3.3.2.1 Capacitor-Based Active Balancing Methods

Active balancing topologies based on capacitors transmit extra energy from the high-charge cell to the low-charge cell by using capacitors as an external energy storage device. In the capacitor-based balancing method, the energy in the selected cell is stored in a capacitor and transferred to another cell. Despite having a lengthy balancing period, it has a straightforward control scheme and high efficiency. Different designs can be made using different numbers of switches and capacitors [9]. Figure 3.6 (a), (b), and (c) exhibit several topologies of capacitor-based cell balancing techniques,

such as switched capacitor, double-tiered capacitor, and single-switched capacitor [35].

The switched capacitor balancing method is very simple because it has only two states. After a certain amount of time in either the upper or lower position, the key switches positions. When compared to the switched shunt resistor balancing method, the disadvantage is the prolonged balancing time and higher cost [35].

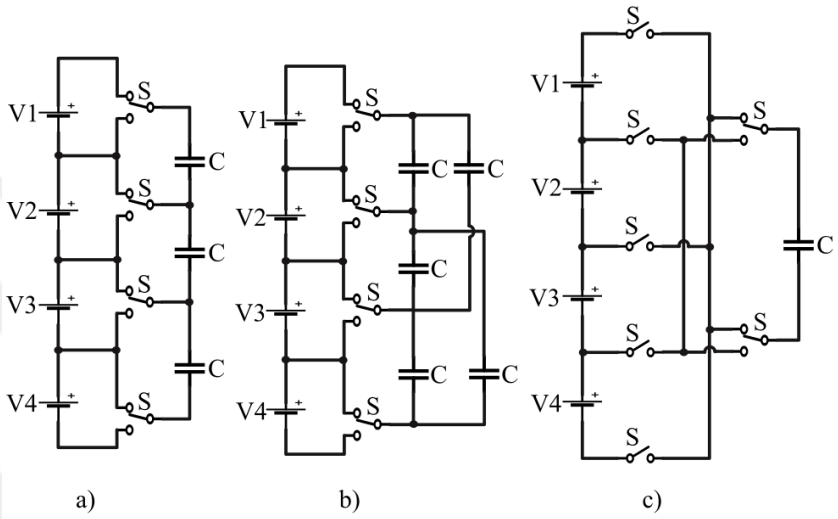

Figure 3.6 Capacitor-based cell-balancing methods

The double-tiered switched capacitor balancing technique is a variation of the switched capacitor approach. It is made by connecting a fresh layer of capacitors in parallel to the switched capacitors [4]. The distinction is that it transfers energy using two capacitor layers. The time spent balancing is cut in half, which gives this approach an edge over the switched capacitor method [35]. As more capacitors are used, the circuit size and cost increase.

In the single-switched capacitor balancing method, cells with high and low SOC levels are determined, and switch positions are swapped between these cells. This approach allows for employing more sophisticated control techniques to speed up the balancing process [35].

3.3.2.2 Inductor and Transformer Based Active Balancing Methods

The active balancing approach based on inductors and transformers uses magnetic components like these to carry out the balancing procedure. High balancing currents might shorten the balancing time. Also, production costs are high, and magnetic transformer losses must be considered [10,36]. In the inductor-based balancing method, balancing is performed using single or multiple inductors, as shown in Figures 3.7 and 3.8, respectively.

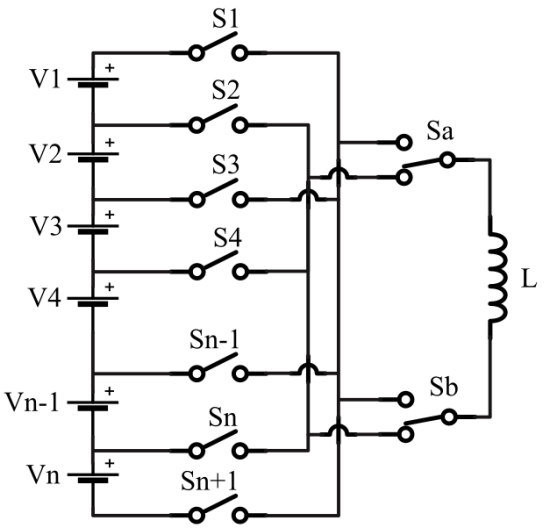

Figure 3.7 Single inductor based cell balancing [6]

Cells with high and low SOC levels are determined, and energy transfer is realized by changing the position of the switches with the control algorithm. The switches are regulated and the surplus energy in the cell is transferred with the use of inductance in the single inductor balancing technique.

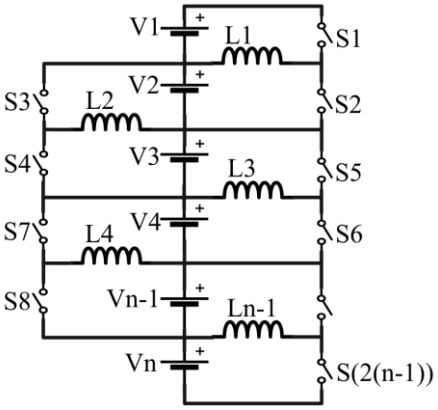

Figure 3.8 Multiple inductors based cell balancing [6]

Balancing can be carried out from battery pack to cell or cell to cell, depending on the direction of energy transfer. The multi-inductor balancing method is faster and more efficient [36]. Balancing speed and efficiency is higher than in capacitor-based topology. Though less expensive, it balances slower than transformer-based topology [6]. In transformer-based balancing, the balancing speed is high. However, the size of the circuit and the high cost and complexity of control for transformer-based circuits make them undesirable. As transformer-based balancing techniques, the multi-winding transformer approach and the multi-transformer method are suggested in the literature. The multi-winding transformer method consists of primary winding, as shown in Figure 3.9, and secondary winding, according to the battery cell number. It has a single core. Due to the growing number of windings in this method, the number of batteries that can be connected in series is constrained. They share the same primary winding and each cell has a separate secondary winding. When compared to the multi-transformer topology, it has less winding. The cost increases as a special multi-winding transformer is required according to the balancing system to be designed. The number of linked cells determines the transformer ratio [37].

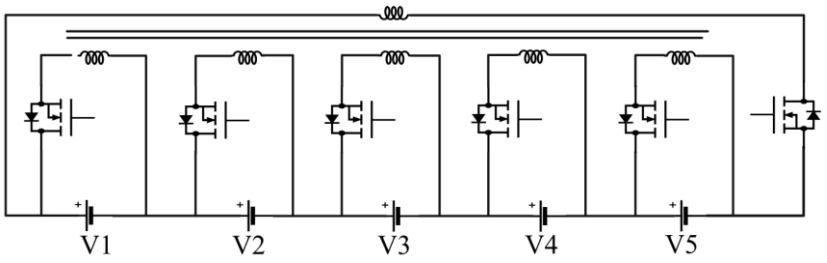

Figure 3.9 Multi-winding transformer based cell balancing method

In the multiple transformer topology, one transformer corresponds to each cell as shown in Figure 3.10. The number of batteries connected in series is no longer limited and can be easily added and removed. As a result, the switches have relatively little current and voltage stress, and equalization happens quickly. However, because each cell contains a transformer, the price is high [37].

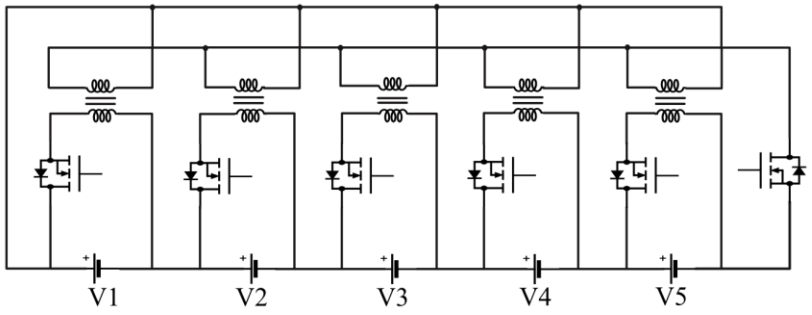

Figure 3.10 Multiple transformer based cell balancing

3.3.2.3 Converter-Based Active Cell Balancing Methods

Converter-based balancing methods are based on balancing battery cells connected in series using DC-DC converters. Due to additional passive components and active switches, they are expensive while being quite effective. They could need a sophisticated control algorithm. Various DC-DC converters, including the cuk converter, the buck-boost converter, the flyback converter, the full bridge converter, and the resonance converter, are used in the literature as balancing techniques [9,10].

Buck-boost converter topology

Figure 3.11 depicts a buck-boost converter-based bidirectional balancing circuit.

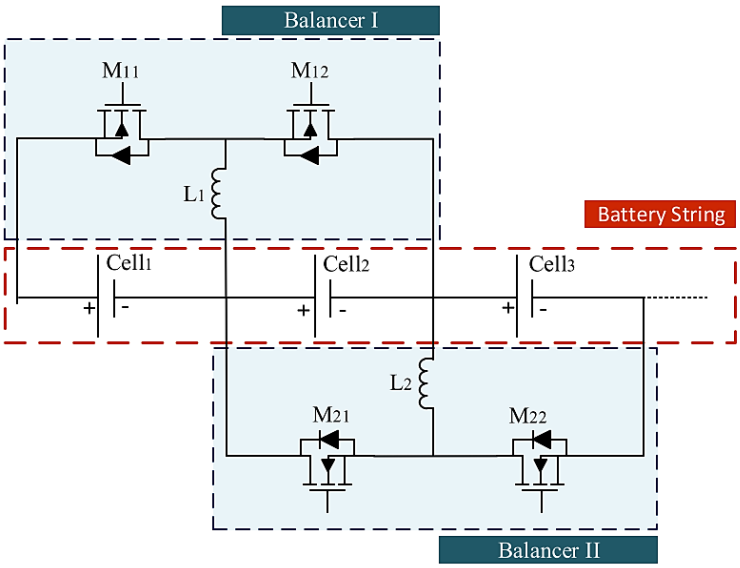

Figure 3.11 Buck-boost converter based cell balancing [5]

A body diode MOSFET and an inductor make up the balance circuit. One of the most popular converter types utilized in active balancing topologies is the buck-boost converter. The energy used for balancing is kept in the inductor [5]. Balancing can be performed both during charging and discharging without the need to design a complex controller. Since balancing occurs between adjacent cells, its speed is low. Energy converters of the buck, boost, and buck-boost types are frequently used circuit topologies. Additionally, there are various designs for transferring energy from the battery cells to the battery pack or the other way around [37].

Cuk converter topology

The cuk converter comprises two uncoupled inductors, an energy transfer capacitor, two MOSFETs with body diodes, and two MOSFETs, as illustrated in Figure 3.12. By acting as a filter, inductors keep harmonics out. In both directions, the output voltage may be either higher or lower than the input. The buck-boost topology and the cuk converter balancing circuit operate on the same principles generally. Contrary to the buck-boost topology, where the inductor is in charge of energy transfer, the cuk converter relies on the capacitor [5].

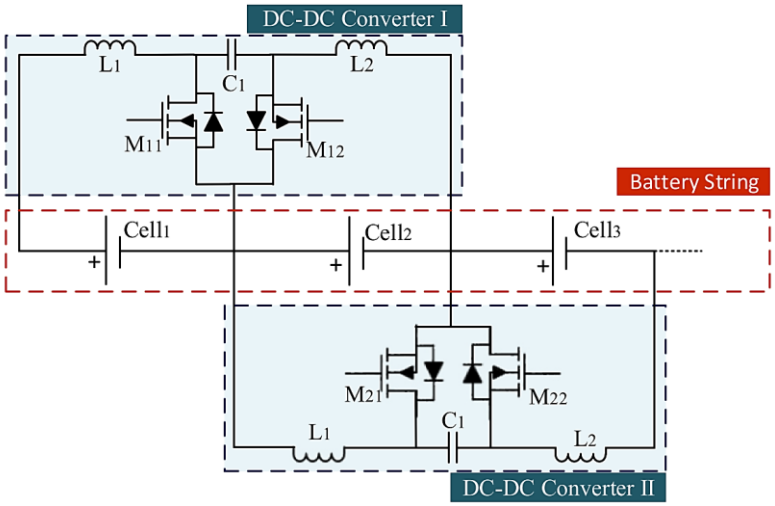

Figure 3.12 Cuk converter-based cell balancing [5]

The cuk converter provides a bidirectional energy transfer direction for nearby battery cells. Cell-to-cell equalization is provided with excellent efficiency by the cuk converter. The balancing procedure is repeated until the battery is balanced with a 50% duty cycle on the switches. This circuit's key benefits are high efficiency, low voltage, and low current strains on the switching components. Because the balancing is between adjacent cells, the balancing speed is low. The circuit is huge and expensive since so many active components are involved [37].

Resonant converter topology

Converters created to lower switching losses are known as resonant converters. By restricting the rates at which the current and voltage rise when the switching elements are switched on and off, the resonance tank, which is composed of an inductor and a capacitor linked in series or parallel, lowers switching losses [5]. Figure 3.13 shows resonant converter based cell balancing topology.

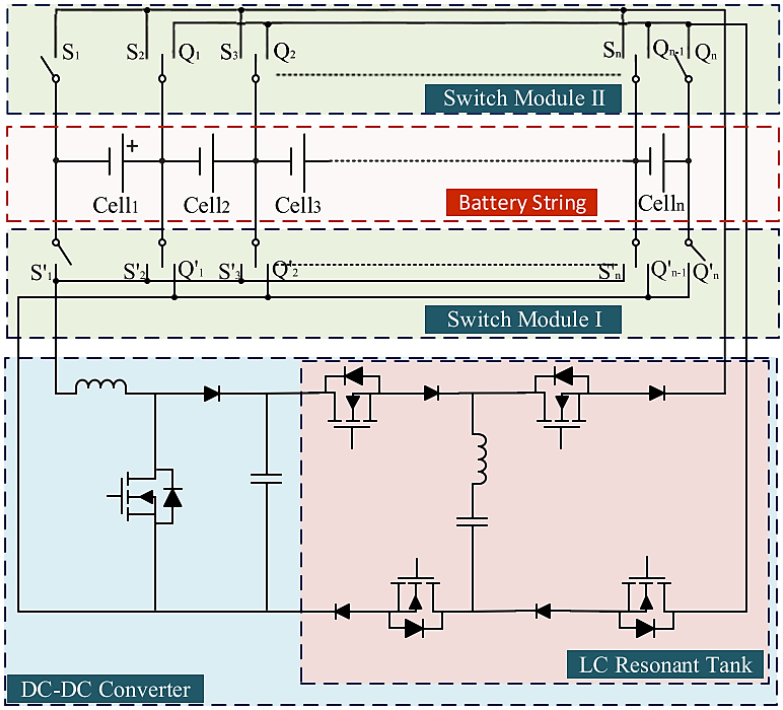

Figure 3.13 Resonant converter-based cell balancing [5]

Flyback converter topology

From the buck-boost converter, the flyback is a standalone DC-DC converter. The flyback converter is frequently used when transferring energy in unidirectional or bidirectional modes. Figures 3.14 and 3.15 show unidirectional and bidirectional flyback converters, respectively. Compared to buck-boost and cuk converters, the circuit size is bigger, and the cost of the transformer also rises [5].

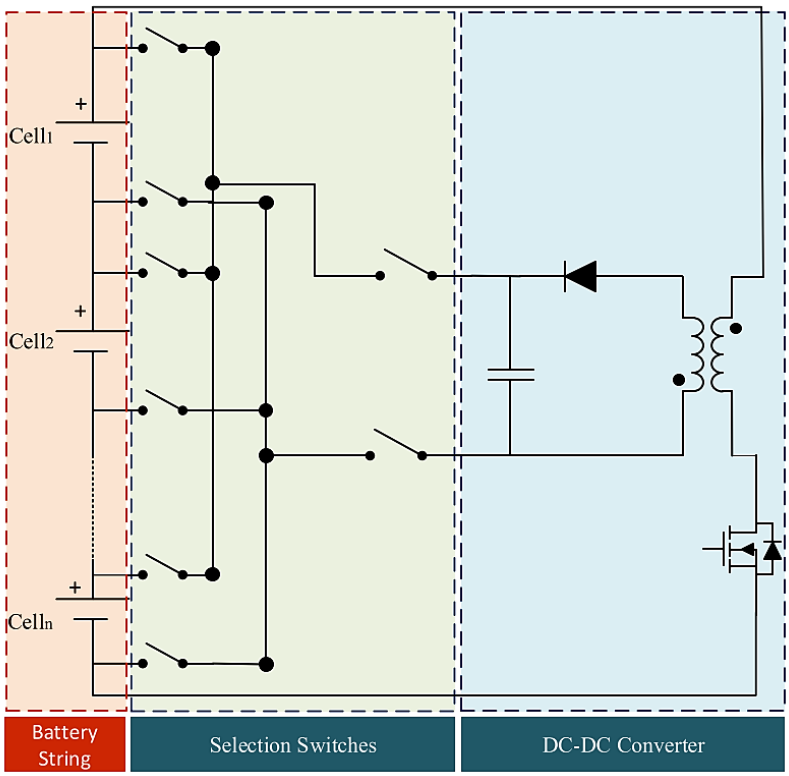

Figure 3.14 Unidirectional flyback-based based cell balancing [5]

Two inductors are coupled to store energy rather than just one. The flyback converter may be used for cell-to- package, package-to-cell, or cell-to-cell balancing based on the bidirectional switching and control mechanism: low current and voltage strains, good efficiency.

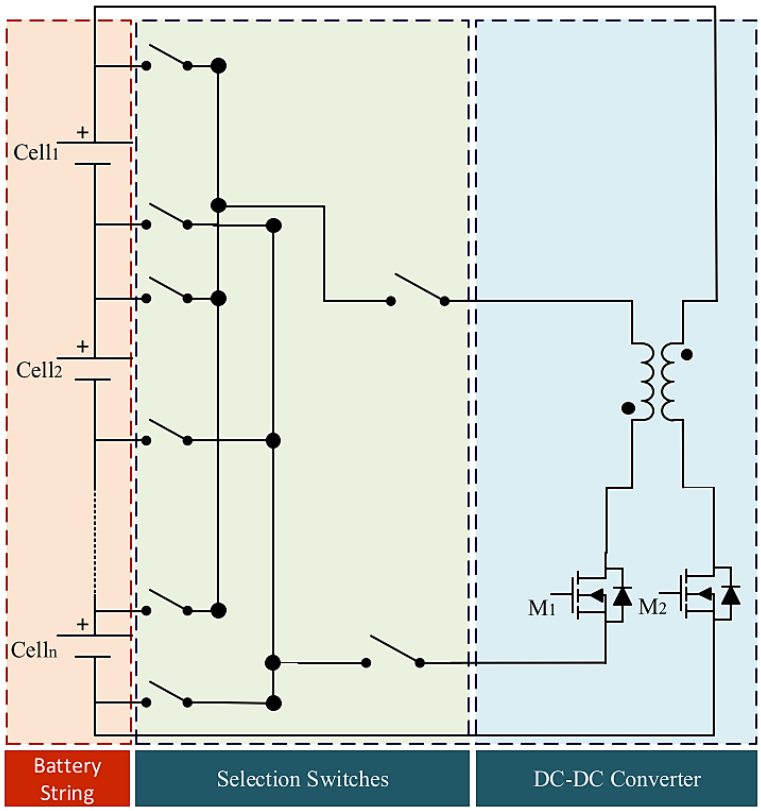

Figure 3.15 Bi-directional flyback converter based cell balancing [5]

As with transformer-based circuits, it has disadvantages such as cost and control complexity. Flyback converters' structural isolation is one of their key characteristics. As a result, they are capable of isolating both parties. The intricacy of this system's design and execution is a drawback [5].

Full-bridge converter topology

When renewable energy sources like wind and solar are connected to the grid, battery energy storage systems comprised of Li-ion battery cells are utilized to reduce the volatility that these sources of energy production at the output. As a result, the harmonic is sent to the grid through unbalanced battery cells, which lowers the capacity. In grid-connected battery energy storage systems, full-bridge converters are an effective converter topology for cell balancing. This converter type's high equalization speed and modular design suit it for high-power applications, as seen in Figure 3.16. However, its cost is significant due to its size and number of switching components [5].

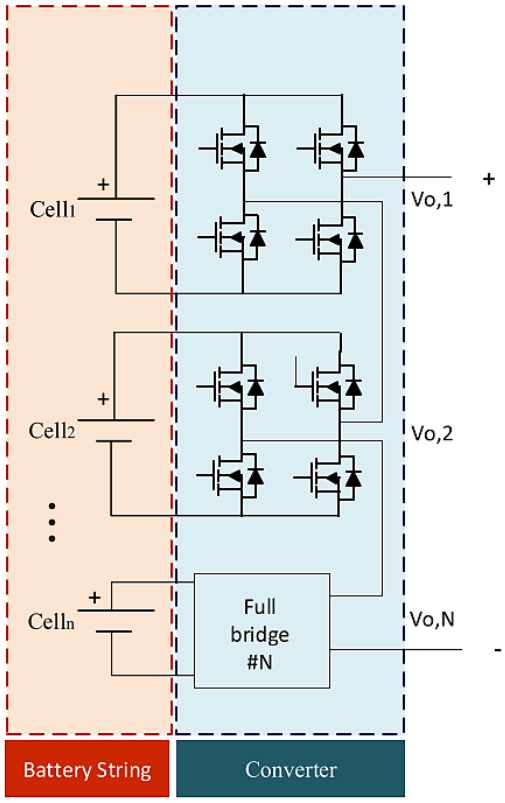

Figure 3.16 Full-bridge converter based cell balancing [5]

Dual active bridge converter topology

A few crictical advantages of dual active bridge power converters are galvanic isolation, high voltage range, power transmission capabilities, soft switching to lower transformer losses, and modular design. The dual active bridge power converter is depicted in Figure 3.17 as consisting of two H-bridges with four switching elements each on either side of the transformer, and a transformer with a significant leakage inductance. The transformer provides galvanic isolation and voltage synchronisation between the high-voltage and the low-voltage sides. Both buck and boost modes can be used with dual active bridge power converters. The dual active bridge power converter-based balancing topology has a high balancing speed and is suited for battery packs with many cells, but it is expensive [5].

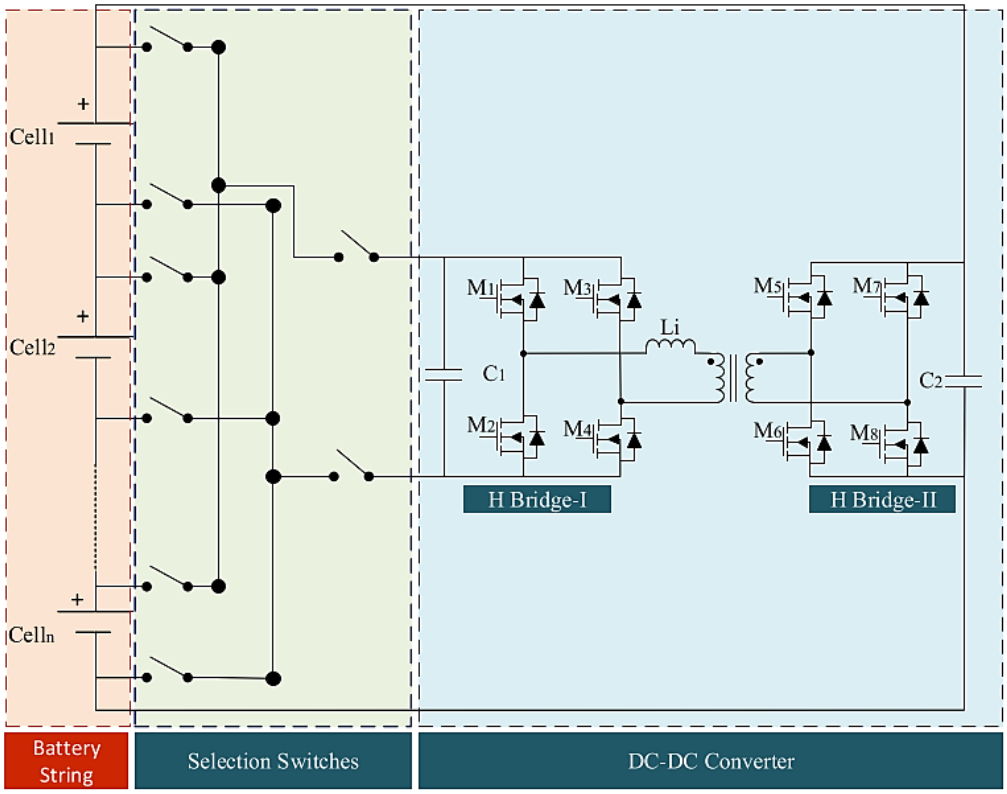

Figure 3.17 Dual active bridge converter based cell balancing [5]

Dual half-bridge converter topology

Applications requiring high voltage balancing can use the dual half-bridge converter, as shown in Figure 3.18. Additionally, this converter's operation follows the same principles as the dual active bridge converter. The output voltage is also half as high due to using a capacitive voltage divider at the input, which also results in half as many switching components as in a dual active bridge converter. Less current spikes are produced by the converter as well [5].

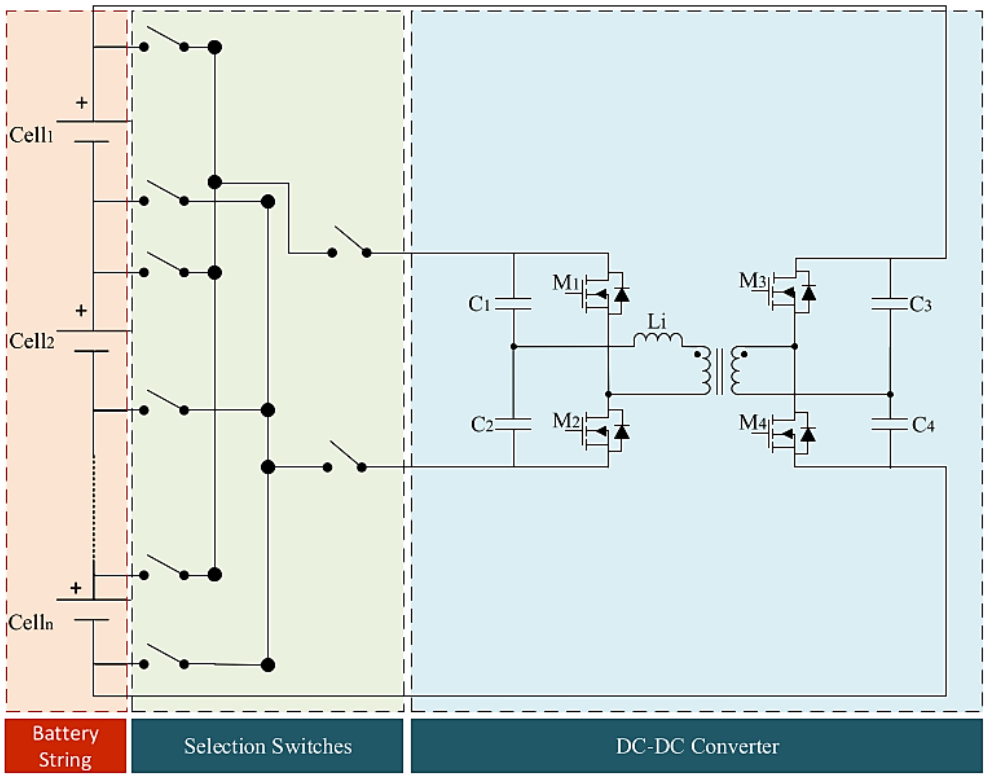

Figure 3.18 Dual half-bridge converter based cell balancing [5]

Push-pull converter topology

The push-pull converter shown in Figure 3.19 is another type of DC-DC converter with transformer isolation. A transformer, two diodes, and two switches comprise the one-way topology.

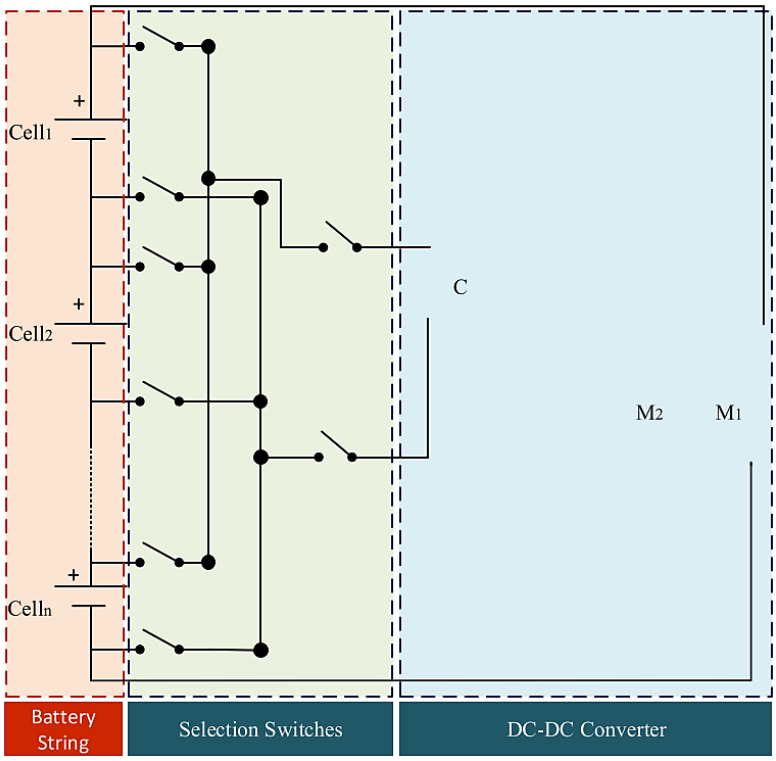

Figure 3.19 Push-pull converter based cell balancing [5]

The switches alter the polarity of the voltage that will be applied to the transformer's primary winding in accordance with the trigger signal. Secondary diodes rectify this voltage waveform before sending it to the output. [5].

Forward converter topology

A DC-DC converter that changes the output voltage is called as a forward converter. When the switch is opened, the transformer's third winding establishes a conduit for the magnetizing current, but when the switch is closed, the first and second windings of the transformer move energy from source to destination. This converter is capable of performing unidirectional and bidirectional balancing. In addition, since it has more circuit elements, it is more complex than other topologies, and transmission losses are higher in it [5]. Figure 3.20 shows forward converter based cell balancing topology.

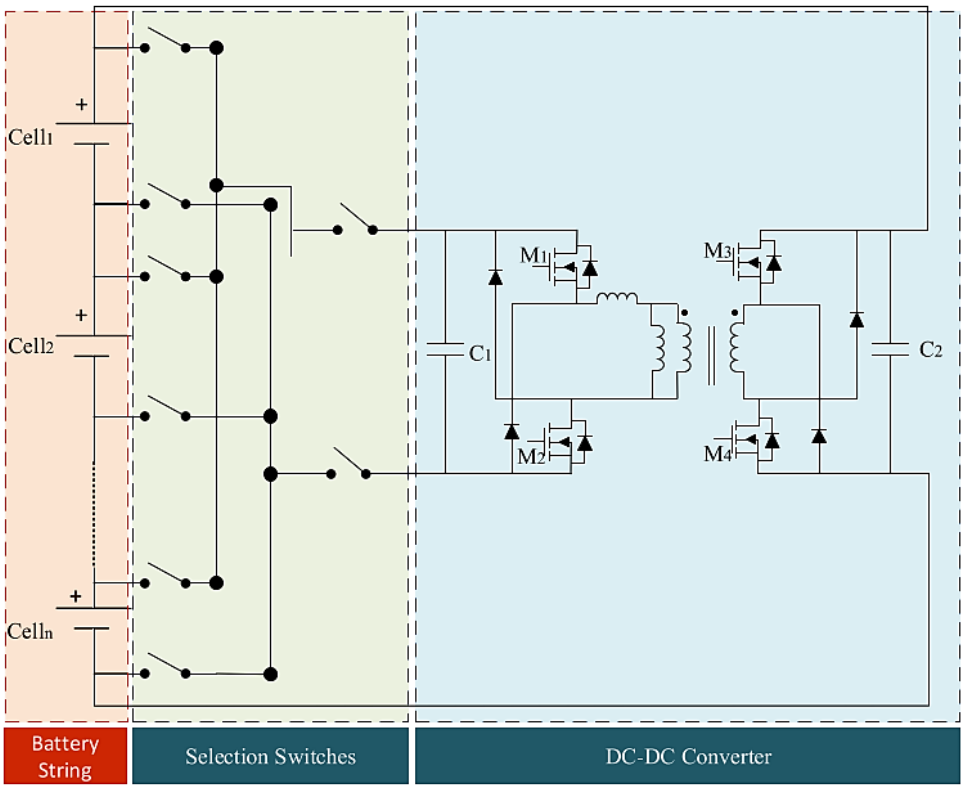

Figure 3.20 Forward converter based cell balancing [5]

CHAPTER 4

PROPOSED CONVERTER BASED TOPOLOGY AND CONTROL TECHNIQUES

4.1 Proposed Topology

In converter-based balancing systems, there are various topologies according to the type of energy transfer. Generally, these are cell-to-cell(a), string(b), and bus(c) topologies, as shown in Figure 4.1, respectively. Between neighboring cells in the cell-to-cell topology, energy is transmitted. Energy is transported from the cell to the battery pack or, conversely, from the battery pack to the cell in the string architecture. In the bus topology, power is transferred between a cell and a bus that is separate from the battery pack. Since the bus topology does not depend on the number of cells linked in series, the bus voltage is low.

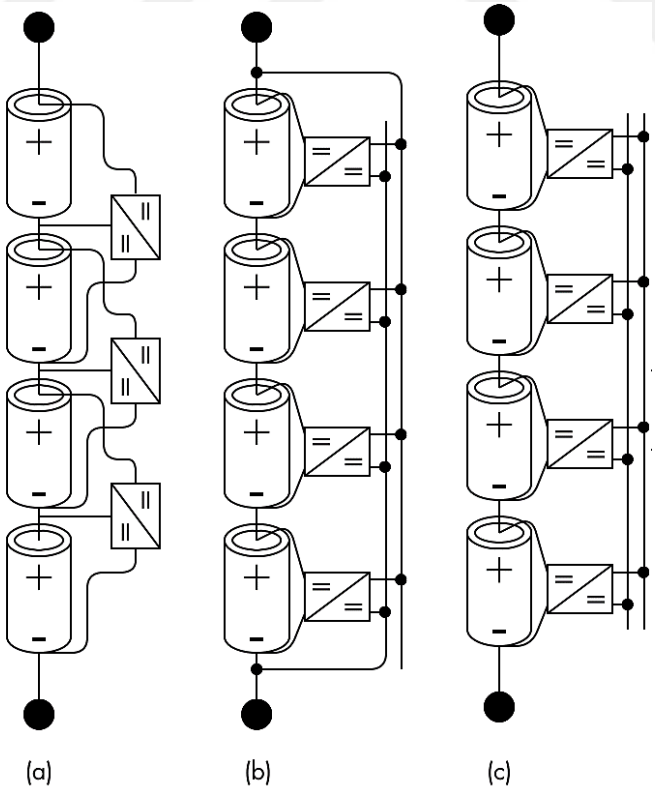

Figure 4.1 Active topologies [4]

Low bus voltage enables the use of less expensive DC-DC converters. No matter how many battery cells are wired in series, the same DC-DC converters may be utilized. In other words, battery cells can be easily added to or removed from the designed system afterward [4].

Only isolated DC-DC converters, which are bidirectional, are linked to the bus. The charger and the load do not impact the bus since they are isolated from the battery pack [4].

4.2 Cuk Converter

A cuk converter is a DC-DC converter that can increase or decrease the voltage applied to its input and has reverse polarity at its output relative to the input [38]. Figure 4.2 shows a cuk converter circuit and its operating modes. The cuk converter circuit comprises a MOSFET, a diode, a resistor, two capacitors, two inductors, and two capacitors. The resistor R in the circuit represents the load.

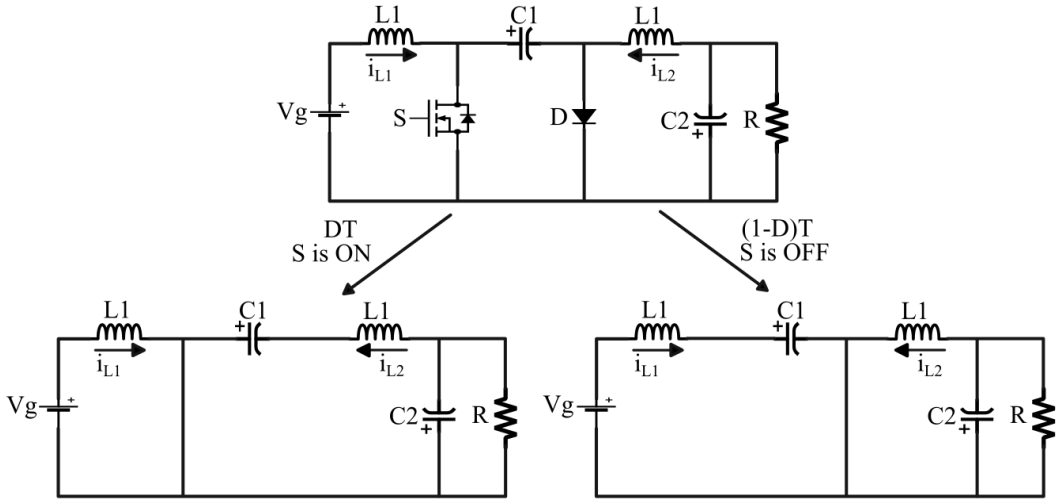

Figure 4.2 Cuk converter operating modes

The circuit is examined in two operational modes according to the on and off states of the switching element. The inductor L1 saves its energy from the source voltage when the S switch is activated. Since the D diode has reverse polarity, no current flows through it. Capacitor C1 discharges its energy through inductor L2, capacitor C2, and load R. The current in inductor L1 attempts to retain its direction by reversing its

polarity when the S switch is off. Capacitor C1 is charged using the energy that is stored in inductor L1. The diode D starts to conduct current. The load R receives the energy from the L2 inductor. The capacitor C2 also supplies power to the load. Energy is transferred from the source to the load through capacitor C1. The D diode in the circuit functions simultaneously with a controlled switch even though it is acts as an uncontrolled switch [39].

The design equations for the cuk converter are represented by Equations.**4.1**, **4.2**, **4.3**, **4.4** and **4.5**.

$$\frac{V_o}{V_g} = \frac{D}{(1-D)} \quad \textbf{(4.1)}$$

$$L_1 = \frac{DV_g}{(\Delta I_{L_1}) f_s} \quad \textbf{(4.2)}$$

$$\mathrm{L_2} = \frac{\mathrm{V_o(1-D)}}{(\Delta \mathrm{I_{L_2}}) \mathrm{f_s}} \quad \textbf{(4.3)}$$

$$\mathrm{C_1} = \frac{\mathrm{D}}{(\mathrm{Rf_s})\left(\frac{\Delta \mathrm{V_{C_1}}}{\mathrm{V_o}}\right)} \quad \textbf{(4.4)}$$

$$\mathrm{C_2} = \frac{(1-\mathrm{D})}{(8\mathrm{L_2 f_s^2})\left(\frac{\Delta \mathrm{V_{C_2}}}{\mathrm{V_o}}\right)} \quad \textbf{(4.5)}$$

The design parameters for the cuk converter circuit are displayed in Table 4.1.

Table 4.1 Cuk converter design parameters

Parameters	**Descriptions**	**Values**
V_g	Input voltage	4.2V
V_o	Output voltage	8V
I_{L1}	Input current	3
f_s	Switching frequency	25kHz
ΔI_{L1}	Current ripple	10%
ΔI_{L2}	Current ripple	10%
ΔV_{C1}	Voltage ripple	20%
ΔV_{C2}	Voltage ripple	1%

The values of the components used in the circuit are calculated using the values selected in Table 4.1 and Equations **4.1**, **4.2**, **4.3**, **4.4**, and **4.5**. As a result of the calculation, element values are selected, as shown in Table 4.2.

Table 4.2 Values of components in the cuk converter circuit

Paremeters	Descriptions	Values
L_1	Input inductor	1000µH
L_2	Output inductor	1000µH
C1	Capacitor 1	25µF
C2	Capacitor 2	250µF
R	Resistor	5Ω

4.2.1 State Space Equations of Cuk Converter

Differential equations are written according to the on and off states of the switching element in the circuit.

During S is on:

$$\frac{di_{L1}}{dt} = \frac{v_g}{L_1} \quad (4.6)$$

$$\frac{di_{L2}}{dt} = \frac{v_{C_1}}{L_2} - \frac{v_{C_2}}{L_2} \quad (4.7)$$

$$\frac{dv_{C1}}{dt} = -\frac{i_{L2}}{C_1} \quad (4.8)$$

$$\frac{dv_{C2}}{dt} = \frac{i_{L2}}{C_2} - \frac{v_{C2}}{RC_2} \quad (4.9)$$

During S is off:

$$\frac{di_{L1}}{dt} = \frac{v_g}{L_1} - \frac{v_{C1}}{L_1} \quad (4.10)$$

$$\frac{di_{L2}}{dt} = -\frac{v_{C2}}{L_2} \quad (4.11)$$

$$\frac{dv_{C1}}{dt} = \frac{i_{L1}}{C_1} \quad (4.12)$$

$$\frac{dv_{C2}}{dt} = \frac{i_{L2}}{C_2} - \frac{v_{C2}}{RC_2} \quad (4.13)$$

State and output equations for both states of the S switch are developed using differential equations.

Large signal model during S is on:

$$\dot{x} = A_1 x + B_1 u \tag{4.14}$$

$$\begin{pmatrix} \dot{i_{L_1}} \\ \dot{i_{L_2}} \\ \dot{V_{C_1}} \\ \dot{V_{C_2}} \end{pmatrix} = \begin{pmatrix} 0 & 0 & 0 & 0 \\ 0 & 0 & \frac{1}{L_2} & -\frac{1}{L_2} \\ 0 & -\frac{1}{C_1} & 0 & 0 \\ 0 & \frac{1}{C_2} & 0 & -\frac{1}{RC_2} \end{pmatrix} \begin{pmatrix} \mathrm{i_{L_1}} \\ \mathrm{i_{L_2}} \\ \mathrm{v_{C_1}} \\ \mathrm{v_{C_2}} \end{pmatrix} + \begin{pmatrix} \frac{1}{\mathrm{L_1}} \\ 0 \\ 0 \\ 0 \end{pmatrix} (v_g) \tag{4.15}$$

Large signal model during S is off:

$$\dot{x} = A_2 x + B_2 x \tag{4.16}$$

$$\begin{pmatrix} \dot{i_{L_1}} \\ \dot{i_{L_2}} \\ \dot{V_{C_1}} \\ \dot{V_{C_2}} \end{pmatrix} = \begin{pmatrix} 0 & 0 & -\frac{1}{L_1} & 0 \\ 0 & 0 & 0 & -\frac{1}{L_2} \\ \frac{1}{C_1} & 0 & 0 & 0 \\ 0 & \frac{1}{C_2} & 0 & -\frac{1}{RC_2} \end{pmatrix} \begin{pmatrix} \dot{i}_{L_1} \\ \dot{i}_{L_2} \\ V_{C_1} \\ V_{C_2} \end{pmatrix} + \begin{pmatrix} \frac{1}{L_1} \\ 0 \\ 0 \\ 0 \end{pmatrix} (v_g) \tag{4.17}$$

Output equations are written for states where S is on and off.

During S is on:

$$y = C_1 x + E_1 u \tag{4.18}$$

During S is off:

$$y = C_2 x + E_2 u \tag{4.19}$$

$$\begin{pmatrix} V_o \\ i_i \end{pmatrix} = \begin{pmatrix} 0 & 0 & 0 & 1 \\ 1 & 0 & 0 & 0 \end{pmatrix} \begin{pmatrix} i_{L_1} \\ i_{L_2} \\ v_{C_1} \\ v_{C_2} \end{pmatrix} \tag{4.20}$$

$$C_1 = C_2 = 0 \tag{4.21}$$

$$E_1 = E_2 = 0 \quad \textbf{(4.22)}$$

v_o is the output voltage of the cuk converter, and i_i is the input current from the source. The average large signal model is obtained by combining the large signal models for the on and off states of the S switch. Equation **4.23** is the state equation, and Equation **4.24** is the output equation.

$$\dot{x} = Ax + Bu \quad \textbf{(4.23)}$$

$$y = Cx + Eu \quad \textbf{(4.24)}$$

$$A = A_1 d + A_2(1-d) \quad \textbf{(4.25)}$$

$$B = B_1 d + B_2(1-d) \quad \textbf{(4.26)}$$

$$C = C_1 d + C_2(1-d) \quad \textbf{(4.27)}$$

$$E = E_1 d + E_2(1-d) \quad \textbf{(4.28)}$$

$$\begin{pmatrix} \dot{i_{L_1}} \\ \dot{i_{L_2}} \\ \dot{V_{C_1}} \\ \dot{V_{C_2}} \end{pmatrix} = \begin{pmatrix} 0 & 0 & \frac{d-1}{L_1} & 0 \\ 0 & 0 & \frac{d}{L_2} & -\frac{1}{L_2} \\ \frac{(1-d)}{C_1} & -\frac{d}{C_1} & 0 & 0 \\ 0 & \frac{1}{C_2} & 0 & -\frac{1}{RC_2} \end{pmatrix} \begin{pmatrix} \dot{i}_{L_1} \\ \dot{i}_{L_2} \\ V_{C_1} \\ V_{C_2} \end{pmatrix} + \begin{pmatrix} \frac{1}{L_1} \\ 0 \\ 0 \\ 0 \end{pmatrix} (v_g) \quad \textbf{(4.29)}$$

The load current is added as one of the inputs of the mathematical model to observe the effect of load changes [40].

By adding the load current as input, the equation is written as follows:

$$\begin{pmatrix} 0 & 0 & \frac{D-1}{L_1} & 0 \\ 0 & 0 & \frac{D}{L_2} & -\frac{1}{L_2} \\ \frac{(1-D)}{C_1} & -\frac{D}{C_1} & 0 & 0 \\ 0 & \frac{1}{C_2} & 0 & -\frac{1}{RC_2} \end{pmatrix} \begin{pmatrix} I_{L_1} \\ I_{L_2} \\ V_{C_1} \\ V_{C_2} \end{pmatrix} + \begin{pmatrix} \frac{1}{L_1} & 0 \\ 0 & 0 \\ 0 & 0 \\ 0 & -\frac{1}{C_2} \end{pmatrix} \begin{pmatrix} V_g \\ I_z \end{pmatrix} = \begin{pmatrix} 0 \\ 0 \\ 0 \\ 0 \end{pmatrix} \quad \textbf{(4.30)}$$

Obtained the average large signal model is composed of steady-state and small-signal model as shown in Figure 4.4. The large signal component is represented by the lower case (d), the steady-state component is represented by the upper case (D), and the small-signal component is represented by the lower case with a symbol ($\hat{d}$).

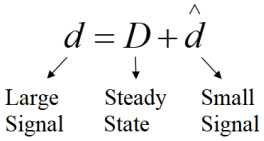

Figure 4.3 Average large signal

$$d = D + \hat{d} \quad \textbf{(4.31)}$$

$$v_{C_2} = V_{C_2} + \widehat{v_{C_2}} \quad \textbf{(4.32)}$$

$$v_{C_1} = V_{C_1} + \widehat{v_{C_1}} \quad \textbf{(4.33)}$$

$$v_g = V_g + \widehat{v_g} \quad \textbf{(4.34)}$$

$$i_z = I_z + \widehat{i_z} \quad \textbf{(4.35)}$$

$$i_{L_1} = I_{L_1} + \widehat{i_{L_1}} \quad \textbf{(4.36)}$$

$$i_{L_2} = I_{L_2} + \widehat{i_{L_2}} \quad \textbf{(4.37)}$$

Compared to the steady-state component, the changes in the small-signal component are extremely small ($\hat{d} \ll D$). By replacing each large-signal component in Equations **4.38** and **4.42** with a small-signal and steady-state component, we get the following equation:

$$\dot{x} = Ax + Bu \quad \textbf{(4.38)}$$

$$(\dot{X + \hat{x}}) = [A_1 d + A_2(1-d)](X + \hat{x}) + [B_1 d + B_2(1-d)](U + \hat{u}) \quad \textbf{(4.39)}$$

$$(\dot{X + \hat{x}}) = [A_1(D + \hat{d}) + A_2(1 - D - \hat{d})](X + \hat{x}) + [B_1(D + \hat{d}) + B_2(1 - D - \hat{d})](U + \hat{u}) \quad \textbf{(4.40)}$$

$$\dot{\hat{x}} = A\hat{x} + B\hat{u} + [(A_1 - A_2)X + (B_1 - B_2)U]\hat{d} \quad \textbf{(4.41)}$$

$$y = Cx + Eu \quad \textbf{(4.42)}$$

$$(Y \dot{+} \hat{y}) = [C_1 d + C_2(1-d)](X + \hat{x}) + [E_1 d + E_2(1-d)](U + \hat{u}) \quad \textbf{(4.43)}$$

$$(Y \dot{+} \hat{y}) = [C_1(D + \hat{d}) + C_2(1 - D - \hat{d})](X + \hat{x}) + [E_1(D + \hat{d}) + E_2(1 - D - \hat{d})](U + \hat{u}) \quad \textbf{(4.44)}$$

$$\hat{y} = C\hat{x} + E\hat{u} + [(C_1 - C_2)X + (E_1 - E_2)U]\hat{d} \quad \textbf{(4.45)}$$

Some assumptions are made:

$$AX + BU = 0 \quad \textbf{(4.46)}$$

$$\dot{X} = \frac{dX}{dt} = 0 \quad \textbf{(4.47)}$$

$$\frac{\hat{d}}{D} \ll 1 \quad \textbf{(4.48)}$$

$$\begin{pmatrix} 0 & 0 & \frac{D-1}{L_1} & 0 \\ 0 & 0 & \frac{D}{L_2} & -\frac{1}{L_2} \\ \frac{(1-D)}{C_1} & -\frac{D}{C_1} & 0 & 0 \\ 0 & \frac{1}{C_2} & 0 & -\frac{1}{RC_2} \end{pmatrix} \begin{pmatrix} I_{L_1} \\ I_{L_2} \\ V_{C_1} \\ V_{C_2} \end{pmatrix} + \begin{pmatrix} \frac{1}{L_1} & 0 \\ 0 & 0 \\ 0 & 0 \\ 0 & -\frac{1}{C_2} \end{pmatrix} \begin{pmatrix} V_g \\ I_z \end{pmatrix} = \begin{pmatrix} 0 \\ 0 \\ 0 \\ 0 \end{pmatrix} \quad \textbf{(4.49)}$$

Equation **4.49** is the steady-state model of a cuk converter. To obtain the small-signal model, subtract the steady-state portion from the average large-signal model and write the equation as follows:

$$\dot{\hat{x}} = A\hat{x} + B\hat{u} + [(A_1 - A_2)X + (B_1 - B_2)U]\hat{d} \quad \textbf{(4.50)}$$

$$\hat{y} = C\hat{x} + E\hat{u} + [(C_1 - C_2)X + (E_1 - E_2)U]\hat{d} \quad \textbf{(4.51)}$$

The small-signal model of the cuk converter is obtained as follows:

$$\dot{\hat{x}} = A\hat{x} + B\hat{u} \quad \textbf{(4.52)}$$

$$\begin{pmatrix} \dot{\widehat{i_{L_1}}} \\ \dot{\widehat{i_{L_2}}} \\ \dot{\widehat{v_{C_1}}} \\ \dot{\widehat{v_{C_2}}} \end{pmatrix} = \begin{pmatrix} 0 & 0 & \frac{D-1}{L_1} & 0 \\ 0 & 0 & \frac{D}{L_2} & -\frac{1}{L_2} \\ \frac{(1-D)}{C_1} & -\frac{D}{C_1} & 0 & 0 \\ 0 & \frac{1}{C_2} & 0 & -\frac{1}{RC_2} \end{pmatrix} \begin{pmatrix} \widehat{i_{L_1}} \\ \widehat{i_{L_2}} \\ \widehat{v_{C_1}} \\ \widehat{v_{C_2}} \end{pmatrix} + \begin{pmatrix} \frac{1}{L_1} & 0 & \frac{V_{C_1}}{L_1} \\ 0 & 0 & \frac{V_{C_1}}{L_2} \\ 0 & 0 & \frac{-I_{L_2}-I_{L_1}}{C_1} \\ 0 & -\frac{1}{C_2} & 0 \end{pmatrix} \begin{pmatrix} \widehat{v_g} \\ \widehat{i_z} \\ \hat{d} \end{pmatrix} \quad \textbf{(4.53)}$$

$$\hat{y} = C\hat{x} + E\hat{u} \quad \textbf{(4.54)}$$

$$\begin{pmatrix} \widehat{v_o} \\ \widehat{i_i} \end{pmatrix} = \begin{pmatrix} 0 & 0 & 0 & 1 \\ 1 & 0 & 0 & 0 \end{pmatrix} \begin{pmatrix} \widehat{i_{L_1}} \\ \widehat{i_{L_2}} \\ \widehat{v_{C_1}} \\ \widehat{v_{C_2}} \end{pmatrix} + \begin{pmatrix} 0 & 0 \end{pmatrix} \quad \textbf{(4.55)}$$

Since the input does not effect on the output, $D = 0$. The small signal model of the cuk converter is used for the controller design. There are three input signs: duty cycle $\hat{d}$, input voltage $\widehat{v_g}$, and load current $\widehat{i_z}$ [40,41]. Various transfer functions are obtained with the small-signal model of the cuk converter.

4.3 Modified Isolated Bidirectional Cuk Converter

The modified isolated bidirectional cuk converter circuit is shown in Figure 4.5. The cuk converter circuit is changed to have a symmetrical construction to achieve the bidirectional power transfer between the battery cells and the energy bus. When we replace the diode in the cuk converter with a MOSFET, the circuit simply becomes symmetrical. Two MOSFETs with body diodes in the circuit determine the direction of energy transfer. Four inductors are used instead of two to reduce di/dt when switches of balancing circuits connected to different battery cells are switched simultaneously. The isolation between the battery string and the energy bus is provided by the C1a and C1b capacitors in the middle [13].

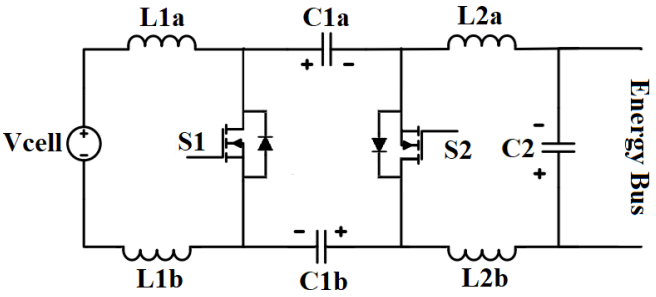

Figure 4.4 The modified isolated bidirectional cuk converter

In the circuit, the equivalent of C1a and C1b is *C1*, the equivalent of L1a and L1b is L1, and the equivalent of L2a and L2b is L2. L1, L2, and C1 are calculated as shown in Equations **4.56**, **4.57** and **4.58** [11].

$$L1 = L1a + L1b \tag{4.56}$$

$$L2 = L2a + L2b \tag{4.57}$$

$$C1 = (C1a * C2b)/(C1a + C2b) \tag{4.58}$$

The modified isolated cuk converter operates in two different transfer modes, battery to bus side and bus to battery side. Each transfer mode has two intervals, depending on whether the switches are closed or open.

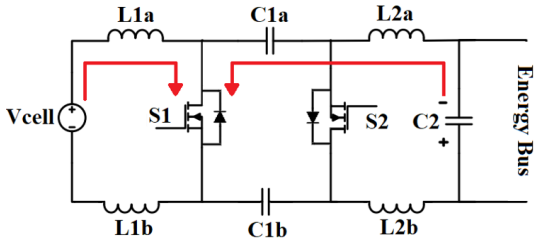

Figure 4.5 Mode-1 interval-1

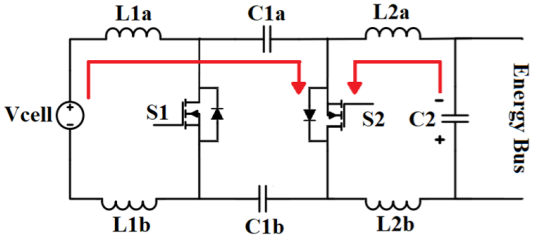

Figure 4.6 Mode-1 interval-2

If energy is transferred from the cell to the bus, S1 MOSFET is controlled by duty, while S2 mosfet works as a diode. In Figure 4.5 S1 is on, S2 is off and in Figure 4.6 S1 is off, S2 works as a diode.

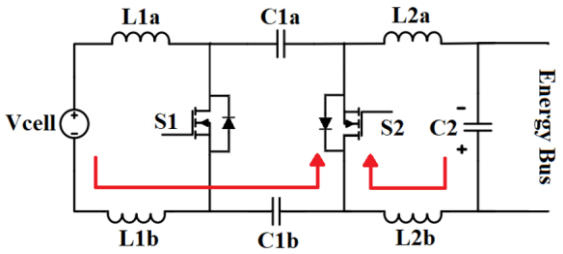

Figure 4.7 Mode-2 interval-1

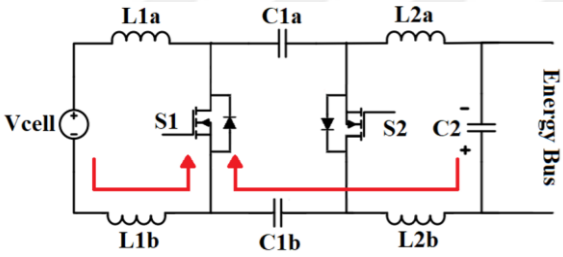

Figure 4.8 Mode-2 interval-2

If energy is transferred from the bus to the cell, S2 MOSFET is controlled by duty, while S1 MOSFET works as a diode [11]. In Figure 4.7 S2 is on, S1 is off, and in Figure 4.8 S2 is off, S1 works as a diode.

Table 4.2 in the preceding section displayed the parameter values utilized in the cuk converter. If we calculate the values of the circuit elements using Equations **4.56**, **4.57** and **4.58**, the circuit takes the form in Figure 4.9.

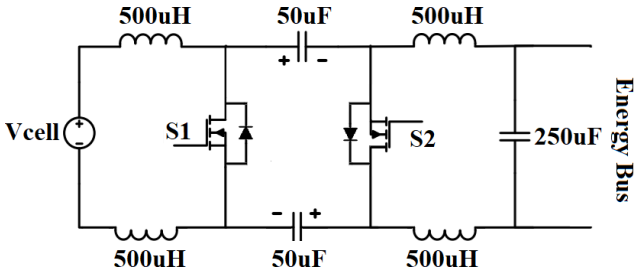

Figure 4.9 The modified cuk converter with component values

4.4 Equalization Circuit and Balancing Algorithm

Figure 4.10 illustrates the energy bus-based topology. In this topology, which has a modular and expandable structure, there are modules for bidirectional energy transfer between each battery cell and the bus. Each module is connected to a battery cell and is independent of each other as it is controlled individually. Excess energy is transferred to the cells with low energy via the bus. The controller determines which cells will receive and send energy by taking the SOC value of each battery cell. If the number of battery cells connected in series changes, the system must not to be completely redesigned. Because of these advantages, a bus-based topology is investigated in this study. The system has five battery cells, each with a different SOC value. Each cell in the series of battery strings is balanced around a calculated reference value. The average SOC value is taken as a reference in this system. The average SOC value is obtained by taking the SOC value of each battery cell. The excess energy of the battery cells whose SOC value is above the reference is transferred to the bus through the converter. Through the converter, the energy in the bus is transferred to the battery cells, whose SOC value is below the reference.

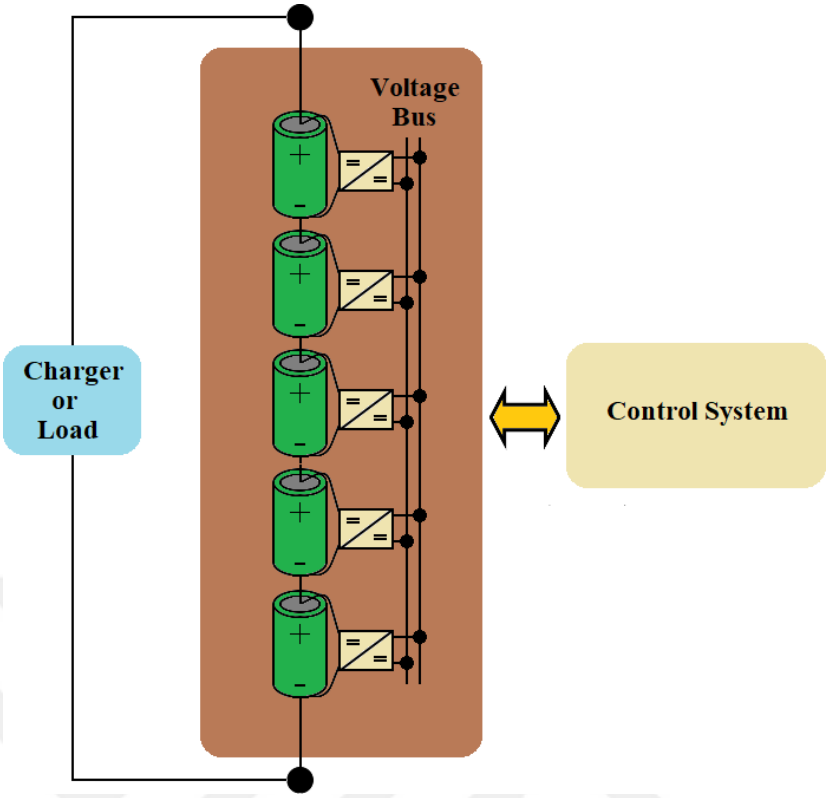

Figure 4.10 Proposed bus topology

The energy transferred from the cells with the SOC value above the reference to the bus must be the same as the energy from the bus to the cells whose SOC value is below the reference; otherwise, the bus voltage cannot be stabilized [4]. As a result, the equality of input and output power is the foundation of the balancing algorithm. Also, each battery cell has a nominal capacity of 2.6Ah and a nominal voltage of 3.7V. Therefore, the charge-discharge currents of the cells are restricted to a maximum of 3A.

Figure 4.11 shows the connection of the modified isolated bidirectional cuk converters in the balancing circuit designed in the Matlab/Simulink environment.

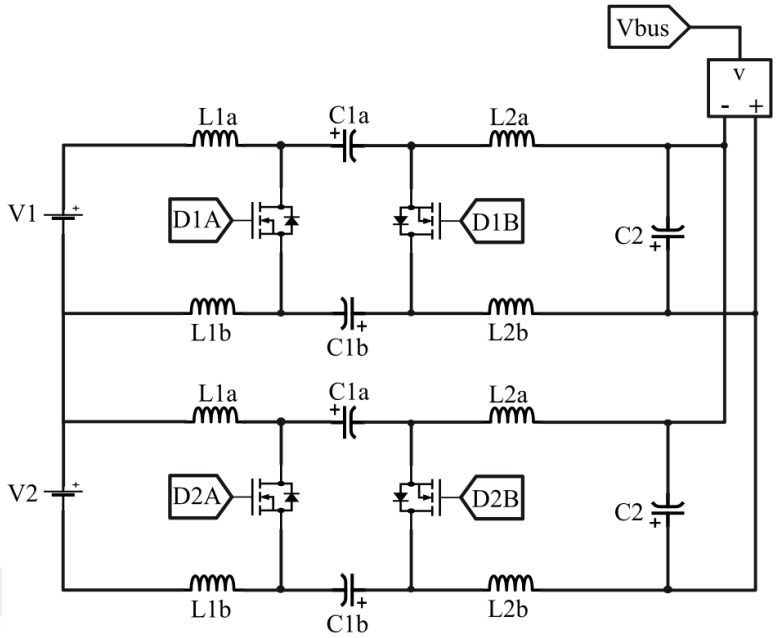

Figure 4.11 The modified cuk converters Matlab/Simulink block diagram

The cell voltage and SOC values are taken and assigned to the variables V1 and SOC1. Likewise, input inductor and output inductor current are taken and assigned to variables such as iL11 and iL12. The control signal of the MOSFETs is controlled by the D1A and D1B variables.

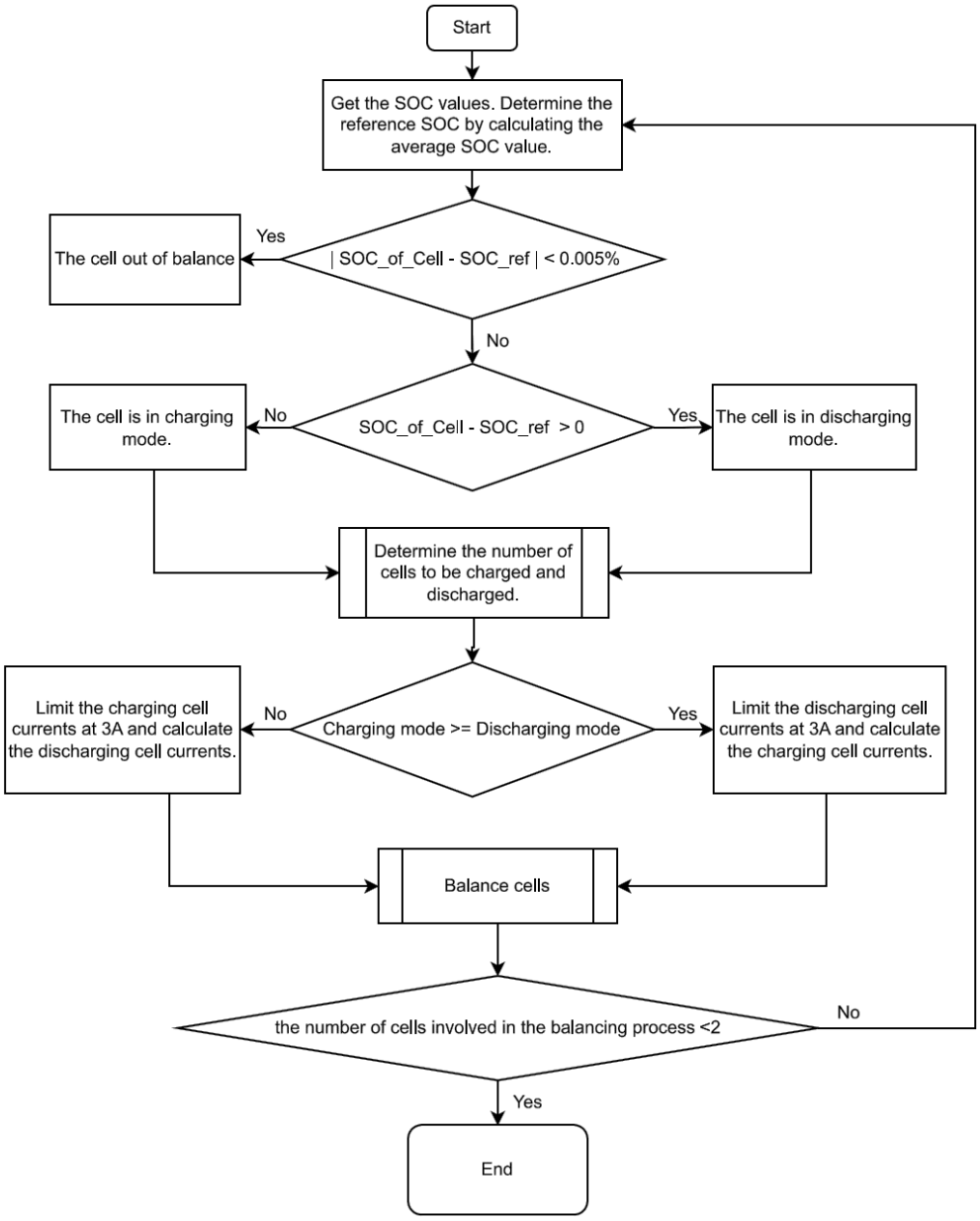

Figure 4.12 The flow chart of proposed active cell balancing control algorithm

Figure 4.12 depicts the flow chart for the proposed active cell balancing system control algorithm. In the balancing algorithm, the SOC values of all battery cells are taken first, and the average SOC value is then calculated. This calculated value is the reference SOC value. This reference is subtracted from each battery cell and takes its absolute value. If the result is less than 0.005%, the relevant battery cell is excluded from the balancing process. Cells with a SOC value greater than the reference value operate in the discharge mode, while cells with a SOC value below the reference value

operate in the charge mode. After determining the number of cells to be charged and discharged, a comparison should be made. If the number of cells to be charged is greater than or equal to the number of cells to be discharged, the currents of the cells to be discharged are limited to 3A and the currents of the cells to be charged are calculated. Similarly, if the number of cells to be discharged exceeds the number of cells to be charged, the charging cell currents are limited to 3A and the discharged cell currents are computed.

4.5 Commonly Used Control Methods in DC-DC Converters

DC-DC converters are used to convert one DC voltage to another DC voltage. While performing this conversion process, the current or voltage must be regulated according to the designed system. Various control techniques are used to regulate voltage or current.

4.5.1 Voltage Mode Control of DC-DC Converter

This single-loop controller measures the output voltage and deducts it from the reference value. It is powered by an error amplifier [42].

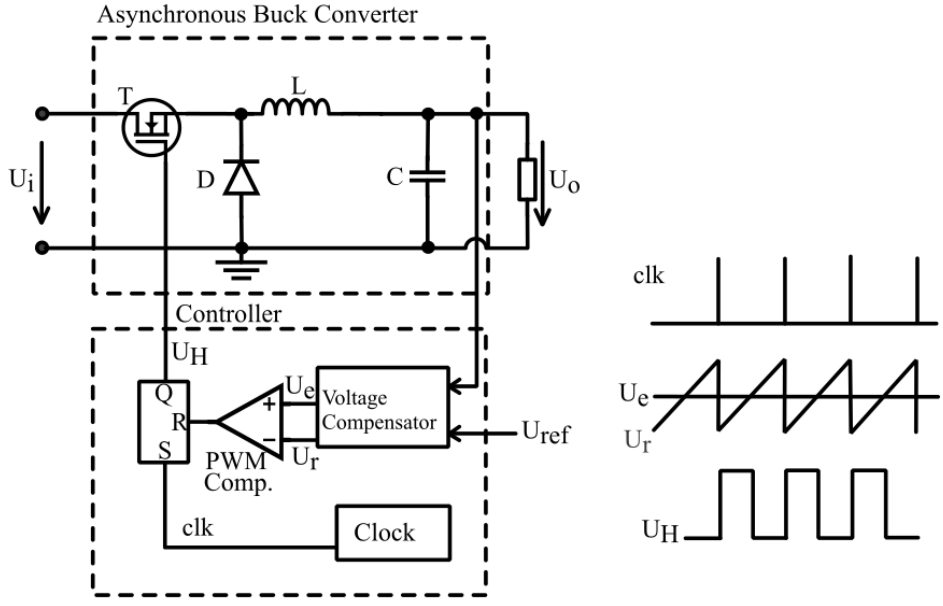

Figure 4.13 Voltage mode control of asynchronous buck converter [43]

The control strategy of the converter includes a voltage feedback loop. The voltage compensator minimizes the controller error, which is the difference between the reference voltage Uref and the output voltage Uo. The output of the voltage compensator is used to reset the output of the RS flip-flop by comparison with the triangular waveform. The switching signal is obtained at the RS flip-flop output [43]. Figure 4.13 shows the voltage mode control structure. Voltage mode control has a straightforward hardware implementation and is flexible. It also provides regulation against fluctuations in load. However, the system is sluggish because the reaction time takes much longer than the switching cycles [44].

4.5.2 Current Mode Control of DC-DC Converter

As can be seen in Figure 4.14, the control structure is similar to voltage mode control. Its main difference from voltage mode control is that the oscillator is only used to generate a fixed-frequency clock signal. The current mode control method includes both current and voltage feedback. The voltage loop error is determined by taking the difference between the voltage measured at the output and the reference voltage. This error is contrasted with the inductor current. The duty cycle of the switching controller is determined by these phases [43].

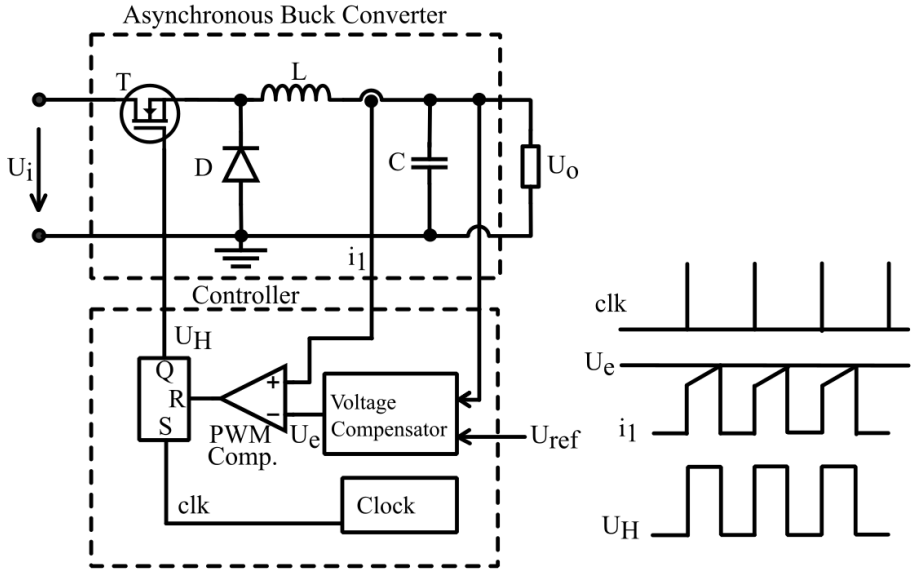

Figure 4.14 Current mode control of asynchronous buck converter [43]

Current mode control is designed to reduce the disadvantages of the voltage mode control method. Its advantages are its performance against overload and improved transient response [42].

4.5.3 Hysteretic Control

The idea behind hysteretic control is to maintain the output voltage within a specified hysteresis band surrounding the reference voltage Vref. This control approach has a rather quick reaction to the converter's input and output voltages. The duty cycle can be altered throughout the entire range of 0 to 1. The dynamic control capabilities allow output filters to be made smaller, which lowers the overall cost of the DC-DC converters [43]. Figure 4.15 shows the hysteretic control structure.

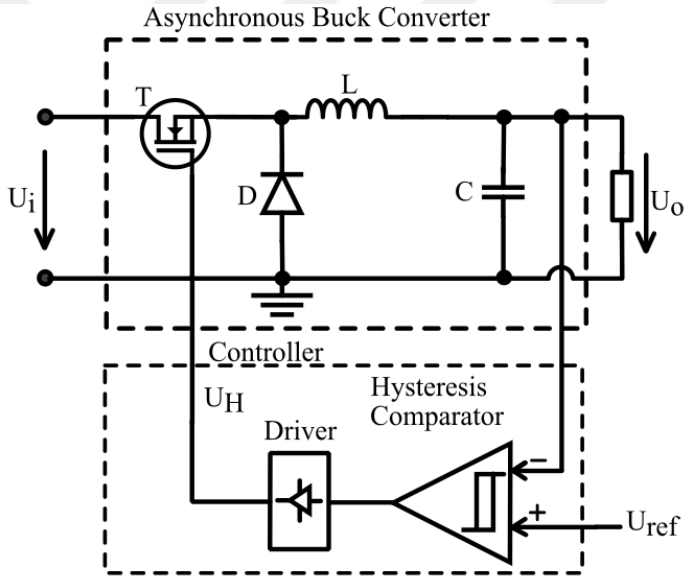

Figure 4.15 Hysteretic control of asynchronous buck converter [43]

The magnitude of the hysteresis range and overshoot, brought on by signal delays and the converter's design, determine how much the output voltage will ripple. For example, the entire output voltage ripple (from Umin to Umax) and the hysteresis range (from UL to UH) are displayed in Figure 4.16 [43].

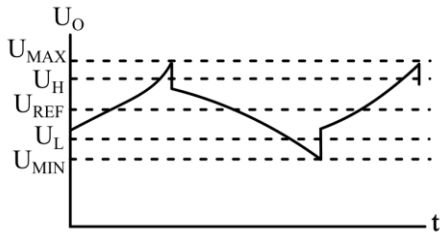

Figure 4.16 Voltage ripple of hysteretic control

4.5.4 Sliding Mode Control

Sliding-mode control is a nonlinear control technique used to manage systems with changeable structures. It operates on the idea of directing the controlled state variable to the desired equilibrium by employing a specific sliding surface as a reference path. In a sliding mode control design, the state variables of the DC-DC converter or variables derived from the state variables, for instance, control error or its derivative, are frequently chosen as variables [43].

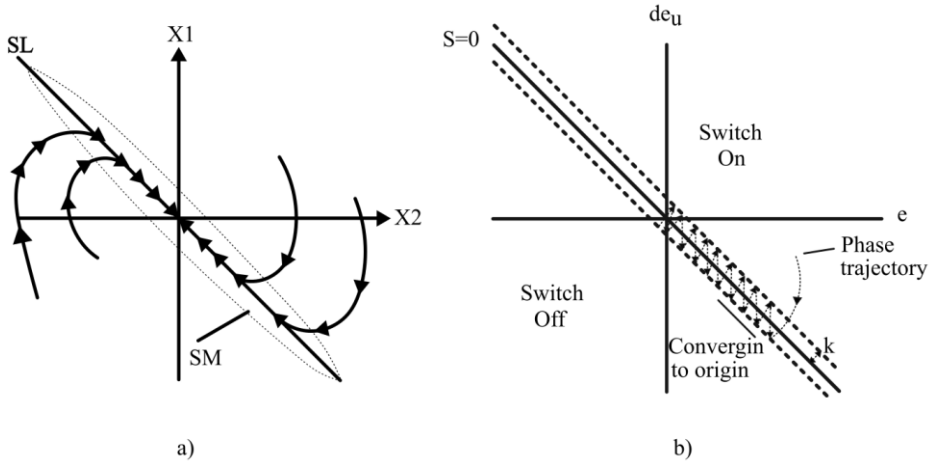

Figure 4.17 Working principle of sliding mode control

Figure 4.17 (a) illustrates the sliding mode control's basic idea. State variables are represented by X1 and X2 [43]. The phase plane is divided into two major sections by the sliding line. Each zone is represented by a switching state. When the orbital system achieves its equilibrium point, it is said to be stable [44].

An infinite switching frequency is necessary to accomplish the ideal floating mode control, which is practically unfeasible. Typically, a hysteresis region is formed around the shift line, which directly limits the switching frequency to the size of the hysteresis region. Figure 4.17 (b) shows how the slip surface is defined at the regulation error e and its derivative deu [43].

One of the critical disadvantages of sliding mode control is the variable switching frequency during load fluctuations, which is unsatisfactory in some applications. To overcome this, fixed-frequency sliding mode control strategies using PWM have been suggested [43]. Practical sliding mode controllers can only work in a quasi-sliding mode at limited switching frequency. Over significant line and load changes, sliding mode controllers demonstrate good stability. In addition to being straightforward to execute, it has high robustness and a fast dynamic response. However, switching frequency variation affects sliding-mode converters. For power electronics applications, these controllers are not accessible in integrated circuit form. The Creating sliding-mode controllers do not follow a standardized process [44].

4.5.5 PID Control

PID control is a commonly applied type of control in DC-DC converters because of its simple implementation, easily comprehensible operating principle, and control efficiency [43]. Reliable for linear systems. In the case of non-linear systems, it is not consistently dependable and satisfactory [44].

The compensator in feedback control systems that is most frequently utilized [42]. The PID controller is defined as:

$$u(t) = K_P e(t) + K_I \int e(t)dt + K_D \frac{de(t)}{d(t)} \quad \textbf{(4.59)}$$

Where e(t) is the compensator input and u(t) is the compensator output. The Laplace transform of the above equation yields the transfer function:

$$G_C(s) = \frac{U(s)}{E(s)} = K_P + \frac{K_I}{s} + K_D(s) \quad \textbf{(4.60)}$$

Phase-lag is the integral term, and phase-lead is the derivative term. The integral term increases the low-frequency gain, and the low-frequency output voltage components are precisely adjusted. The derivative term enhances the system's stability and transient response time at high frequency by increasing the phase margin and cross-over frequency. A faster system response time will result from an increase in the proportional term, while an unstable system will result from an excess of the proportional gain. The derivative term in a PID controller is sensitive to system noise and measurement error, which can cause duty cycle oscillation during a steady-state. Therefore, PI controller is often used in practical applications [42].

The PI controller is a closed-loop control method widely used in control systems in industrial areas. There are two parts to it: proportional gain and integral gain. Proportional gain improves system stability and transient response. The integral gain reduces the steady-state error of the system [45]. By comparing the value at the system's output with the reference value at the input, the PI controller detects the error that may occur, corrects it, and sends it to the system. Because of its simple implementation, the PI controller is one of the most popular controllers used to control DC-DC converters. The integral of the error signal and the error signal itself are proportional to the control signal. The mathematical formula of the PI controller is shown in Equation **4.61**.

$$y(t) = K_P e(t) + K_I \int e(t)dt \qquad (\mathbf{4.61})$$

Figure 4.18 depicts a PI controller schematic. The error $e(t)$ is the difference between the setpoint $r(t)$ and the output $y(t)$. K_p represents proportional gain, and K_i represents integral gain. Reducing the error signal is the main purpose of the control function.

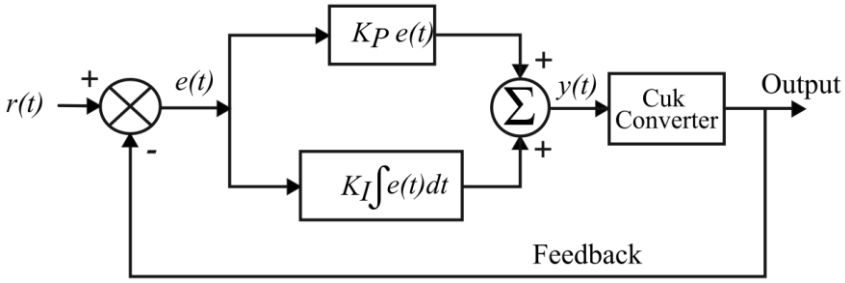

Figure 4.18 Block diagram of PI controller with cuk converter

4.5.6 Fuzzy Logic Control

4.5.6.1 Fuzzy Logic

Classical logic is a two-valued logic system, and according to classical logic, the result of something is either true or false. In other words, the result can be 1 or 0 in classical logic. However, according to fuzzy logic, the result of something can be a value between 1 and 0 [46].

People make definitions in daily life with too many fuzzy expressions without realising it. Since the structure of the human brain is similar to the fuzzy logic system. Fuzzy logic involves mathematically expressing the weights of linguistically fuzzy expressions and drawing inferences. Classical logic uses certain expressions such as true or false, hot or cold. That is, it makes no distinction as to how true or false a statement is or how hot or cold a body of water is [47]. Fuzzy logic deals with how true or false the statement is, or how hot or cold the water is. So fuzzy logic deals with intermediate values.

In his essay from 1965, Zadeh introduced the idea of fuzzy logic for the first time. In his study, Zadeh suggested that the membership degree of the set to which an element belongs should be defined by fuzzy sets that form the basis of fuzzy logic rather than the exact sets that form the basis of classical logic [47].

The general features of fuzzy logic are expressed by Zadeh as follows:

- In fuzzy logic, reasoning based on approximations is employed rather than thinking in terms of precise values.

- In fuzzy logic, everything is represented with a certain degree in the range of 0 and 1.
- Fuzzy inference is made with rules defined between linguistic expressions.
- Every logical system can be expressed as fuzzy.
- A fuzzy logic mathematical model is very suitable for systems that are difficult to obtain.
- Fuzzy logic can act according to unknown or incomplete information.

4.5.6.2 Fuzzy Set

An element either belongs to or does not belong to a set in definite sets, which serve as the foundation of classical logic. According to the defined set space, the membership degree value that the element can take can be 0 or 1. Fuzzy sets, which form the basis of fuzzy logic, consist of membership functions. That is, the membership degree value of an element can be between 0 and 1, according to the membership functions defined for the relevant fuzzy set. If an element is not included in a membership function, the membership degree value is 0, but if it is fully included, the membership degree value is 1. If it is uncertain whether an element is included in the membership function, the degree of membership takes a value between 0 and 1 according to the degree of uncertainty [46].

In classical sets, an element is either a member of the set or not. In fuzzy sets, the element may partially belong to a set [48]. Classical sets can be expressed as shown in Equation **4.62**.

$$\mu A(x) = \begin{cases} 1, & if\ x \in A \\ 0, & if\ x \notin A \end{cases} \quad (\mathbf{4.62})$$

In Equation **4.59**, *A* represents the cluster, *x* represents the cluster element of the space set, and *μA(x)* represents the membership degree value. Here *x* values take {0,1} values.

In classical sets, the boundaries are strictly defined. For example, according to the classic set example as shown in Figure 4.19, any temperature below 20°C is considered cold. As a result, 19°C takes the value 1 as cold, and 21°C takes the value 1 as hot.

However, in real life, the boundaries may not be expressed as precisely as they are.

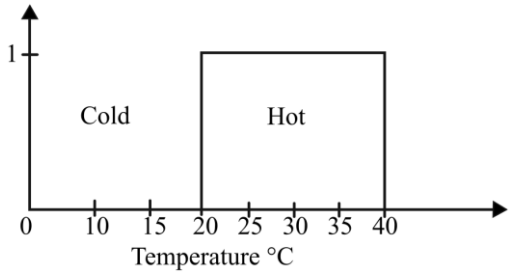

Figure 4.19 Classic set

For example, a temperature of 19°C can be a member of both the hot and cold clusters to a certain extent. For this reason, fuzzy sets are used to overcome these limitations in classical sets. In fuzzy sets, an element can be a partial member of that set. In classical sets, the membership of an element can only take 0 or 1 values depending on whether it belongs or not, while in fuzzy sets it can take values in the range of [0,1]. As this value increases, the degree to which the relevant element belongs to the cluster also increases. The element's degree of membership in the pertinent cluster is represented by this value, which is known as the membership degree. The fuzzy set *A* in the universal set *U* is expressed as *μA(x)*.

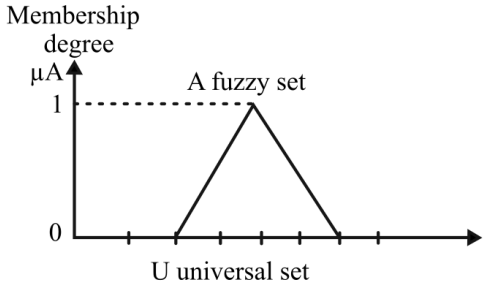

Figure 4.20 Fuzzy set

The fuzzy set *A* in the universal set *U* as shown in Figure 4.20 is defined by the membership function in Equation **4.63**.

$$\mu A: U \longrightarrow [0,1] \qquad (\mathbf{4.63})$$

Membership degrees of *x* elements in the fuzzy set *A* in the universal set *U* represent a set of ordered pairs in the form of *μA(x)*. This set is expressed in Equation **4.64**.

$$A = \{(x, \mu A(x) \mid x \in A)\} \quad \textbf{(4.64)}$$

4.5.6.3 Membership Functions

Any element *x* in the universal set *U* is expressed with the *μA(x)* function in the fuzzy set *A*. It takes the value *μA(x)=0* if any *x* element is definitely not a member of the fuzzy set *A*. However, if the element *x* is definitely a member of the fuzzy set *A*, it takes the value *μA(x)=1*. In other uncertain cases, the element *x* is a member of the fuzzy set *A* to a certain degree. In this case, the degree of membership can take any value between $0 < \mu A(x) < 1$. Membership functions are used to calculate this value.

The curve that changes with the values of the set members is called the membership function. The x-axis shows the members, while the y-axis shows the membership degrees. Values on the x-axis can range from 0 to 1. There are several ways to choose membership functions. The triangular, trapezoidal, and Gaussian membership functions are frequently used membership functions, as illustrated in Figure 4.21.

The shortest and most concise way to define membership functions is to formulate the membership function mathematically. Which membership function should be used to solve the problem is usually decided by considering the user experience and the type of problem.

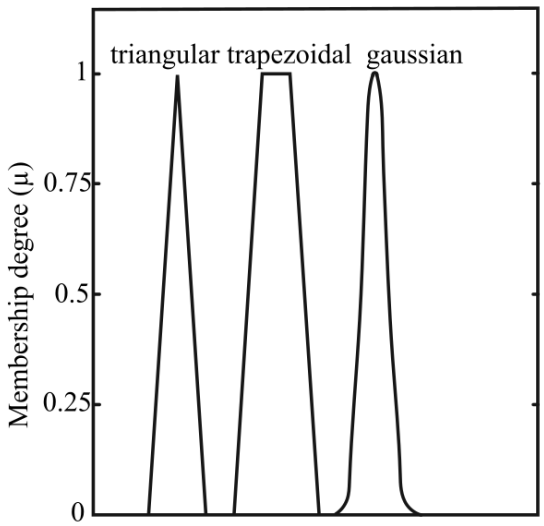

Figure 4.21 The most commonly used membership function types

4.5.6.4 Fuzzy Logic Structure

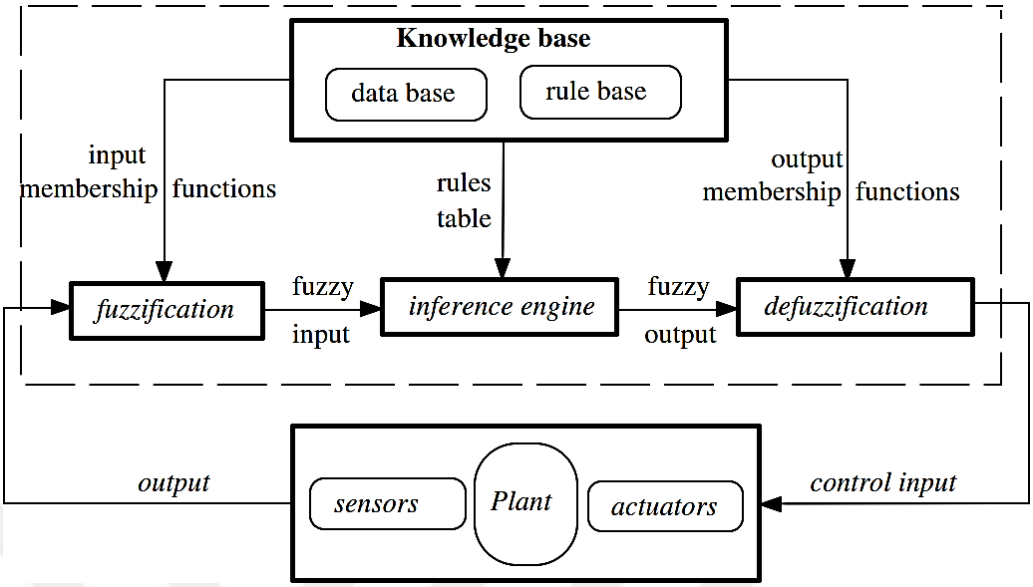

Figure 4.22 Block diagram of a fuzzy control system [49]

Fuzzy logic controllers consist of fuzzification, knowledge base, fuzzy inference engine, and defuzzification units. Figure 4.22 depicts the construction of fuzzy logic controllers.

Fuzzification

For the data entering the system to comply with the fuzzy logic structure, it is called fuzzification when it is expressed with linguistic variables and made suitable for the fuzzy logic structure. It measures the value of the input variables and maps the input information to the appropriate fuzzy sets with the membership function, that is, converting a real value to a linguistic variable value [46].

It is not important that the information entered to be exact; it can also be approximate. The variables obtained after the fuzzification process are linguistic, and all the values of the input variables are transferred here as membership degrees [47].

In the fuzzying process, more than one membership function is used. The membership degrees of membership functions range from 0 to 1. Membership functions are used to determine the sensitivity of the system. Defining and delimiting membership functions

is very important, for fuzzification of input variables and precision. The smooth and stable operation of the system is possible because of the accuracy of the membership functions.

Knowledge Base

The rule base determines the control objectives and control strategy. The rule base is the part where the rules of the fuzzy system are located. The rules in the rule base are the most important part of the fuzzy system. The rule base is used in the operations performed in the inference system. While creating these rules, the experience and knowledge of the experts are used. If the expert does not know the system well, the correct rules cannot be created, and the system will not work correctly. The rule base created with the help of an expert is subjective, as it is created by utilizing the experience and knowledge of the expert. The rule base symbolizes the relationship between the inputs to the system and the output obtained [46].

The if-then pattern often defines expert knowledge and consists of cause and effect. These generated if-then patterns are called fuzzy conditional statements and are easily manipulated in fuzzy logic. These rules form the basis of the fuzzy system. Causes and consequences in fuzzy control rules can be more than one. Therefore, fuzzy control rules are better formulated in linguistic rather than numerical terms [46].

The rule "IF *x*=A and *y*= B, THEN *z*=C" can be defined. Here, while *x*, *y*, and *z* express linguistically defined variables, A, B, and C express the fuzzy sets of these variables. While creating the rules, *and* - *or* expressions are used. For the output, the *and* operator is used when all of the input variables need to be supplied simultaneously, and the *or* operator is used when providing any of the input variables is sufficient. In this case, *or* and *and* operators are used in fuzzy logic controllers. When the *or* operator is used, the largest of the numbers, $max\{\mu A(x), \mu B(x)\}$ is preferred. When the *and* operator is used, the smallest number, $min\{\mu A(x), \mu B(x)\}$ is preferred.

Fuzzy Inference Engine

In the inference unit, fuzzy values are processed and inferences are made similarly, considering human beings' ability to make decisions and make inferences. Fuzzy results

are created by applying the fuzzy expressions from the fuzzifier to the rules in the rule base. Firstly, it is determined to what extent the value entered into the system belongs to the membership set and function. The rules in the rule base and the output values are determined using the obtained values.

The most often employed fuzzy inference system is the Mamdani system. The Mamdani method was first used by Professor Mamdani in 1975 to control the steam engine. In the Mamdani fuzzy inference system, a rule base should be created by the expert with linguistic knowledge, and input variables should be defined with membership functions. Then, the defuzzification process is performed with the specified operators. The final fuzzy output sets need to be clarified [47].

In the Mamdani-type fuzzy inference mechanism, membership degrees are first calculated for each input variable. According to the calculated membership degrees, some rules in the fuzzy logic controller become active. Then, with the help of fuzzy logic operators in activated rules, the value indicating the degree of belonging in the relevant cluster is calculated for each rule. Afterward, trimming is performed according to the membership functions determined at the output. Finally, the membership functions of all the previously clipped rule results are summed into a single fuzzy set. Figure 4.23 shows the Mandani fuzzy inference system.

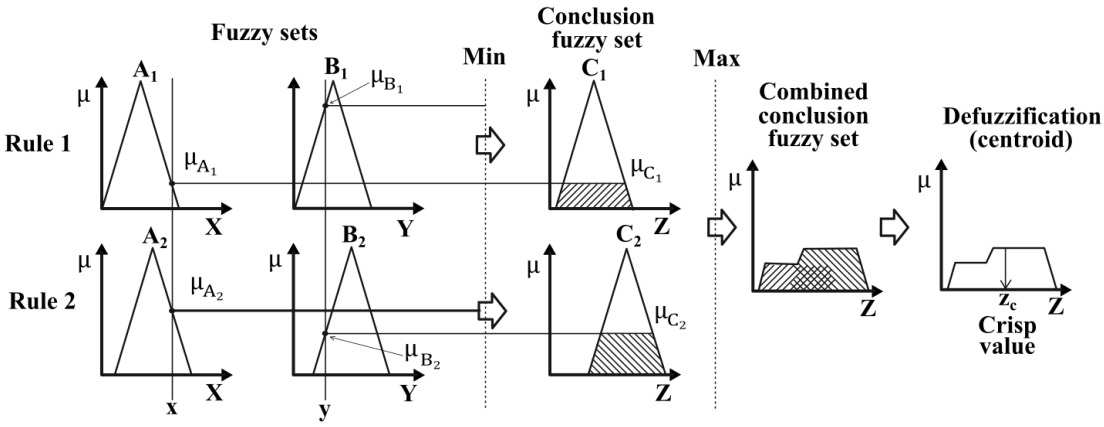

Figure 4.23 Mamdani fuzzy inference system [50]

If ‘x’ is ‘A_1’ and ‘y’ is ‘B_1’ then ‘Z’ is ‘C_1’.

If ‘x’ is ‘A_2’ and ‘y’ is ‘B_2’ then ‘Z’ is ‘C_2’.

Defuzzification

The values obtained from the fuzzy inference engine are fuzzy values, which do not mean anything for the system to be controlled. In order to use the fuzzy output in practical applications in real life, defuzzification is needed. Defuzzification is the procedure used to transform the fuzzily calculated results of the fuzzy inference engine into exact numerical values. The three most commonly used defuzzification methods are centroid, weighted average, mean max membership, and max membership methods [51].

The centroid method is the most popular defuzzification technique and is the most used method in practical applications. With this method, the physical center of gravity of the area of the fuzzy output obtained as a result of the fuzzy inference engine is calculated. The mathematical expression of this method is given in Equation **4.65**.

$$z^* = \frac{\int \mu(z) z dz}{\int \mu(z) dz} \quad (\mathbf{4.65})$$

$\int$ denotes an algebraic integration. The centroid method is shown in Figure 4.24.

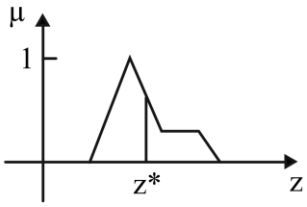

Figure 4.24 Centroid defuzzification method [52]

The weight average method is a defuzzification method and is frequently used in applications where fuzzy logic controllers are used because it is more efficient with its ability to reach the result with less calculation. The mathematical expression of this method is given in Equation **4.66**.

$$z^* = \frac{\sum \mu(\bar{z}) \bar{z}}{\sum \mu(\bar{z})} \quad (\mathbf{4.66})$$

$\bar{z}$ is the centroid of each symmetric membership function, and $\sum$ is the algebraic sum. The weighted average approach is created by dividing each membership function's

output by its corresponding maximum membership value. Figure 4.25 shows the weighted average defuzzification method.

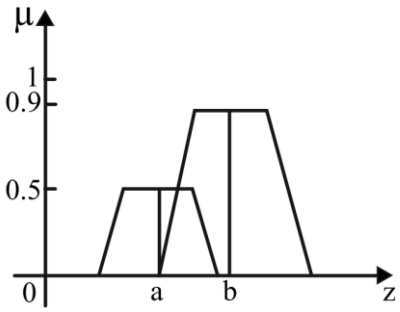

Figure 4.25 Weighted Average defuzzification method [52]

In the fuzzy output obtained from of the fuzzy inference engine, the defuzzification process involves calculating the average of the values belonging to the highest membership degree. The same results can be obtained for outputs with different shapes since this method does not focus on the entire shape obtained at the output but only on the part with the values with the maximum membership [51]. z^* represents the defuzzified value. The max membership defuzzification method is graphically illustrated in Figure 4.26.

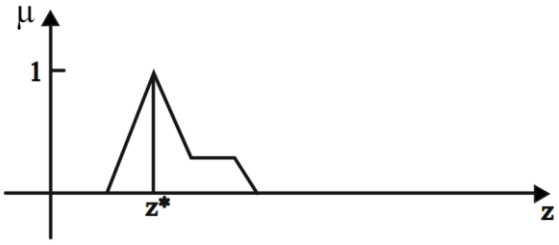

Figure 4.26 Max membership defuzzification method [52]

The center of the maxima is another name for the mean max membership. This method is expressed in Equation **4.67**.

$$z^* = \frac{a+b}{2} \quad \textbf{(4.67)}$$

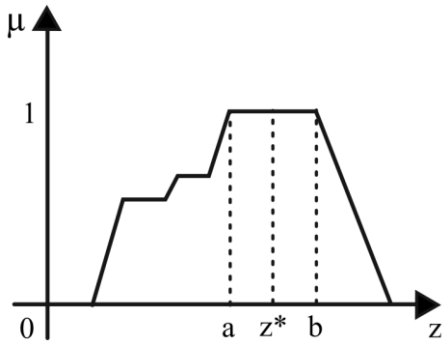

Figure 4.27 Mean max membership defuzzification method [52]

Figure 4.27 depicts the mean max membership defuzzification technique.

4.6 Designed PI Controller

The small signal model of the cuk converter is given in Equations **4.52**, **4.53**, **4.54**, and **4.55**. Using these equations, transfer functions for PI control design are easily obtained.

In mode-1, as shown in Figure 4.28, energy transfer is carried out from the cell to the bus side. In this mode, double-loop PI control is designed to control cell current and bus voltage.

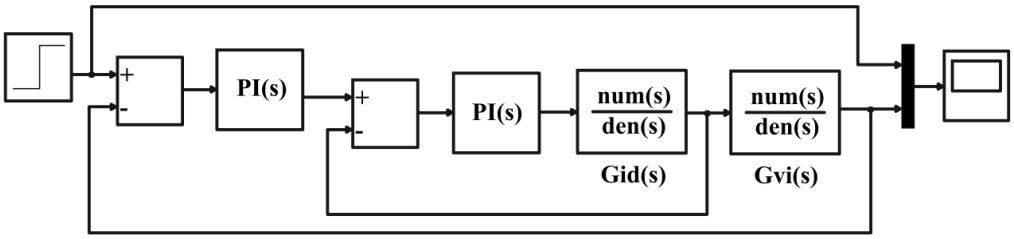

Figure 4.28 Mode-1 double loop PI control Matlab/Simulink block diagram

The following transfer functions for mode-1 are calculated in the Matlab program:

$$Gvd = \frac{\widehat{v_o}}{\hat{d}} = \frac{2.46e08s^2 - 2.4e12s + 3.395e15}{s^4 + 3937s^3 + 4.192e07s^2 + 8.631e10s + 9.522e13} \quad (\mathbf{4.68})$$

$$Gid = \frac{\hat{i}_j}{\hat{d}} = \frac{1.23e04s^3 + 1.116e08s^2 + 8.171e11s + 2.533e15}{s^4 + 3937s^3 + 4.192e07s^2 + 8.631e10s + 9.522e13} \quad (\mathbf{4.69})$$

$$Gvi = \frac{\widehat{v_o}}{\hat{i}_i} =$$

$$\frac{2.46e08s^6+2.691e11s^5+1.081e16s^4+5.298e18s^3+1.045e23s^2+2.319e26s+3.375e29}{1.23e04s^7+1.187e08s^7+1.437e12s^5+8.244e15s^4+4.098e19s^3+1.336e23s^2+2.107e26s+1.645e29} \quad \textbf{(4.70)}$$

The inner loop PI control parameters that control the reference current are $K_p = 2$ and $K_i = 950$. For the bus voltage to remain constant at 8 volts, the outer loop PI control parameters are $K_p = 0$ and $K_i = 166.6$. Kp and Ki values are determined by the PID tuner in the Matlab/Simulink program. Figure 4.29 shows the double loop PI control for mode-1.

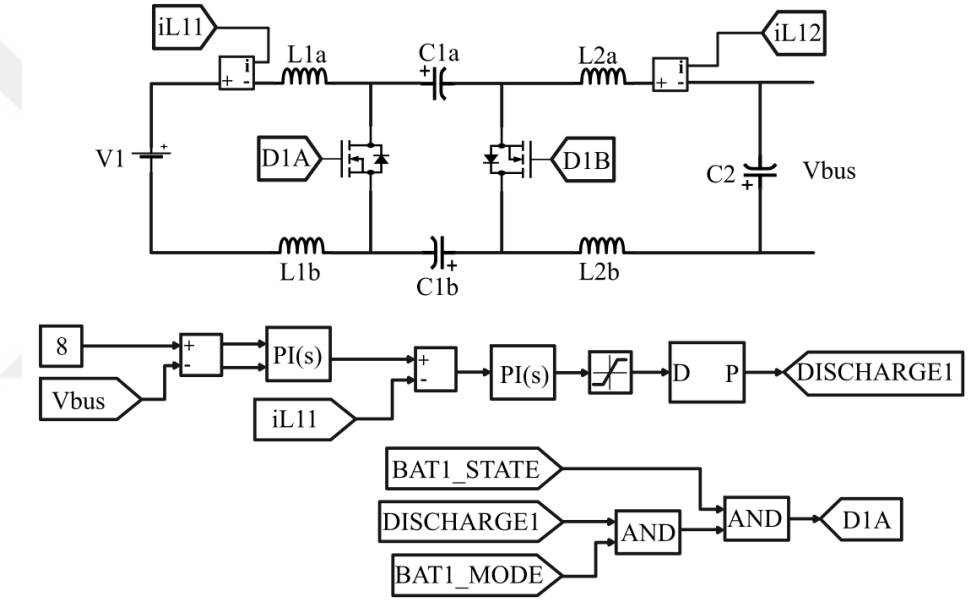

Figure 4.29 The converter with double loop PI control Matlab/Simulink block diagram for mode-1

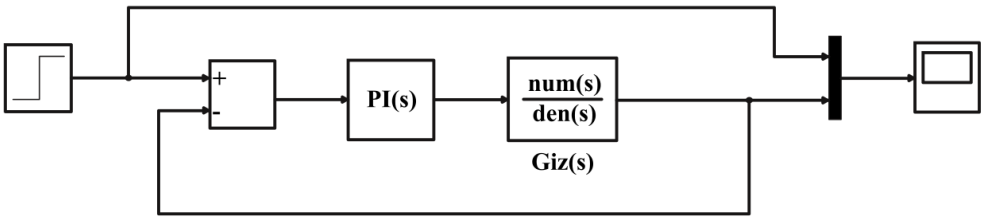

Figure 4.30 Mode 2 Matlab/Simulink block diagram

Figure 4.30 shows PI control block diagram for mode-2. The following transfer function for mode-2 is calculated in the Matlab program:

$$Giz = \frac{\hat{i}_j}{\hat{i}_z} = \frac{1.805e14}{s^4+1.405e06s^3+4.195e07s^2+3.084e13s+3.443e14} \quad (\mathbf{4.71})$$

In mode-2, energy is transferred from the bus to the cell. PI control is designed to efficiently transfer energy from the bus to cells with low SOC levels. The PI control parameters that control the reference current for this mode are $K_p = 0.31$ and $K_i = 9.71$. Kp and Ki values are determined by the PID tuner in the Matlab/Simulink program. Figure 4.31 shows the PI control for mode-2.

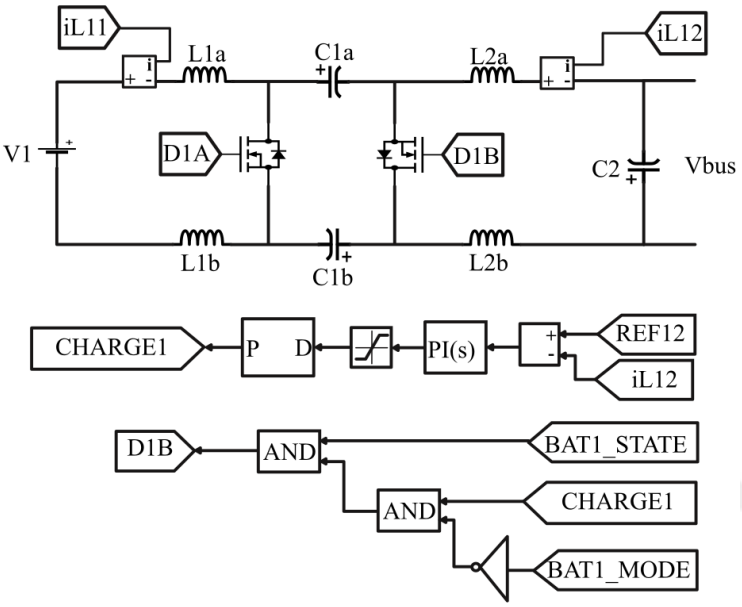

Figure 4.31 The converter with PI control Matlab/Simulink block diagram for mode-2

Figures 4.32, 4.33, 4.34 and 4.35 show the simulation model of the system that is designed with the PI control method.

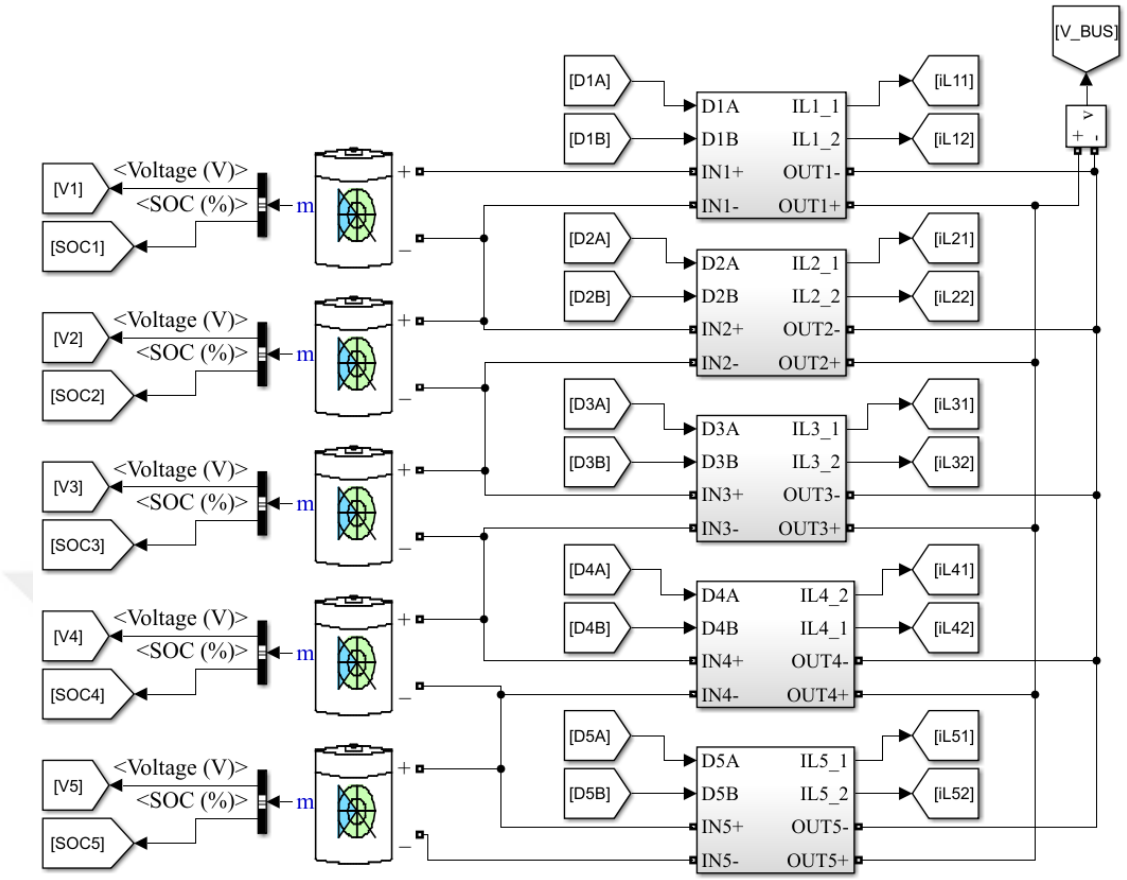

Figure 4.32 Modified bidirectional cuk converter Matlab/Simulink block diagram for PI control

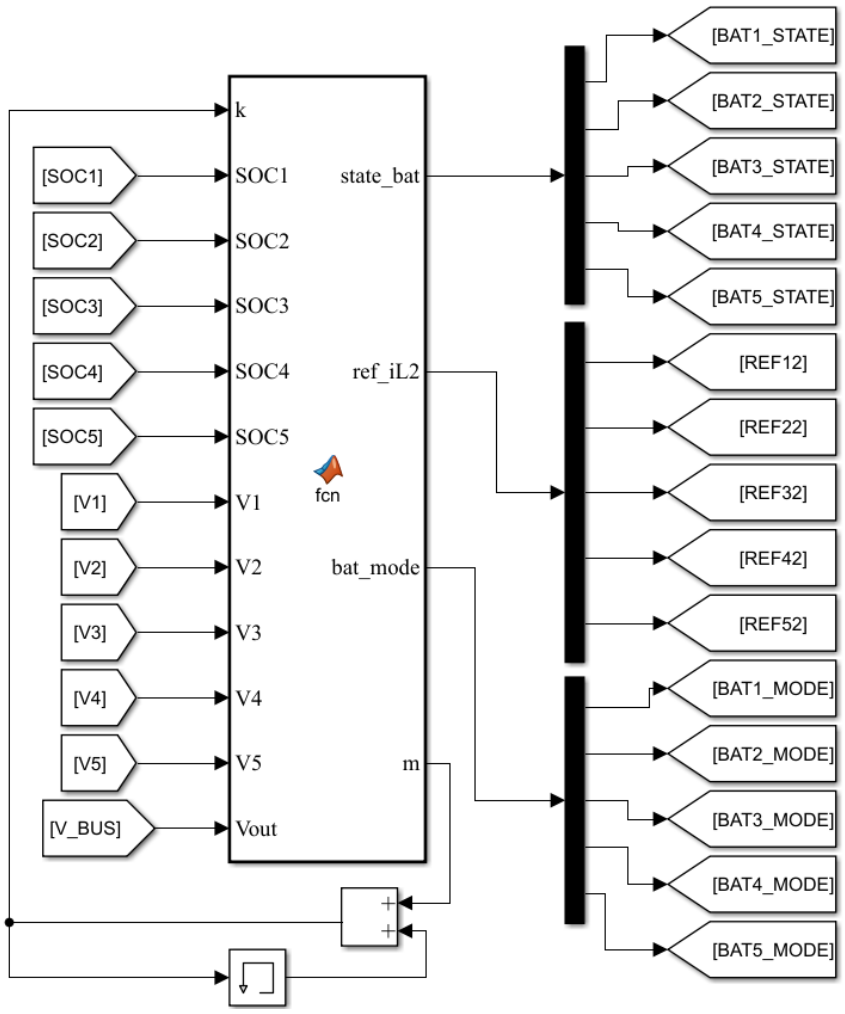

Figure 4.33 Equalization control function Matlab/Simulink block diagram for PI control

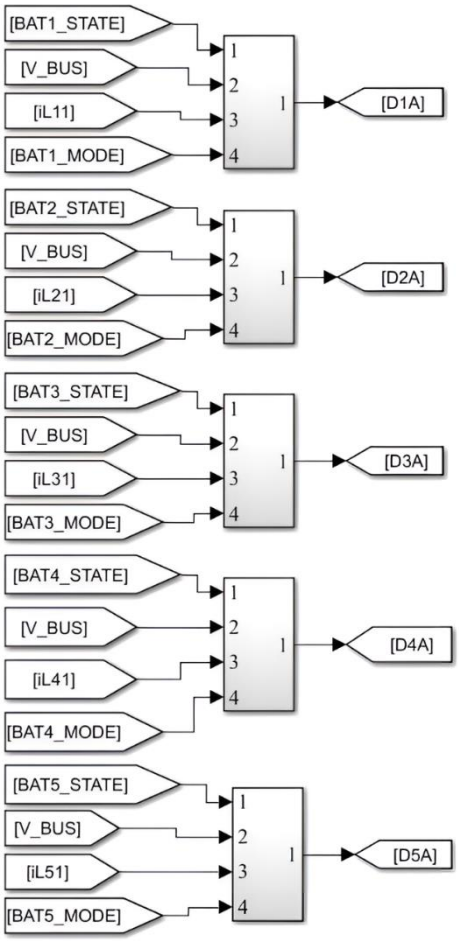

Figure 4. 34 Mode-1 discharging control Matlab/Simulink block diagram for PI controller

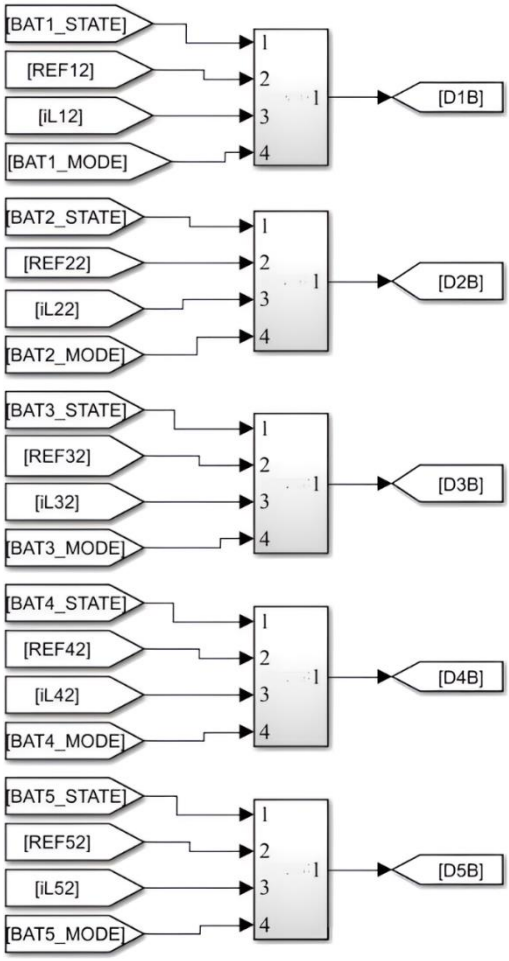

Figure 4.35 Mode-2 charging control Matlab/Simulink block diagram for PI controller

4.7 Designed Fuzzy Logic Controller

Due to its straightforward architecture, DC- DC converters frequently utilize fuzzy logic controller. Fuzzy logic controller has the primary advantage over traditional control methods in that a system's accurate mathematical model is unnecessary. Instead of mathematical models, linguistic norms based on system behavior and human experience are used [53] [54]. The fuzzy controller is a system with two inputs and one output. As stated in Equation **4.72**, *e(k)* is the difference between the output and the reference value. In Equation **4.73**, *de(k)* represents the difference between consecutive errors, that is, the variation of the error [49,55,56].

$$e(k) = R(k) - O(k) \tag{4.72}$$

$$de(k) = e(k) - e(k-1) \tag{4.73}$$

In equation **4.72**, *R(k)* and *O(k)* represents the reference and the output respectively. *e(k)* and *d(k)* form the inputs of the fuzzy controller. The fuzzy controller output *du(k)* represents the change in the duty cycle. As shown in Equation **4.74**, the duty rate *d(k)* at the kth sampling time is calculated by adding the fuzzy controller output *du(k)* and the duty cycle *d(k-1)* of the previous sampling period.

$$d(k) = d(k-1) - du(k) \tag{4.74}$$

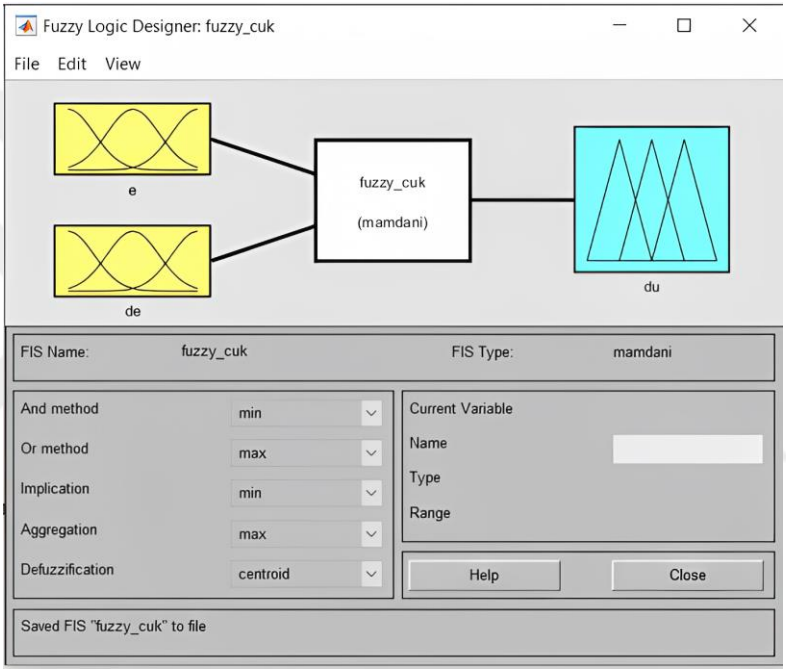

Figure 4.36 Fuzzy logic designer

A Mamdani-based control system is designed. Max-min technique and center of gravity method were used in the inference engine and defuzzification. Figure 4.36 shows the fuzzy logic designer tool in the Matlab/Simulink environment

The fuzzy rule base consists of IF-Then rules. Fuzzification is the conversion of input data into suitable language values. First, membership functions are defined for the inputs. For the input variables, five fuzzy levels (NB) negative large, (NS) negative small, (Z) zero, (PS) positive small, and (PB) positive large are selected as fuzzy set values. Figure 4.37 shows the membership functions for inputs and output.

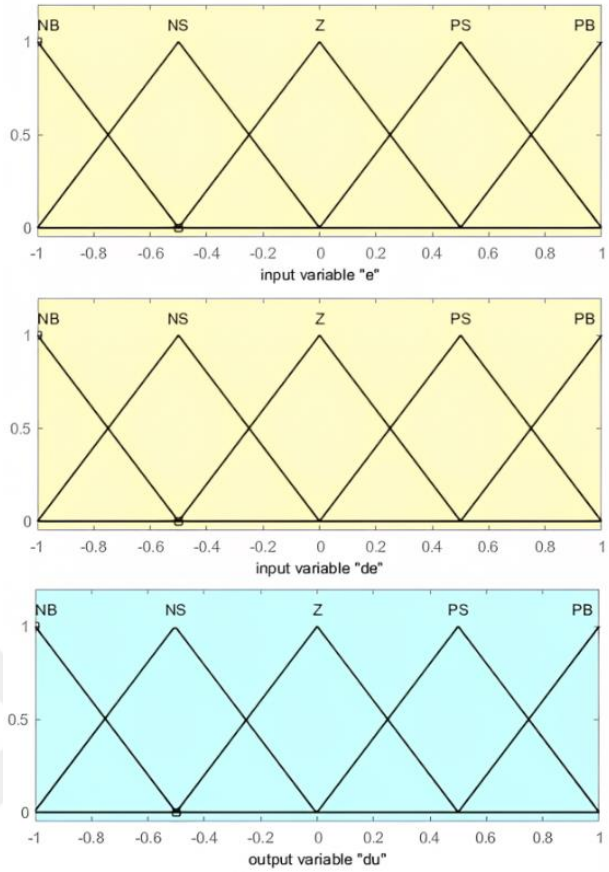

Figure 4.37 The Membership functions

The number of fuzzy levels is determined by the input resolution, and increasing the number of these levels enhances the input resolution. The triangle membership function was chosen for the controller input due to its simplicity and widespread use. For the given inputs, the fuzzifier unit determines the degree of membership in each language variable. Control rules are obtained by analyzing system behaviour. An example rule is like "If *e* is NB and *de* is PS, then *output* is NS". Here *e*, *de*, and *output* represent membership degrees. Table 4.3 shows the rule base.

Table 4.3 The rules

		Change of error				
		NB	**NS**	**Z**	**PS**	**PB**
Error	**NB**	NB	NB	NB	NS	Z
	NS	NB	NB	NS	Z	PS
	Z	NB	NS	Z	PS	PB
	PS	NS	Z	PS	PB	PB
	PB	Z	PS	PB	PB	PB

Fuzzy control rules are developed within the scope of certain criteria based on the system's behavior. If the converter's output is distant from the reference point, the duty cycle change must be big for the output to rapidly return to the reference point. If the converter's output approaches the reference point, a slight modification in the duty cycle will be sufficient. The duty cycle should stay constant if the output is steady and has reached the reference point. The duty cycle change should be negative if the output exceeds the reference point. If the converter's output greatly exceeds the reference point, the duty cycle change must be negative and big to swiftly return the output to the reference point [55,56]. Figure 4.38 depicts the surface view of the developed fuzzy logic control's rules.

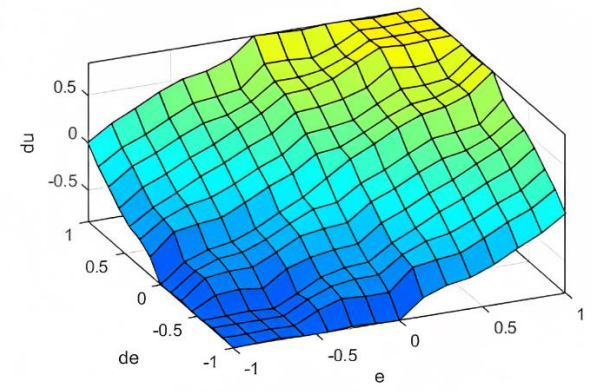

Figure 4.38 Rule surface

According to the direction of energy transfer, fuzzy control designs have been made for both modes separately. Mode-1 is shown in Figure 4.39. In this mode, excess energy will be taken from the battery and transferred to the bus.

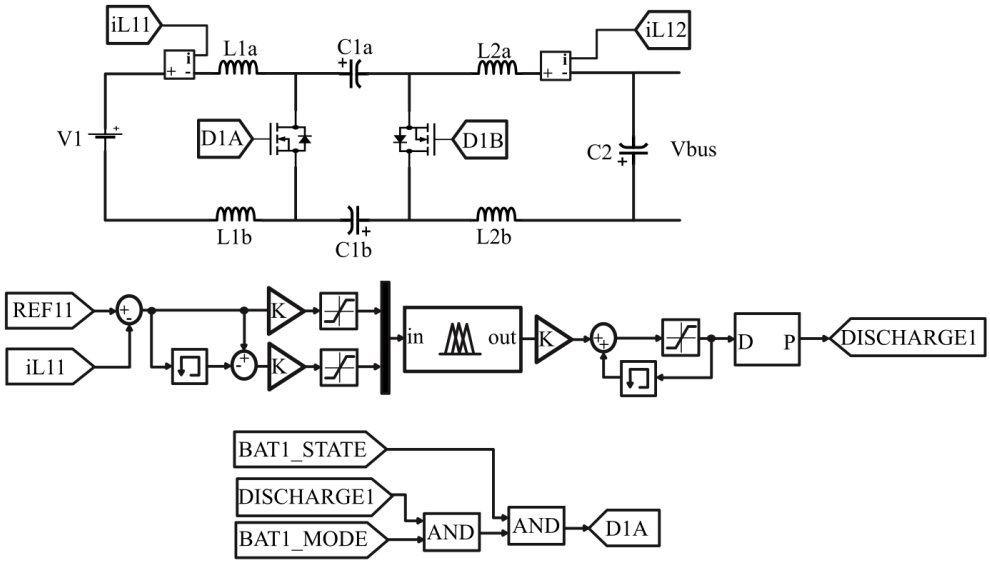

Figure 4.39 The converter with FLC Matlab/Simulink block diagram for mode-1

In Mode-2, energy is transferred from the bus to the battery cell. The FLC design for this mode is shown in Figure 4.40.

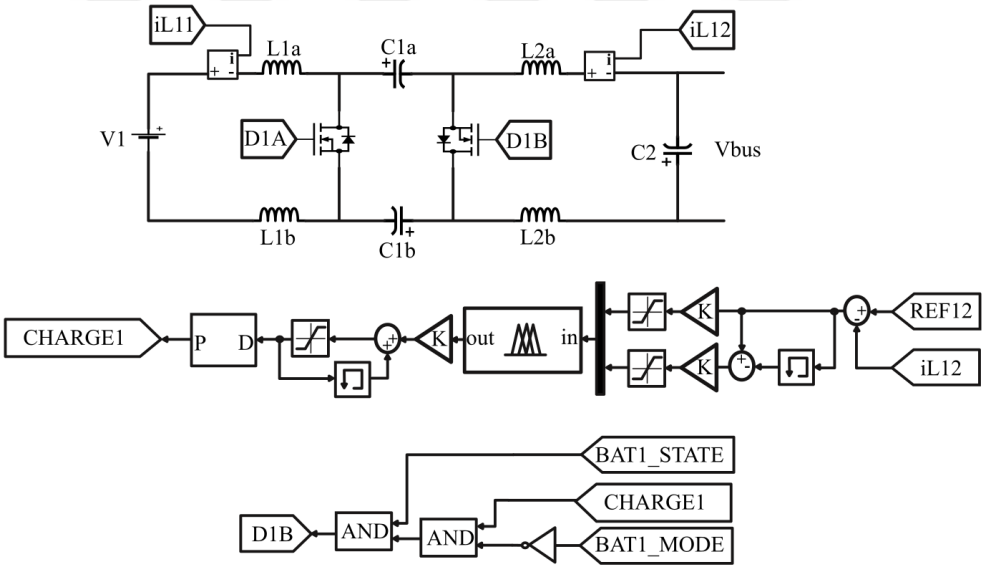

Figure 4.40 The converter with FLC Matlab/Simulink block diagram for mode-2

Figures 4.41, 4.42, 4.43 and 4.44 show the simulation model of the system designed with the FLC method. The fuzzy controller design for the modified bidirectional cuk converter is thus implemented in the Matlab/Simulink program.

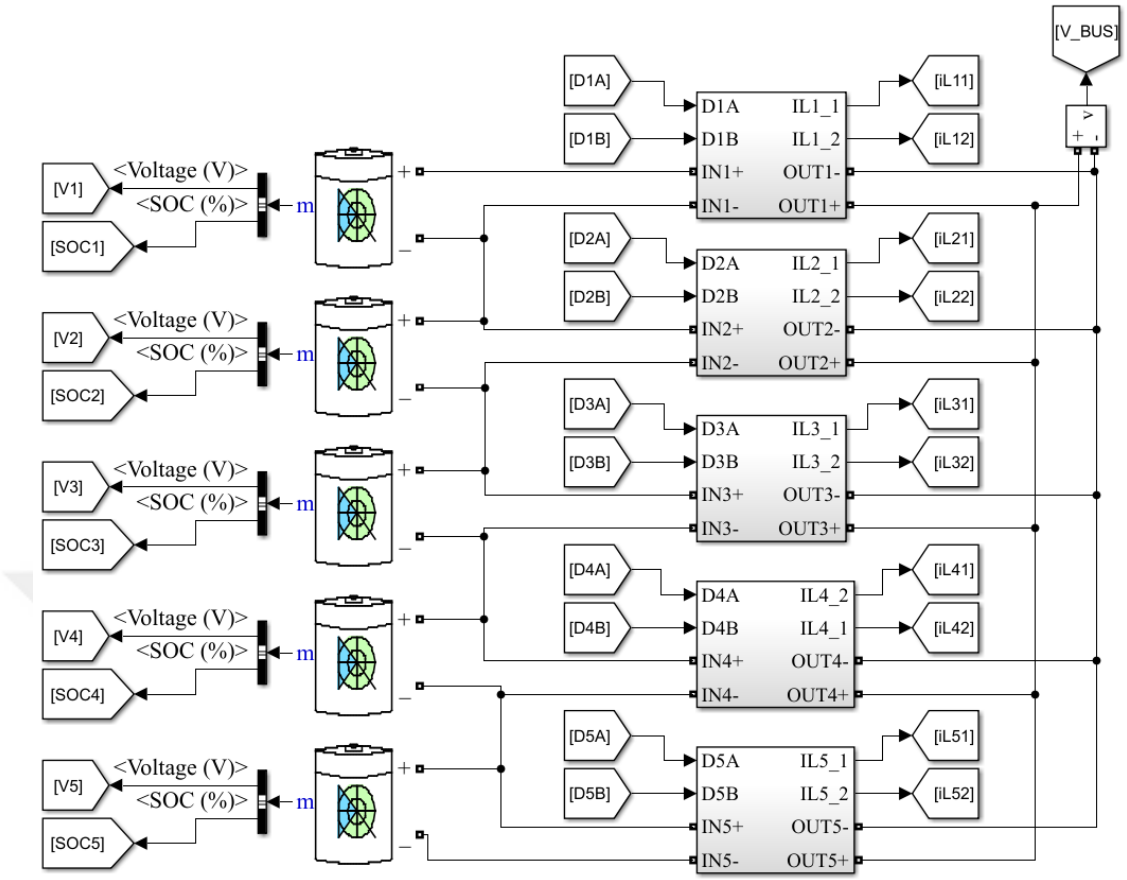

Figure 4.41 Modified bidirectional cuk converter Matlab/Simulink block diagram for FLC

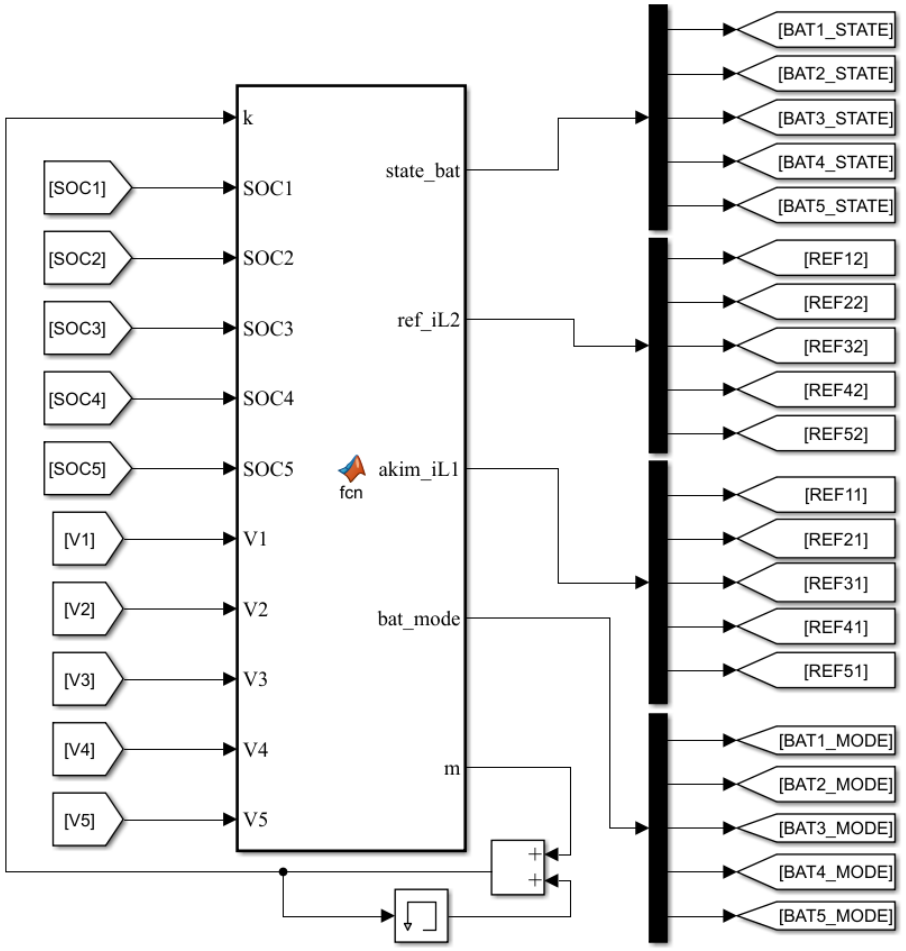

Figure 4.42 Equalization control function Matlab/Simulink block diagram for FLC

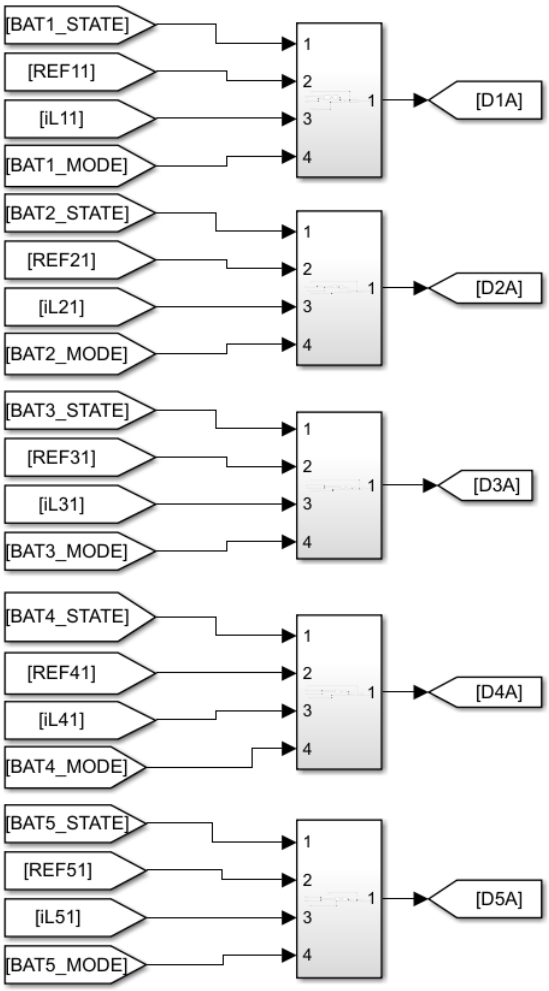

Figure 4.43 Mode-1 discharging Matlab/Simulink block diagram for FLC

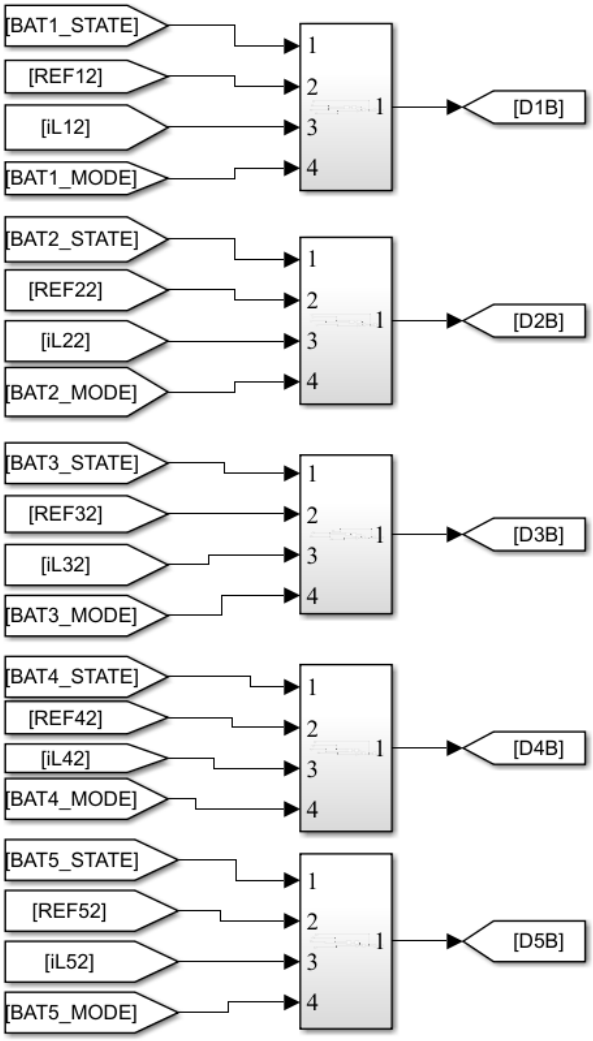

Figure 4.44 Mode-2 charging Matlab/Simulink block diagram for FLC

CHAPTER 5

SIMULATION RESULTS

The diagram of the circuit designed for the proposed converter-based bus topology and the values of the electronic elements used in the circuit are shown in Figure 4.9. The transducers designed in this way are connected one under the other, as shown in Figure 4.11, and become the one in Figure 4.32. By using the flow chart shown in Figure 4.12, the balancing control functions shown in Figures 4.33 and 4.42 have been created separately for FLC and PI control. Figures 4.34, 4.35 and figures 4.43, 4.44 show mode-1 (discharging) and mode-2 (charging) for the PI control and FLC methods, respectively. In both control methods, battery cells with different SOC values are connected in series under the same conditions and simulated.

Except for abnormal situations, there is not much difference between the battery SOC values. For this reason and to keep the simulation time short, the battery SOC values are close to each other. The initial SOC (%) of each battery cell is 74, 74.1, 74.2, 74.5, and 74.6, respectively. Figure 5.1 shows the SOC changes of battery cells in an idle state. Figure 5.2 shows the SOC changes of battery cells while the battery pack is charged with a 21V power supply. Figure 5.3 shows the SOC changes of battery cells as the battery pack is discharged with a load of 5Ω.

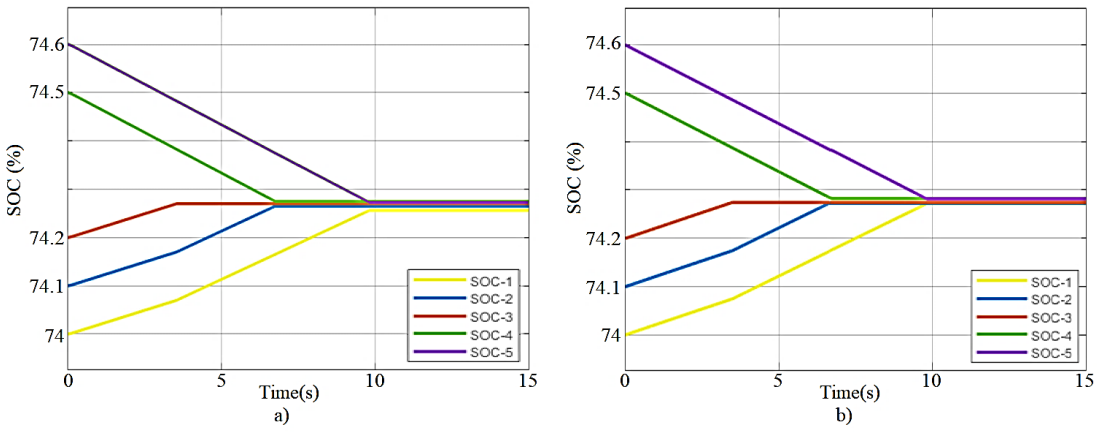

Figure 5.1 SOC variation at idle state; a) PI control, b) FLC

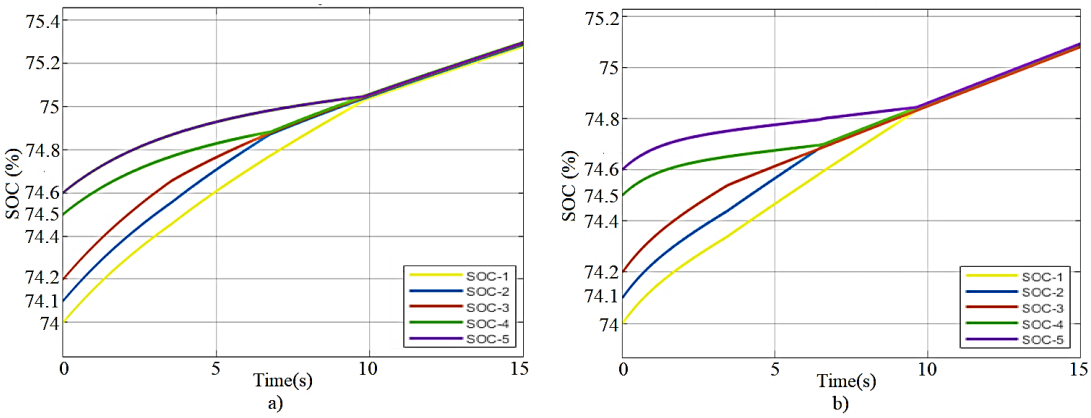

Figure 5.2 SOC variation at charging state; a) PI control, b) FLC

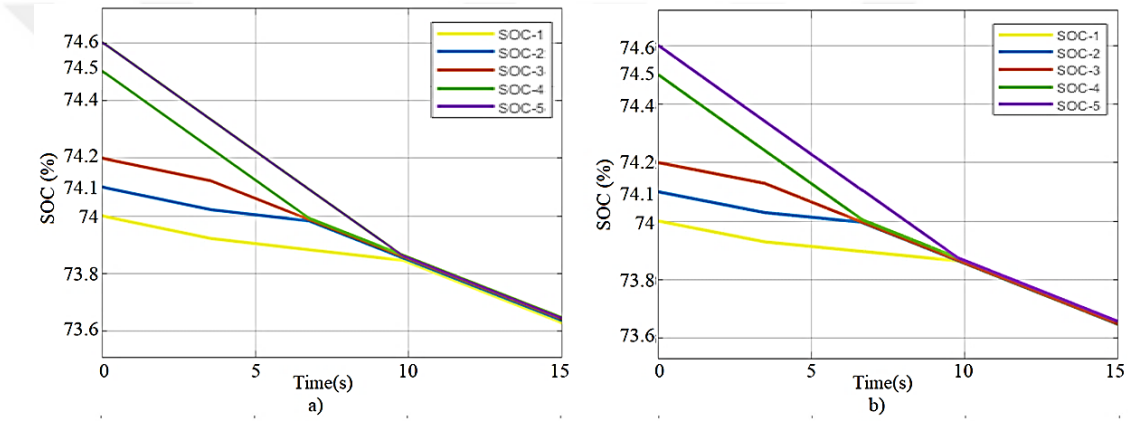

Figure 5.3 SOC variation at discharging state; a) PI control, b) FLC

In Table 5.1, the balancing times of the systems designed with FLC and PI control methods are given comparatively in the three states of the battery pack.

Table 5.1 The comparison of balancing time

Method	Idle state (second)	Charging state (second)	Discharging state (second)
PI Control	9.811	9.828	9.805
FLC	9.808	9.636	9.775

The waveform of the current change in the cells during the balancing process is shown in Figure 5.4. Figure 5.4 (a) shows cell current changes for PI control. Figure 5.4 (b) shows cell current changes for FLC. Initially, three cells with SOC values lower than the reference receive energy from the bus, while two cells with SOC values higher than the reference transfer energy to the bus. Battery cells that reach the limits of the

calculated average SOC reference value are excluded from the energy transfer process as they have reached equilibrium. As the number of cells participating in the balancing process changes, the reference current values of the battery cells in the energy transfer process also change. The balancing module of the battery cell that reaches the reference SOC value is disabled, and the current in the transfer process becomes zero. When the balancing process is completed, all battery cell current values become zero because no energy is transferred.

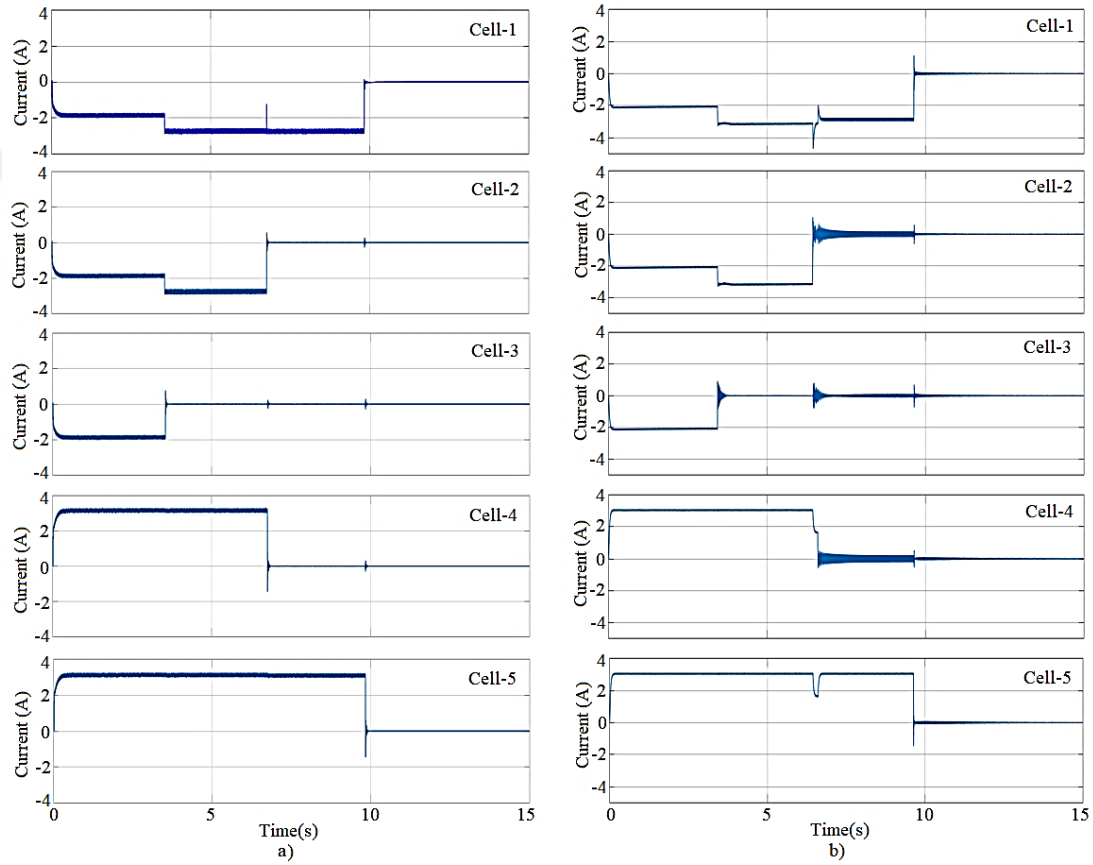

Figure 5.4 Cell current variation in the balancing process

In order to provide a stable and efficient balancing between cells in series connected battery strings, the power to be transferred to the bus side and the power to be drawn from the bus must be equal. This situation ensures that the bus voltage remains constant without deviations. As seen in Figure 5.5, the bus voltage remains constant around 8V during the balancing process and drops to zero when the balancing process is finished.

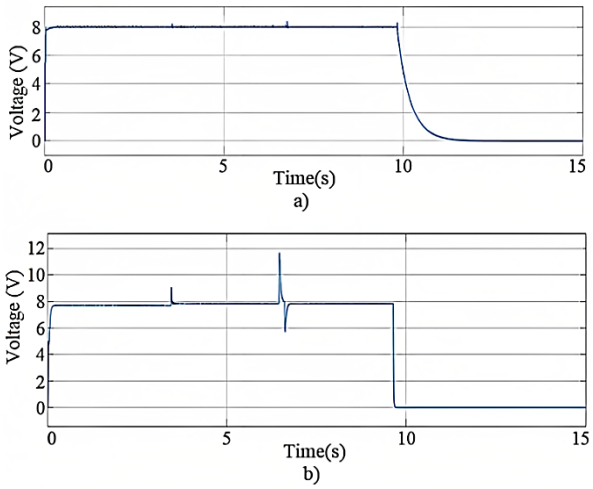

Figure 5.5 Bus voltage variation; a) PI control, b) FLC

Table 5.2 Comparison of current and voltage changes

Parameters	Description	PI control rise time (second)	FLC rise time (second)	PI control settling time (second)	FLC settling time (second)
Vbus	Bus Voltage	0.017	0.064	0.333	0.15
Cell-1	Cell Current 1	0.147	0.043	0.333	0.15
Cell-2	Cell Current 2	0.147	0.043	0.333	0.15
Cell-3	Cell Current 3	0.147	0.043	0.333	0.15
Cell-4	Cell Current 4	0.147	0.052	0.333	0.15
Cell-5	Cell Current 5	0.147	0.052	0.333	0.15

Figure 5.4 shows the systems' responses designed with PI control and FLC method to reference current changes. As given in Table 5.2 when compared to FLC, PI control has a faster transient response and less maximum deviation from steady state. On the other hand, the FLC method has a faster rise and settling time. As seen in Figure 5.5, spikes are seen in the reference current changes in the FLC method.

CHAPTER 6

CONCLUSION

This thesis presents an active balancing topology for balancing battery cells with different SOC values in series-connected battery strings. Bus-based topology was created with modified isolated bidirectional cuk converter modules. The proposed topology has converter modules connected to each battery cell. Excess energy is transferred bi-directionally via a bus where the balancing modules are connected in parallel. In the balancing process, the energy that the converter modules will transfer is calculated and regulated by the balancing algorithm. The equalization system designed with five series-connected battery cells with different SOC values has been verified in the Matlab/Simulink program. As a result, the balancing process was carried out successfully with both control methods, and a comparative analysis was made.

As a result of the designed balancing circuit and the simulations, it has been seen that both balancing methods eliminate the imbalances in the battery pack, but the PI control method is more stable than the FLC method.

In future studies, if the designed active balancing circuit model is physically applied to a battery pack, the responses of the balancing system to changes in ambient conditions can be determined. With the data to be obtained, improvements can be made in the battery pack or balancing circuit design.

REFERENCES

[1] Hoque, M. M., Hannan, M. A., Mohamed, A. & Ayop, A., "Battery charge equalization controller in electric vehicle applications: A review", Renewable and Sustainable Energy Reviews, (*75*), 1363-1385, 2017.

[2] Andrea, D., "Battery management systems for large lithium-ion battery packs", Artech house, 2010.

[3] Naguib, M., Kollmeyer, P. & Emadi, A., "Lithium-Ion Battery Pack Robust State of Charge Estimation", Cell Inconsistency, and Balancing: Review, IEEE Access, (*9*), 50570-50582, 2021.

[4] Andrea, D., "Lithium-Ion Batteries and Applications: A Practical and Comprehensive Guide to Lithium-Ion Batteries and Arrays, from Toys to Towns, Volume 2, Applications, Artech House, 2020.

[5] Turksoy, A., Teke, A. & Alkaya, A., "A comprehensive overview of the dc-dc converter-based battery charge balancing methods in electric vehicles", Renewable and Sustainable Energy Reviews, (*133*), 110274, 2020.

[6] Hemavathi, S., "Overview of cell balancing methods for Li-ion battery technology", Energy storage, (*203*), 1-12, 2020.

[7] Qi, J. & Lu, D. D. C., "Review of battery cell balancing techniques", Australasian Universities Power Engineering Conference (AUPEC), 1-6, 2014.

[8] Cao, J., Schofield, N. & Emadi, A., "Battery balancing methods: A comprehensive review", IEEE Vehicle Power and Propulsion Conference, 1-6, Harbin, China, 2008.

[9] KAYMAZ, H. & HANÇAR, Y., "Elektrikli araç batarya yönetim sistemleri için hücre eşitleme yöntemleri", Akıllı Ulaşım Sistemleri ve Uygulamaları Dergisi, (*4*), (1), 59-73, 2021.

[10] Khanal, A., Timilsina, A., Paudyal, B. & Ghimire, S., "Comparative Analysis of Cell Balancing Topologies in Battery Management Systems", Proceedings of the IOE Graduate Conference, 845-851, Lisbon, Portugal, 2019.

[11] Zhong, H., Li, J. & Wang, Y. X., "A bus-based battery equalization via modified isolated cuk converter governed by adaptive control", Chinese Automation Congress (CAC), 2824-2828, Hangzhou, China, 2019.

[12] Ling, R., Dan, Q., Wang, L. & Li, D., "Energy bus-based equalization scheme with bi-directional isolated Cuk equalizer for series connected battery strings", IEEE Applied Power Electronics Conference and Exposition (APEC), 3335-3340, Charlotte, NC, USA, 2015.

[13] Wu, Z., Ling, R. & Tang, R., "Dynamic battery equalization with energy and time efficiency for electric vehicles", Energy, (*141*), 937-948, 2017.

[14] Ling, R., Dan, Q., Zhang, J. & Chen, G., "A distributed equalization control approach for series connected battery strings", The 26th Chinese Control and Decision Conference (2014 CCDC), 5102-5106, Changsha, China, 2014.

[15] Şükran, E. & Güngör, Z. A., "Geçmişten Günümüze Batarya Teknolojisi", Avrupa Bilim ve Teknoloji Dergisi, (*32*), 947-955, 2021.

[16] Turğut, M., "Elektrikli araçlar için batarya yönetim sistemi tasarımı ve geliştirilmesi", Master's thesis, Karabük Üniversitesi Fen Bilimleri Enstitüsü/Mekatronik Mühendisliği Anabilim Dalı, 2018.

[17] AVGIN, M., YILMAZ, A. & ÜNSAL, M., "Lityum ion bataryaların deşarj durumu davranışlarının genetik ifade programlama ile kestirimi", Kahramanmaraş Sütçü İmam Üniversitesi Mühendislik Bilimleri Dergisi, (*17*), (1),10-15, 2014.

[18] KUL, B., "Geçmişten Günümüze Piller", Takvim-i Vekayi, (*8*), (1), 104-115, 2020.

[19] Nair, N. K. C. & Garimella, N., "Battery energy storage systems: Assessment for small-scale renewable energy integration", Energy and Buildings, (*42*), (11), 2124-2130, 2010.

[20] Tuğru, M. S., "Atık çinko-karbon ve alkali pillerden çinko ve karbonun geri kazanılması", Master's thesis, ESOGÜ Fen Bilimleri Enstitüsü, 2009.

[21] Baker, J., "New technology and possible advances in energy storage", Energy Policy, (*36*), (12), 4368-4373, 2008.

[22] Yu, H., Xie, T., Paszczyñski, S. & Wilamowski, B. M. "Advantages of radial basis function networks for dynamic system design", IEEE Transactions on Industrial Electronics, (*58*), (12), 5438-5450, 2011.

[23] Horiba, T., "Lithium-ion battery systems", Proceedings of the IEEE, (*102*), (6), 939-950, 2014.

[24] Atabay, M., "Lityum-iyon Bataryaların Fotovoltaik Sistemlerde Uygulanabilirliliğinin Diğer Batarya Tipleri ile Karşılaştırılmalı Olarak Araştırılması", MSc Thesis, Ege Üniversitesi Fen Bilimleri Enstitüsü, 2006.

[25] Geisbauer, C., Wöhrl, K., Koch, D., Wilhelm, G., Schneider, G. & Schweiger, H. G., "Comparative study on the calendar aging behavior of six different lithium-ion cell chemistries in terms of parameter variation", Energies, (*14*), (11), 3358, 2021.

[26] Larminie J. & Lowry, J., "Electric vehicle technology explained", John Wiley & Sons, 2012.

[27] Li, C., Wang, Z. Y., He, Z. J., Li, Y. J., Mao, J., Dai, K., et al., “An advance review of solid-state battery: Challenges, progress and prospects”, Sustainable Materials and Technologies, (*29*), e00297, 2021.

[28] Kim, J. G., Son, B., Mukherjee, S., Schuppert, N., Bates, A., Kwon, O., et al., “A review of lithium and non-lithium based solid state batteries”, Journal of Power Sources, (*282*), 299-322, 2015.

[29] Sakuda, A., “Favorable composite electrodes for all-solid-state batteries”, Journal of the Ceramic Society of Japan, (*126*), (9), 675-683, 2018.

[30] Karthikeyan, S., Narenthiran, B., Sivanantham, A., Bhatlu L. D. & Maridurai, T., “Supercapacitor: Evolution and review”, Materials Today: Proceedings, (*46*), 3984-3988, 2021.

[31] https://www.cap-xx.com, 16/04/2023.

[32] Yong, J. Y., Ramachandaramurthy, V. K., Tan, K. M. & Mithulananthan, N., “A review on the state-of-the-art technologies of electric vehicle, its impacts and prospects”, Renewable and sustainable energy reviews, (*49*), 365-385, 2015.

[33] Zhang, R., Xia, B., Li, B., Cao, L., Lai, Y., Zheng, et al., “State of the art of lithium-ion battery SOC estimation for electrical vehicles”, Energies, (*11*), (7), 1820, 2018.

[34] Ma, S., Jiang, M., Tao, P., Song, C., Wu, J., Wang, J., et al., “Temperature effect and thermal impact in lithium-ion batteries: A review”, Progress in Natural Science: Materials International, (*28*), (6), 653-666, 2018.

[35] Daowd, M., Antoine, M., Omar, N., Van den Bossche P. & Van Mierlo, J., “Single switched capacitor battery balancing system enhancements”, Energies, (*6*), (4), 2149-2174, 2013.

[36] Lee, Y., Jeon, S., Lee H. & Bae, S., “Comparison on cell balancing methods for energy storage applications”, Indian Journal of Science and Technology, (*9*), (17), 92316, 2016.

[37] Carter, J., Fan, Z.& Cao, J., “Cell equalisation circuits: A review”, Journal of Power Sources, (*448*), 227489, 2020.

[38] Bildirici, M. & Karaarslan, A., “Analysis of cuk converter using PI and OCC control method”, 13th Int. Conf. Technical Phys. Probl. Eng., 2077-3528, Van, Turkey, 2017.

[39] Karaarslan, A., “Modeling and performance analysis of cuk converter using PI and OCC method”, Int. J. Technical Phys. Probl. Eng, (*10*), (3), 1-5, 2018.

[40] Mokal, B. P. & Vadirajacharya, K., “Extensive modeling of DC-DC cuk converter operating in continuous conduction mode”, International Conference

on Circuit, Power and Computing Technologies (ICCPCT), 1-5, Kollam, India, 2017.

[41] GÜNGÖR, O. & YÜKSEK, H. İ., "Modeling of Boost and Cuk Converters and Comparison of Their Performance in MPPT", Sigma Journal of Engineering and Natural Sciences, (*11*), (1), 83-101, 2020.

[42] Lynser, F. B., Sun, M., Sungoh, M., Taggu, N. & Konwar, P., "Comparative Analysis of Different Control Schemes for DC-DC Converter: A Review", ADBU Journal of Electrical and Electronics Engineering (AJEEE), (*2*), (1), 8-13, 2018.

[43] LešO, M., Žilková, J., Biroš M. & Talian, P., "Survey of control methods for DC-DC converters", Acta Electrotechnica et Informatica, (*18*), (3), 41-46, 2018.

[44] Verma, S., Singh, S. & Rao, A., "Overview of control Techniques for DC-DC converters", Research Journal of Engineering Sciences, (*2*), (8), 18-21, 2013.

[45] Babu, M. V. G. & Naik, D., "Comparative analysis of PI, IP, PID and fuzzy controllers for speed control of DC motor", International Research Journal of Engineering and Technology (IRJET), 500-504, 2017.

[46] Pehlivan, İ., "Bulanık mantık kontrolörler ile klasik PID kontrolörlerin karşılaştırılması ve bir bulanık mantık kontrolör tasarımı", PhD Thesis, Sakarya Universitesi, 2001.

[47] Zadeh, L., "Fuzzy sets", Inform control, (*8*), 338–353, 1965.

[48] Zimmermann, H. J., "Fuzzy set theory", Wiley interdisciplinary reviews: computational statistics, (*2*), (3), 317-332, 2010.

[49] Eker, I. & Torun, Y., "Fuzzy logic control to be conventional method", Energy conversion and management, (*47*), (4), 377-394, 2006.

[50] Cho, H. C., Lee, D. H., Ju, H., Park, H.C., Kim H. Y. & Kim, K. S., "Fire damage assessment of reinforced concrete structures using fuzzy theory", Applied Sciences, (*7*), (5), 518, 2017.

[51] Bai, Y. & Wang, D., "Fundamentals of fuzzy logic control—fuzzy sets, fuzzy rules and defuzzifications, Advanced fuzzy logic technologies in industrial applications", 17-36, 2006.

[52] Morim, A., Fortes, E. S., Reis, P., Cosenza, C., Doria, F. & Gonçalves, A., "Think fuzzy system: developing new pricing strategy methods for consumer goods using fuzzy logic", International Journal of Fuzzy Logic Systems, (*7*), (1), 1-17, 2017.

[53] Corcau, J. I. & Dinca, L., “Fuzzy Logic Controller in a Cuk Converter for Aerospace Application”, International Symposium on Power Electronics, Electrical Drives, Automation and Motion (SPEEDAM), 856-860, Sorrento, Italy, 2022.

[54] Ismail, N. N., Musirin, I., Baharom, R. & Johari, D., “Fuzzy logic controller on DC/DC boost converter”, IEEE International Conference on Power and Energy, 661-666, Kuala Lumpur, Malaysia, 2010.

[55] Duranay, Z. B. & Guldemir, H., “Study of fuzzy logic control of DC-DC buck converter”, Turkish Journal of Science and Technology, (*12*), (2), 23-31, 2017.

[56] Ueno, F., Inoue, T., Oota, I. & Sasaki, M., “Regulation of Cuk converters using fuzzy controllers”, Thirteenth International Telecommunications Energy Conference-INTELEC 91, 261-267, Kyoto, Japan, 1991.

CURRICULUM VITAE

PERSONAL INFORMATION

Name Surname : Eyüp KÖSEOĞLU

Date of Birth :

Phone :

E-mail :

EDUCATION

High School : Iskitler Technical High School

Bachelor : Marmara University, Faculty of Technical Education, Teacher Training in Electronics and Communication Programme

WORK EXPERIENCE

Electronics Technician : Ministry of National Defense, Istanbul Shipyard Command, 2010-2015

Electronics Teacher : Ministry of Education, 2015-…

TOPICS OF INTEREST

- Electronics
- Microcontrollers
- Electrical Systems
- Power Electronics

PRESENT ORGANIZED SOURCES / PRESENTATION

E. Koseoglu A. Karaarslan, Active Cell Balancing with Modified Bidirectional Cuk Converter in Battery Management System, ICES2023 6th International Conference on Engineering Sciences, Ankara, Turkey